

**MICRORNA REGULATION OF TUMOR-INITIATING CELLS IN METASTASIS AND
CHEMORESISTANCE**

By

Ruth White

A DISSERTATION

Presented to the Department of Cell and Developmental Biology
and the Oregon Health & Science University
School of Medicine
in partial fulfillment of
the requirements for the degree of
Doctor of Philosophy
July 2011

School of Medicine

Oregon Health & Science University

CERTIFICATE OF APPROVAL

This is to certify that the PhD dissertation of
Ruth White
has been approved

Dr. Xiao-Jing Wang, PhD Mentor

Dr. Susan Olson, Thesis Committee Chair

Dr. Charles Lopez

Dr. Soren Impey

Dr. Melissa Wong

TABLE OF CONTENTS

TABLE OF ABBREVIATIONS.....ix

ACKNOWLEDGEMENTS.....xi

ABSTRACT.....xiii

CHAPTER ONE: INTRODUCTION.....1

 1.1. Squamous Cell Carcinoma of the Head and Neck and Skin.....1

 1.2. Aberrations of TGFβ Signaling in Squamous Cell Carcinoma.....5

 1.3. Tumor-initiating Cells.....18

 1.4. Metastasis and the Epithelial-to-Mesenchymal Transition.....23

 1.5. ABC Transporters: Tumor-initiating Cell-Associated Regulators of
 Chemoresistance and Metastasis.....27

 1.6. microRNAs: Small RNAs Playing a Large Role in Cancer and Metastasis.....29

 1.7. MicroRNA Regulation of Tumor-Initiating Cells in Metastasis and
 Chemoresistance.....36

**CHAPTER TWO: MICRORNA-9 REGULATES TUMOR-INITIATING CELL
MIGRATION, INVASION AND CHEMORESISTANCE IN MURINE SKIN SQUAMOUS
CELL CARCINOMA.....39**

MATERIALS AND METHODS.....40

 2.1 Mouse Strains.....40

 2.2 Targeting mutations to hair follicle bulge stem cells.....40

 2.3 Histology and Immunostaining.....42

 2.4 Tumor cell isolation and Fluorescence Activated Cell Sorting.....44

2.5 Tumor cell grafting and passaging of whole tumor cells.....	47
2.6 Analysis of Gene and miRNA Expression.....	48
2.7 TaqMan Low Density miRNA Arrays.....	50
2.8 Bioinformatics and Statistical Analysis.....	52
2.9 Cell culture.....	55
2.10 Luciferase Assays for miRNA activity.....	57
2.11 Invasion/Migration Assays.....	57
2.12 Cell Growth Assays.....	58
2.13 Cell Cycle Analysis.....	59
2.14 Drug Resistance Assays.....	59
2.15 <i>In Vivo</i> Tumor Growth Assay.....	59
RESULTS.....	61
2.16 Metastatic Squamous Cell Carcinoma (SCC) Model Development.....	61
2.17 Identification and Characterization of Tumor-Initiating Cells in SCC....	74
2.18 MicroRNAs as Potential Regulators of Stem Cells and Metastasis.....	82
2.19 Increased miR-9 expression in Kras mutant cells.....	91
2.20 Increased miR-9 in the Passaged Tumor SP is not a Result of Increased c-Myc Expression.....	94
2.21 miR-9 regulation of tumor cell growth <i>in vitro</i> and <i>in vivo</i>	95
2.22 miR-9 expression is associated with increased SP size and chemoresistance.....	105
2.23 miR-9 Regulation of Tumor Cell Invasion and Migration.....	118

DISCUSSION.....	122
2.24 Smad4 loss and Kras activation targeted to the murine hair follicle bulge stem cells generates metastatic SCC.....	122
2.25 Tumor Passaging Induces EMT and Increases Metastasis.....	123
2.26 The Side Population and SP ⁻ /CD34 ⁺ /CD49f ⁺ Population are Tumor-Initiating	125
2.27 The Side Population, but not the SP ⁻ /CD34 ⁺ /CD49f ⁺ Size, Correlates with Metastasis.....	126
2.28 Oncogenic and Metastatic miRNA Profile of the Passage 1 Tumor Side population.....	127
2.29 Regulation of miR-9 Expression in the K15.Kras ^{G12D} .Smad4 ^{-/-} Tumors.....	132
2.30 miR-9 Slows Cell Proliferation <i>in vitro</i> , but may Promote Tumor Growth <i>in vivo</i>	133
2.31 miR-9 Expression is Associated with SP size and Chemoresistance in a Context Dependent Manner.....	135
2.32 miR-9 Increases Invasion and Migration of Tumor Cells.....	137
CHAPTER THREE: THE ROLE OF MICRORNA-9 IN HEAD AND NECK SQUAMOUS CELL CARCINOMA METASTASIS.....	139
METHODS.....	140
3.1 Generation of Stably Transduced Tumor Lines.....	140
3.2 Analysis of Gene and miRNA Expression.....	141
3.3 Invasion/Migration Assays.....	142

3.4 Cell Cycle Analysis.....	143
3.5 Statistical Analysis.....	143
3.6 Clinical Sample Collection.....	144
RESULTS.....	145
3.7 miR-9 Overexpression Inhibits Human HNSCC Cell Cycling.....	145
3.8 miR-9 does not Affect the Expression of ABCB1 in Human HNSCC.....	147
3.9. miR-9 Regulation of HNSCC Cell Invasion and Migration.....	148
3.10 miR-Expression in Human Tumors.....	151
DISCUSSION.....	157
3.11 miR-9 Does Not Increase ABCB1 Expression in Human HNSCC Cells..	157
3.12 miR-9 Increases Invasion of Human HNSCC Cells.....	158
3.13 miR-9 Expression may be Associated with Metastasis in Human HNSCC.....	158
CHAPTER FOUR: INCREASED SOX2 EXPRESSION IN THE SP⁻/CD34⁺/CD49f⁺ TUMOR-INITIATING CELL POPULATION FROM XENOGRAFTED TUMORS.....	161
METHODS.....	162
4.1 Tumor cell isolation and Fluorescence Activated Cell Sorting.....	163
4.2 Analysis of Gene Expression.....	165
4.3 Cell culture.....	167
4.4 Cell Growth Assays.....	167
4.5 Invasion/Migration Assays.....	169
RESULTS.....	169

4.6 Sox2 is increased in the SP ⁻ /CD34 ⁺ /CD49f ⁺ TIC from Passage 1	
Tumors.....	169
DISCUSSION.....	175
4.7 The CD34 ⁺ /CD49f ⁺ TIC Population has Increased Expression of the Stem Cell Gene, Sox2, after Passaging.....	175
CHAPTER FIVE: SUMMARY AND CONCLUSIONS.....	177
CHAPTER SIX: FUTURE DIRECTIONS.....	181
6.1 Studying the Tumor-Initiating and Metastatic Potential of the SP ⁻ /CD34 ⁺ /CD49f ⁺ Cell Populations.....	181
6.2 Transcriptional Regulation of miR-9 in SCC.....	182
6.3. The Role of miR-9 in SCC Chemoresistance.....	183
6.4 The role of miR-9 in SCC Metastasis.....	184
6.5 Does Sox2 Contribute to Tumor-Initiation and Chemoresistance in the SP ⁻ /CD34 ⁺ /CD49f ⁺ Population?.....	185
CHAPTER SEVEN: REFERENCES.....	187
APPENDIX A: ANTIBODIES.....	216
APPENDIX B: LENTI/RETROVIRAL STUDY VECTORS.....	217
APPENDIX C: GENOTYPING PRIMERS.....	218
APPENDIX D: TAQMAN® GENE EXPRESSION PROBES.....	219
APPENDIX E: TAQMAN® MICRORNA EXPRESSION PROBES.....	220
APPENDIX F: HUMAN SAMPLES.....	221
APPENDIX G: CURRICULUM VITAE.....	221

**APPENDIX H: SMAD4 LOSS IN MICE CAUSES SPONTANEOUS HEAD AND NECK
CANCER WITH INCREASED GENOMIC INSTABILITY AND
INFLAMMATION.....225**

TABLE OF ABBREVIATIONS

General Terms	
AACR	American Association for Cancer Research
Abcb1a	ATP binding cassette transporter b1a
ABC	ATP binding cassette
ALDH1	Aldehyde Dehydrogenase 1
ALK5	Activin-like kinase
BCC	Basal Cell Carcinoma
bHLH	Basic Helic Loop Helix
BMP	Bone Morphogenic Protein
CAF	Carcinoma Associated Fibroblast
EGFR	Epidermal Growth Factor Receptor
EMT	Epithelial-to-Mesenchymal Transition
ER	Estrogen Receptor
FA	Fanconi Anemia
Fanc/Brca	Fanconi Anemia/Brca pathway
I-Smad	Inhibitory Smad
miR	microRNA
miRNA	microRNA
MMP2	Matrix Metalloprotease 2
MMP9	Matrix Metalloprotease 9
MRP	Multidrug Resistance Related Protein
NFkb	Nuclear Factor kappa b
PI3K	Phosphoinositide-3 kinase
PR	Progesterone Receptor
pre-miRNA	Precursor microRNA
pri-miRNA	primary microRNA transcript
PTEN	Phosphatase and Tensin Homolog
R-Smad	Receptor Smad
RISC	RNA Induced Silencing Complex
SA	Sebaceous Adenoma
SBE	Smad Binding Element
SCC	Squamous Cell Carcinoma
SEM	Standard Error of the Mean
siRNA	Short Interfering RNA
Sox2	Sex Determining Region Y-Box 2
SPCC	Spindle Cell Carcinoma
STAT3	Signal Transducer and Activator of Transcription 3
tet	tetrocycline
TGFβ	Transforming Growth factor beta

TGF β RII	Transforming Growth factor beta Receptor II
TGF β RI	Transforming Growth Factor beta Receptor I
TIC	Tumor Initiating Cell
UV	Ultraviolet
ZEB	Zinc Finger E-Box Binding Homeobox

Materials and Methods	
K15	Keratin 15
WT	Wild Type
OCT	Optimal Cutting Temperature
H&E	Hematoxylin and Eosin
IHC	Immunohistochemistry
IF	Immunofluorescence
BSA	Bovine Serum Albumin
PCR	Polymerase Chain Reaction
PBS	Phosphate Buffered Saline
GFP	Green Fluorescent Protein
RFP	Red Fluorescent Protein
qRT-PCR	Quantitative Real Time Polymerase Chain Reaction

ACNOWLEDGEMENTS

- Xiao-Jing Wang, for her excellent mentorship and support, and the opportunity to conduct this research.
- My thesis committee members: Drs. Susan Olson, Charles Lopez, Soren Impey, Melissa Wong and Xiao-Jing Wang for their scientific and moral support during this thesis work.
- Dr. Shi-Long Lu for contributing the miR-9 methylation and expression data (figure 33) and for his advice and support.
- Dr. Sophia Bornstein for laying the groundwork for this project.
- Karen Helm, Lester Acosta and Christine Childs at the UC Denver Health Sciences Cancer Center Flow Cytometry Core for helping develop sorting protocols and analysis of flow data.
- Kazutoshi Murao and Shawna Johnson (Dennis Roop Lab, UC Denver) for teaching me the tumor initiating cell sorting and grafting techniques.
- Antonio Jimeno (UC Denver) for supplying primary and passaged human HNSCC samples.
- Molly Kulesz-Martin for supplying primary human HNSCC samples.
- Pamela Garl, for moral and administrative support.
- David Castillo for contributing to the Sox2 project (Figure 37).
- The Wang lab, both old and new, for their ideas and support.
- Drs. Sophia Bornstein, Kristina Hoot Young and Philip Owens for looking after their “little sister” during the early years.

- My friends and family whose advice, love and support has helped me persevere: Donna Albertson, John White, Amelia White and the Geiger's, Dan Pinkel, Phoebe White, Ben White, Jarred Power, Erin Meadows, Kristina Hoot Young, and Sophia Bornstein.

ABSTRACT

Tumor-initiating cells (TICs) are operationally defined as tumor cells with the ability to initiate tumor formation upon grafting into immunocompromised mice. TICs have been characterized as drug resistant and as possible sources of metastatic cells, although the latter function is poorly understood. In order to gain a better understanding of the role of these cells in metastasis, we have studied TICs from a mouse model of skin squamous cell carcinoma (SCC) initiated by activation of Kras and inactivation of Smad4 in the hair follicle bulge stem cells. These mice develop tumors that are metastatic to the lung. Lung metastasis in this model was shown to be greatly increased by xenografting (passaging) the tumors. Two TIC populations were defined within this tumor model, the Hoechst dye excluding side population (SP) and the SP⁻/CD34⁺/CD49f⁺ population. We observed that the size of the SP, but not the SP⁻/CD34⁺/CD49f⁺ cell fraction, closely correlated with the presence of lung metastasis, and further that there is a significant increase in the size of the SP fraction in the more metastatic, passaged tumors compared to the primary tumors. A screen of miRNA expression in the SP from highly metastatic passaged tumors compared to the SP from primary tumors revealed differential expression of a number of miRNAs, including miR-9. Expression of miR-9 closely correlates with SP size and spindle cell carcinoma (SPCC) histology. miR-9 regulates the expression of the ABC transporter, Abcb1a, in a context specific manner leading to increased SP size and chemoresistance. miR-9 also increases the invasion and migration of skin and HNSCC cell lines *in vitro* and may promote *in vivo* tumor growth in

immunocompetent mice. In human head and neck SCC (HNSCC), higher expression of miR-9 was found in passaged tumors with metastasis positive lymph node status compared to negative node status based on pathological staging. However, no association between miR-9 expression and node status was found in primary HNSCC. Lastly, we found increased expression of the stem cell gene, Sox2, in the SP⁻/CD34⁺/CD49f⁺, but not the SP⁺, cells from the passaged tumors. Sox2 overexpression inhibited invasion and migration, further suggesting that the SP⁻/CD34⁺/CD49f⁺ population is a TIC with functions distinct from the SP⁺

CHAPTER ONE

INTRODUCTION

1.1. Squamous Cell Carcinoma of the Head and Neck and Skin

Head and neck squamous cell carcinoma (HNSCC) includes tumors of the nasal cavity, paranasal sinuses, oral cavity, pharynx and larynx, and is the sixth most common cancer worldwide with ~650,000 new cases and ~350,000 cancer related deaths each year [1]. Despite advances in surgery, radiotherapy, and chemotherapy, there has been little improvement in the five-year survival of HNSCC in the last 30 years [2]. HNSCC patients commonly present with locally advanced disease involving both vital structures and regional lymph nodes with ~10% of patients presenting with distant metastases. Despite initial success in local control, ~50% of patients relapse with either local or distant disease progression [3].

The major risk factors for HNSCC are alcohol, tobacco, and betel (areca) nut use [4]. While tobacco use increases HNSCC risk 3-9 fold, the combination of alcohol and tobacco use synergistically increases HNSCC risk ~100-fold [5]. In addition, human papillomavirus (HPV) is responsible for a subset of HNSCCs located primarily in the hypopharynx [6]. A number of cancer susceptibility syndromes including Fanconi anemia, xeroderma pigmentosum, ataxia telangiectasia, and Bloom syndrome also increase HNSCC risk [7]. Noticeably, all of these syndromes linked to HNSCC susceptibility have extensive DNA repair defects and genomic

instability. Accordingly, understanding the molecular pathophysiology of these diseases may provide valuable information about the genetic aberrations responsible for sporadic HNSCC.

As with other epithelial cancers HNSCC results from the accumulation of genetic and epigenetic aberrations that affect numerous cellular processes including proliferation, apoptosis, inflammation, angiogenesis, and DNA repair [8, 9]. Genetic alterations at 17p13 (encoding p53) and 9p21 (encoding p14 and p16) have both been reported in HNSCC [10, 11]. A number of oncogenic pathways such as EGFR/STAT3 and PI3 kinase/PTEN/Akt are also activated in HNSCC [12]. Epithelial growth factor receptor (EGFR) is a tyrosine kinase receptor that regulates cell growth, migration and survival and is overexpressed in 80-90% of HNSCCs [13]. STAT3, a transcription factor that can be activated by both EGFR and interleukin signaling [14], is also commonly activated in HNSCCs [15]. EGFR overexpression correlates with both aggressive tumor behavior and poor clinical outcome [16, 17] and targeted therapy against EGFR is now being clinically applied [18]. While the incidence of activating Ras mutations is infrequent in HNSCC in the Western world (5-10%)[19, 20], Ras mRNA is overexpressed in a majority of human HNSCCs [20], and Ras mutations occur in ~35% of oral cancers associated with chewing tobacco exposure in southern Asia [21].

Skin SCC is the second most common type of skin cancer in the US behind basal cell carcinoma and accounts for ~20% of all cutaneous malignancies [22]. The

major risk factors for skin SCC are ultraviolet (UV) radiation and immunosuppression (e.g. organ transplant patients) [23, 24]. Approximately 60% of skin SCCs arise from UV-induced precancerous lesions called Actinic Keratoses [25]. While the majority of skin SCCs can be effectively treated if caught early, a subset of aggressive tumors can progress and metastasize, particularly in immunocompromised patients. Various studies have shown the rate of metastasis in skin SCC to range from 0.1-10% [26]. While the majority of skin SCC metastasizes to the regional lymph nodes, subsequent metastases can occur in the lung, liver, bone and brain [26]. Among the risk factors for metastasis of skin SCC are histologic differentiation [27, 28] and immunosuppression [29]. Poorly differentiated tumors and those with greater vertical tumor thickness have increased risk of metastasis [27]. One rare subset of poorly differentiated, metastatic SCC seen in both skin and HNSCC are spindle cell carcinomas (SPCC). Histological characterization of these poorly differentiated tumors is based on the elongated spindle shape of the cells and a loss of keratinization [30].

Mutations of p53 are believed to occur early in skin SCC development as a result of UV exposure, and patches of p53 mutant epidermis can be seen in normal, UV exposed skin [31-34]. Similar to HNSCC, loss of p16 has also been frequently detected in skin SCC. While mutation of p16 is relatively infrequent [35], loss of the short arm of chromosome 9, is frequently seen in skin SCC [36, 37]. Ras mutation in skin SCC is seen at UV sensitive sites at codons 12, 13, and 61 [38] at a frequency of approximately 10-20% [39-42]. One question currently under debate is the origin

of skin tumors of different phenotypes. Many studies in transgenic animals have shown that different gene mutations in the basal keratinocyte layer can result in tumors with different phenotypes such as SCC, basal cell carcinoma (BCC) or hair follicle tumors such as sebaceous adenomas (SA) [43]. One hypothesis for this diversity is that different gene mutations target individual stem cells in the hair follicle bulge and the type of mutation dictates tumor differentiation. The other hypothesis for tumor heterogeneity suggests that different subsets of cells in the epidermis differentially respond to aberrant signaling pathways (Figure 1). By targeting the hair follicle bulge stem cells directly it would be possible to start to understand which of these mechanisms contributes to skin tumor heterogeneity.

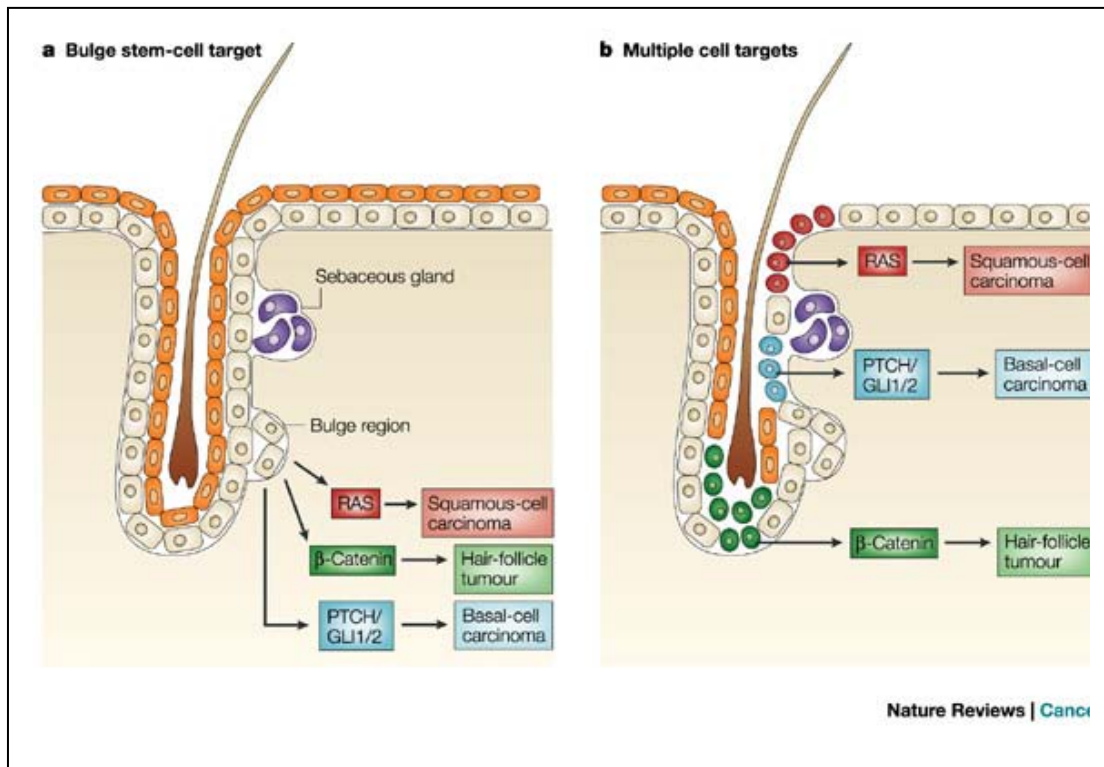


Figure 1. *Two models for the origin of skin tumor heterogeneity. Aberrations in different signaling pathways have been shown to result in specific epithelial tumor*

phenotypes. The origin of such tumors has been under debate. One hypothesis (a) states that the mutations occur in the pluripotent stem cell population of the hair follicle bulge. The type of mutation then directs the pathway of differentiation of the epithelial stem cell during tumor formation. The other hypothesis (b) suggests that different sub-populations of cells within the hair follicle respond differentially to aberrant signaling pathways. Adapted by permission from Macmillan publishers Ltd: Nature Reviews cancer, 2003. 3(6): p. 434-43, Copyright 2003 [43].

1.2. Aberrations of TGF β Signaling in Squamous Cell Carcinoma

TGF β Signaling Overview

While skin SCC and HNSCC have different etiologies, both tumor types frequently exhibit aberrations of the TGF β signaling pathway. The TGF β superfamily includes the TGF β ligands, bone morphogenic proteins (BMPs) and activins/inhibins [44]. TGF β ligands signal through two types of transmembrane serine/threonine kinase receptors, TGF β receptor I (TGF β RI), also known as activin receptor-like kinase 5 (ALK5), and TGF β receptor II (TGF β RII) (Figure 2); a total of five TGF β RII and seven TGF β RI family members with differing tissue distributions have been described [45]. Canonical TGF β signaling is mediated through Smad family members; there are eight different Smads that are divided into three groups: receptor-activated Smads (R-Smads), inhibitory Smads (I-Smads) and the common Smad (co-Smad or Smad4) [45]. After ligand binding, TGF β RII phosphorylates TGF β RI, which in turn phosphorylates R-Smads: TGF β ligands signal through the R-Smads 2 and 3, while BMPs employ R-Smads 1, 5, and 8 [46]. Phosphorylated R-

Smads form heterotrimers with Smad4 and translocate to the nucleus where they regulate gene expression at Smad binding elements (SBEs) [47] (Figure 2). Smad complexes interact with a variety of transcription factors and transcriptional co-activators and co-repressors that regulate binding at TGF β -responsive target genes and provide an additional layer of tissue and gene specificity [46]. I-Smads attenuate TGF β signaling by competing with R-Smads for binding at TGF β RI and by recruiting ubiquitin ligases to degrade TGF β RI and R-Smads [47, 48]. In non-cannical (Smad-independent) TGF β signaling, ligand bound TGF β receptors can activate other signaling pathways including the MAP kinase pathway, phosphatidylinositol-3-kinase (PI3K)/AKT, and Rho GTPase; activation of these pathways likely enhances tumor growth after disruption of canonical TGF β -Smad signaling [49].

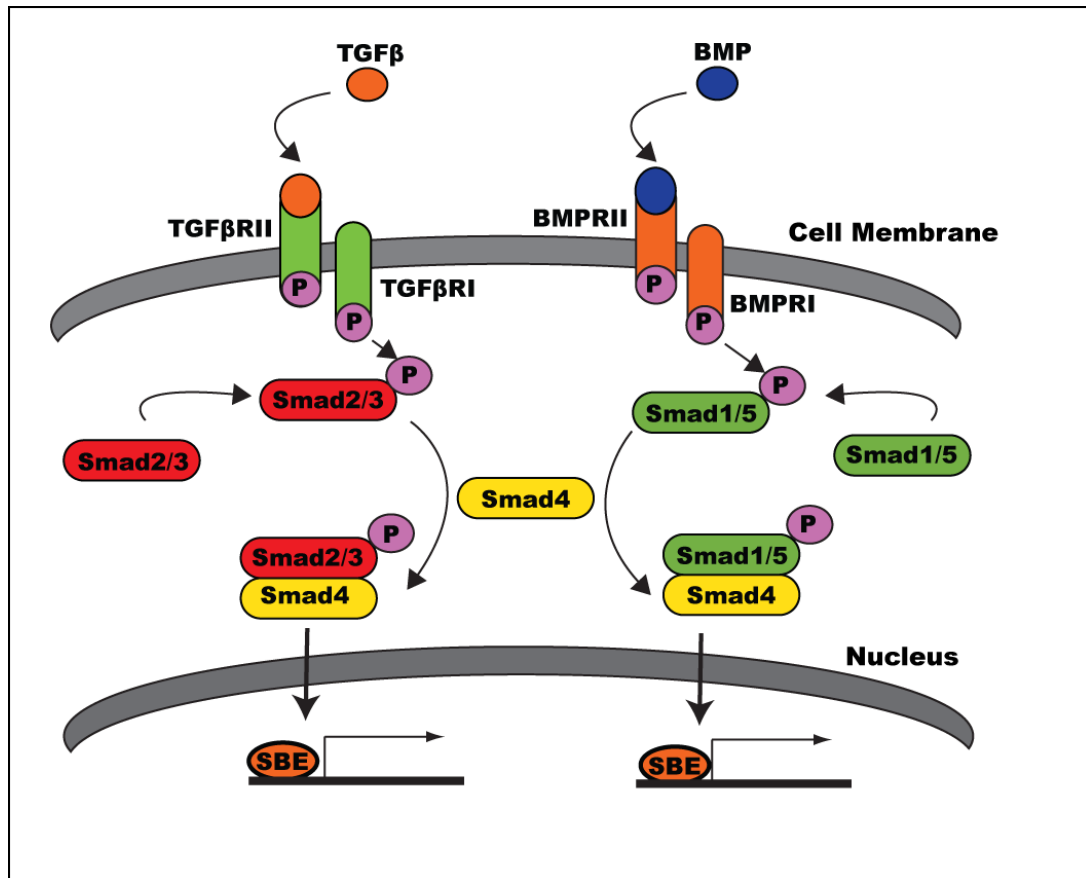


Figure 2. TGFβ/BMP signaling regulates tissue homeostasis.

TGFβ and BMPs signal through different R-Smads. Phosphorylated R-Smads heterotrimerize with Smad4, translocate into the nucleus and mediate gene transcription by binding Smad binding elements (SBEs) in the promoters of TGFβ and BMP responsive genes. Interactions with transcriptional coactivators and corepressors provide an additional layer of regulation.

TGF β as a regulator of epithelial homeostasis

TGF β signaling regulates tissue homeostasis by modulating cell growth, differentiation, apoptosis, migration, inflammation, and angiogenesis [45, 50-52]. In epithelial cells, TGF β inhibits proliferation and promotes both apoptosis and differentiation [45]. By inducing expression of the cell cycle regulators, p15Ink4b and p21Cip1, TGF β inhibits cell cycle progression [53, 54]. In addition, TGF β down regulates c-myc expression through interactions between Smads and transcriptional co-repressors [55]. TGF β promotes differentiation by down-regulating Inhibitor of Differentiation/DNA binding (Id) proteins [56]. TGF β promotes apoptosis through both Smad dependent and Smad independent mechanisms [57, 58]. TGF β RI directly interacts with the E3 ubiquitin ligase, TRAF6, causing apoptosis through TAK1-p38/JNK [59, 60] while Smads activate apoptosis through activation of ATM, p53, and BIM and repression of AKT [61, 62]. Given the numerous activities of TGF β on epithelial homeostasis, it is not surprising that TGF β signaling disruption is common in many cancers including HNSCC [63], however, studies in mouse models and human HNSCC samples illustrate that different TGF β signaling disruptions promote epithelial carcinogenesis through both unique and overlapping mechanisms.

Mouse Models

Mouse models of skin and head and neck cancer have demonstrated the importance of the TGF β pathway in both tumor initiation and progression in these

two organs [20, 64-68]. Since TGF β signaling disruption typically causes embryonic lethality, systems allowing conditional and tissue-specific genetic manipulation are required. The commonly used systems include tetracycline to de-repress or activate the tet operon (tet-off or tet-on), tamoxifen to activate an estrogen receptor (ER) fusion protein or RU486 to activate a progesterone receptor (PR) fusion protein [69, 70]. Keratinocyte targeting is accomplished by placing the transactivator under the control of the keratin 5 or 14 promoter that is expressed in basal keratinocytes of the skin and oral epithelium [71, 72]. In the inducible PR gene-switch system, the transactivator is a fusion protein containing a Gal4 DNA binding domain, a RU486-responsive PR domain, and a p65 transactivation domain [73]. Mice with the transactivator are then crossed with animals harboring a target that consists of a series of Gal4 DNA binding sites and a minimal tata promoter upstream of the gene of interest. In this system, local RU486 application causes gene activation (Figure 3A). In conditional gene deletion systems, target genes or sequences are flanked by LoxP sites (“floxed”), which can then be excised by Cre recombinase. Tissue specificity is achieved by placing the Cre recombinase under the control of a keratin promoter and temporal control is achieved by a Cre recombinase-PR fusion protein that is inducible by application of RU486 [74] (Figure 3B). In addition to genetic deletion, this system can also be used to “knock-in” oncogenes, for example, when a floxed stop codon is placed upstream of oncogenic Kras^{G12D} [75].

Although single genetic alterations do not typically induce tumor formation, chemical carcinogenesis can be used to determine whether these genetic

modifications affect susceptibility to tumor development. For example, a single dose of 7, 12-dimethylbenz[a]anthracene (DMBA) to the skin or oral epithelium can be used to induce tumor-initiating H-Ras mutations [76]. Other carcinogens such as 4-nitroquinoline-1 oxide (4-NQO) have also been used to induce HNSCC through DNA adduct formation and H-ras mutations [77, 78]. These inducible animal models of skin and HNSCC are valuable resources for the study of TGF β signaling aberrations in the development and progression of SCC.

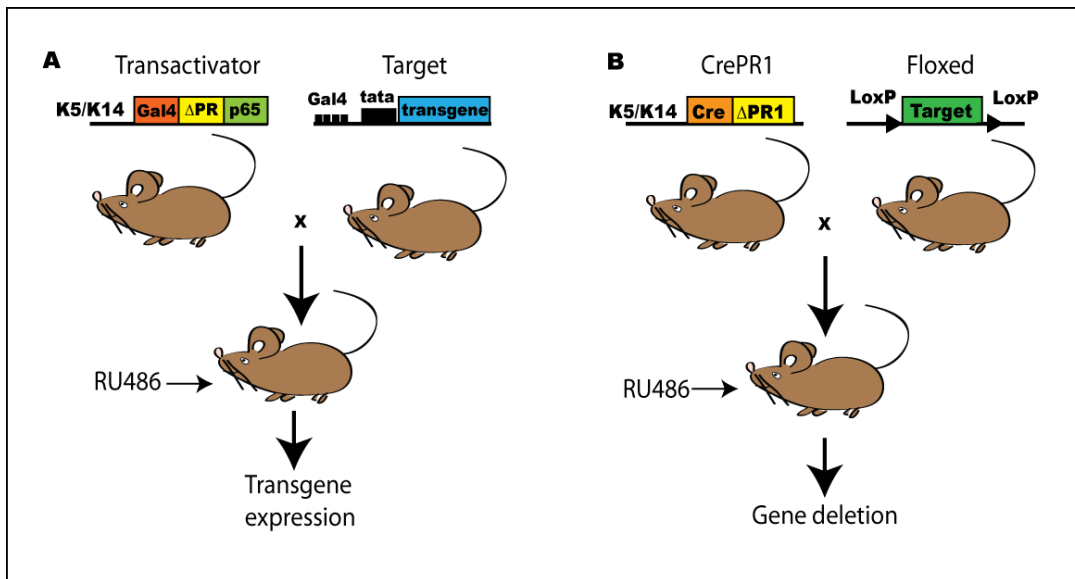


Figure 3. Conditional mouse models facilitate tissue-specific manipulation of TGF β signaling.

A. The epithelial gene-switch system requires both transactivator and target transgenes. The transactivator is a fusion protein consisting of a Gal4 DNA binding domain, a RU486-inducible truncated progesterone receptor (Δ PR) and the NF- κ B p65 transactivation domain and is under the control of a keratin promoter that restricts

expression to basal keratinocytes. The target consists of Gal4 binding sites and a minimal tata promoter upstream of the inducible transgene. RU486 treatment causes translocation of the transactivator into the nucleus where it binds the Gal4 sites upstream of the target and induces expression of the gene of interest. B. The inducible knockout system uses Cre/LoxP technology. Expression of an RU486-inducible Cre recombinase-progesterone receptor (Δ PR) fusion protein is directed by a keratin promoter. RU486 treatment causes nuclear translocation of the Cre recombinase where it excises sequences flanked by LoxP sites.

Defective TGF β Signaling in Skin SCC and HNSCC

While downregulation of TGF β RII, Smad4, and Smad2 is common in human skin SCC and HNSCC, alterations of TGF β RI and Smad3 are relatively rare [79, 80], suggesting discrete roles for these molecules in suppressing epithelial tumor formation. In contrast TGF β 1 ligand overexpression is common in human skin and HNSCC and is likely related to defective TGF β signaling in tumor epithelial cells [81, 82]. A number of mouse models have been used to illustrate how these various TGF β signaling defects promote skin and head and neck SCC development *in vivo* [20, 64, 65, 82, 83].

The Role of the TGF β 1 Ligand

While canonical TGF β 1 signaling inhibits epithelial proliferation, TGF β overexpression promotes tumorigenesis through paracrine effects on the tumor stroma leading to increased inflammation and angiogenesis [82]. This dual role of

TGF β 1 was demonstrated in mouse models with conditional epithelial TGF β 1 overexpression [66, 82, 84]. While TGF β 1 overexpression initially inhibits the growth of chemically induced skin tumors, it paradoxically increases the malignant conversion of papillomas to carcinomas [66]. Similarly, TGF β 1 overexpression early in skin carcinogenesis inhibits tumor formation, while overexpression in established tumors promoted progression to metastatic spindle cell carcinoma (SPCC) [66, 84].

Increased TGF β 1 expression is seen in ~80% of human HNSCC and correlates with more advanced disease and reduced survival [63, 82]. Non-malignant tissue adjacent to HNSCCs also frequently exhibits increased TGF β 1, suggesting that TGF β 1 overexpression is an early event in HNSCC development [82]. To study TGF β 1 overexpression, our lab developed a conditional gene switch model where TGF β 1 overexpression in oral keratinocytes can be induced by RU486 [82]. Although TGF β 1 expression at levels similar to those seen in human HNSCC did not cause tumor formation, these mice exhibit increased angiogenesis and inflammation in the stroma, which subsequently caused marked epithelial hyperplasia [82]. In this model, increased angiogenesis in the oral mucosa was mediated by the endothelial TGF β RI receptor, ALK1, and TGF β -dependent inflammation was comprised of CD4+ T cells, granulocytes, and macrophages, likely stimulated by increased interleukin-1 β and tumor necrosis factor- α [82].

TGF β 1 can be either an immunosuppressor or a pro-inflammatory cytokine [85, 86]. TGF β 1 suppresses tumor immunity by suppressing the activity of dendritic

cells and natural killer cells that mediate tumor immunity but are functionally inactivated in HNSCC [86, 87]. TGF β 1 also recruits and activates T regulatory cells that suppress tumor immune responses and are elevated in HNSCC patients [87, 88]. In contrast, TGF β 1 is important for T cell differentiation and the maturation and activation of Th17 cells [89-91] and contributes to the chronic inflammation associated with carcinogenesis by attracting both neutrophils and monocytes [92]. In summary, TGF β 1 inhibits anti-tumor immunity while activating tumor-promoting inflammation. Loss of functional TGF β signaling causes a compensatory increase in TGF β 1 production that paradoxically stimulates tumor growth by affecting the tumor stroma, increasing invasion, inflammation, and angiogenesis [20, 64, 83].

Smad4 is a Potent Tumor Suppressor in the Skin and Oral Cavity

Smad4 was initially identified as a tumor suppressor in the pancreas [93] and was later characterized as a key mediator of TGF β signaling [94]. Since Smad4 mediates both TGF β and BMP signaling, Smad4 loss abrogates signaling of both pathways. Smad4 loss or inactivation is common in many malignancies including skin SCC and HNSCC [95, 96]. In skin SCC Smad4 is lost at the mRNA level in approximately 85% of poorly differentiated tumors, and loss of heterozygosity (LOH) at the Smad4 locus is seen in around 60% of poorly differentiated tumors [95]. Loss of chromosome 18q, a region encoding both Smad2 and Smad4, is common in HNSCC [97-100] and LOH at the Smad4 locus also occurs in ~50% of HNSCC [98, 100]. Although loss of 18q is associated with reduced survival in HNSCC [101], it is unknown whether this is related strictly to Smad4 loss, the simultaneous

loss of both Smad2 and Smad4, or loss of other genes contained within this region. Somatic inactivation of Smad4 has been reported in 22-40% of HNSCCs [102, 103] and while point mutations are relatively infrequent [98], loss of a single Smad4 allele occurs in 30%-50% of HNSCC [64, 98, 100]. In cases where a single copy of Smad4 is lost, additional mutation from another allele is rare in HNSCC [98]. Studies using Smad4 knockout mouse models have shown that loss of a single copy of the Smad4 gene confers 50% of reduction of the Smad4 mRNA and protein [104, 105], and this reduction is sufficient to increase skin and HNSCC susceptibility [64]. We examined Smad4 expression in human HNSCC, and found that 86% of tumors and 67% of adjacent non-malignant mucosa had reduced Smad4 expression suggesting that Smad4 loss is an early event in HNSCC development [64]. Although we found LOH at the Smad4 locus in 33% of HNSCC, the higher frequency of Smad4 loss at the mRNA and protein levels suggests that other epigenetic, posttranscriptional or posttranslational modifications contribute to reduced Smad4 expression in HNSCC [64].

Since Smad4 loss or inactivation is common in tumorigenesis, a number of mouse models have been created to assess the role of Smad4. In combination with other oncogenic alterations, Smad4 deletion causes tumors in the colon [106, 107], pancreas [108, 109], forestomach [110] and liver [111] indicating that Smad4 loss can promote tumor progression. In addition, Smad4 deletion causes spontaneous tumors in the stomach [112], skin [67, 68] and mammary gland [113], demonstrating that Smad4 can initiate tumor formation in certain tissues.

Epidermal Smad4 deletion blocks growth inhibition by TGF β , leading first to hyperproliferation and subsequently to skin SCC [67, 68]. We developed a conditional mouse model to delete Smad4 in the oral keratinocytes and found that these mice developed HNSCC starting at 29 weeks [64]. These tumors resembled human HNSCC histologically and also occasionally metastasized to regional lymph nodes [64].

Ras Mutation Cooperates with Smad4 in Tumor Formation

The Ras family of genes, encodes small GTPases that act as molecular switches in transducing signals to the nucleus. The Ras proteins can induce a number of downstream pathways including the oncogenic PI3K, and mitogenic Raf/MEK/ERK pathways [114]. Ras mutations are some of the most common genetic aberrations in human cancer. Kras mutations are seen in approximately 75-100% of pancreatic cancers, 50% of colorectal cancers and 50% of lung adenocarcinomas [114], and activation of Ras is frequently associated with poor prognosis and therapeutic resistance [115, 116]. Inducible mouse models of Kras activation have shown that the constitutively active Kras G12D protein is a potent activator of lung adenocarcinoma [75]. Further studies with these mice have shown that Kras activation in the oral cavity leads to the production of benign epithelial papillomas [117]. These studies show that Kras may be an important regulator of tumor initiation.

A number of studies have shown that the combination of activating Kras mutations with alterations in TGF β signaling can lead to aggressive tumor formation. When combined with Smad4 deletion, activating Kras mutations in the pancreas lead to invasive ductal adenocarcinoma [108, 118]. In the oral cavity, TGF β RII deletion is insufficient to form SCC, however, addition of Ras mutation, either by crossing the mice with the LSL-Kras^{G12D} mice, or by HRas mutation generated by treatment with DMBA, induces metastatic tumor formation [20]. While Smad4 deletion was sufficient for generating HNSCC in mice, we investigated whether spontaneous Ras activation was responsible for initiating tumor formation after Smad4 deletion. While only a small number of tumors exhibited Ras mutations, the remaining tumors had increased Ras protein levels [64], suggesting that Ras activation may also function as an initiating event after Smad4 deletion.

Smad4 Loss Increases Genomic Instability by Inhibiting DNA Repair.

Since cancers are the result of an accumulation of oncogenic changes we were surprised by spontaneous HNSCC formation after Smad4 deletion and hypothesized that Smad4 might affect genetic stability and facilitate acquisition of additional genetic alterations. Indeed, Smad4 knockout tumors had increased centrosome numbers and reduced expression of several Brca/Fanc family members responsible for double strand DNA repair [64]. We subsequently also demonstrated Smad4 regulated expression of Fanc/Brca genes [64]. This was particularly interesting because germline mutations in the Fanc/Brca pathway lead to Fanconi anemia (FA) in humans, a syndrome characterized by bone marrow failure and

markedly increased susceptibility to HNSCC [119]. Other studies have shown down-regulation of Fanc/Brca genes in sporadic HNSCC [120-123] and mice with epithelial specific deletion of Brca1 develop oral SCCs [124], suggesting that Smad4 loss promotes HNSCC formation by deregulating DNA repair. While less is known about Smad4 regulation of genomic integrity in skin, recent studies in the Wang lab have shown that mice with Smad4 loss in the epidermis are more susceptible to UV induced skin carcinogenesis and that a number of additional DNA damage repair genes show decreased expression in the skin of these mice (Wang lab unpublished data).

Smad4 Loss Increases Inflammation

Inflammation associated with Smad4 loss is important for tumorigenesis. Smad4 deficient intestinal cells recruit immature myeloid cells expressing MMP2, MMP9 and the chemokine receptor CCR1 to the tumor invasion front [106] and Smad4 deletion in T cells causes intestinal tumors, indicating that Smad4 loss in both epithelial and inflammatory cells can promote cancer development [125]. Smad4 loss in the oral mucosa causes leukocyte infiltration of macrophages, granulocytes, T lymphocytes, and proinflammatory Th17 cells prior to tumor formation and this is likely mediated by increased TGF β expression [64]. Indeed, these mice exhibit significantly increased levels of TGF β ligand in both the HNSCC and the adjacent mucosa that occurs within 1 week of Smad4 deletion [64]. Abrogation of TGF β signaling and increased TGF β elaboration can increase tumor invasion and migration though increases in BMP signaling through Smads 1 and 5

[126, 127]. We found that Smad4 knockout mice also exhibited increased Smads 1/5/8 [64], suggesting that BMP signaling may contribute to the increased inflammation and a tumor-promoting microenvironment environment.

These studies have shown the importance of Smad4 in maintaining epithelial homeostasis and the contribution of Smad4 loss to epithelial tumor formation. However, since these mouse models result in Smad4 deletion in the entire basal keratinocyte layer, the question of which population of cells receiving the mutation is responsible for initiating tumor formation remains.

1.3. Tumor-initiating Cells

Overview of Tumor-initiating Cells

Despite great strides in understanding aberrations in cancer cells at the molecular level and the increasing sensitivity with which drugs can be specifically targeted to these aberrant molecules, treatment failure occurs routinely. Thus, there is concern that the key tumor-initiating and propagating cells are not appropriately targeted by cancer therapies. The cancer stem cell hypothesis provides a possible explanation. This hypothesis states that distinct population of cells within a tumor have the ability to initiate tumor formation and drive tumor progression, metastasis and recurrence [128]. These tumor-initiating cells (TICs) display characteristics of normal adult stem cells such as the capability for self-renewal and differentiation [128]. They also are thought to be resistant to conventional therapy through mechanisms including drug efflux and resistance to

DNA damage [129]. The source of cancer stem cells is largely unknown and hypothesized to be either adult tissue stem cells that develop oncogenic properties leading to tumor formation, or tumorigenic progenitor cells that acquire the stem cell property of self-renewal [130]. These observations thereby suggest that deregulation of pathways that regulate stem cell behavior, i.e. maintenance of self-renewal or commitment to differentiation, is a key event in initiation of tumor formation and maintenance.

Sox2 Regulates Stem Cell Behavior

An example of a gene that may promote stem-like behavior in tumor cells is the SRY (Sex determining region-Y)-box 2 or Sox2 gene. This gene is an intronless transcription factor highly expressed in embryonic stem cells, and certain tissue stem cells [131]. It is predicted to regulate the expression of several hundred genes including the activation of pluripotency genes and down regulation of lineage specific genes [131]. Sox2 is such an important stem cell factor that it is one of 4 genes needed to reprogram fibroblasts in to induced pluripotent stem (iPS) cells [132]. Because of this powerful role in the regulation of normal tissue stem cells, it is likely that Sox2 plays an important role in the regulation and perhaps induction of tumor-initiating cells.

Identification of Tumor-initiating Cells

Tumor-initiating cells were first identified in human acute myeloid leukemia, where it was shown that a small subset of about 0.1-1% of the total population of

leukemic cells could initiate leukemia when xenografted in to immunodeficient mice. The resulting leukemia displayed the same tumor heterogeneity as the original disease [133]. Interestingly, the tumor-initiating cells expressed a number of cell surface markers associated with normal hematopoietic stem cells [133]. Engraftment of tumor cells in nude mice has now become the gold standard for the identification of TICs. Based on the AACR consensus definition, the TIC containing population should be able to reestablish the tumor heterogeneity seen in the original tumor and the TICs must exhibit self-renewal through serial passaging [134].

Following the studies of hematopoietic TICs, markers of normal tissue stem cells have been used for the isolation of solid tumor TICs. This approach has been problematic in many solid tumors due to a lack of information about these normal stem cell markers. Additionally, many known stem cell markers are not found exclusively on the stem cell population, making it difficult to obtain a pure population of stem cells. One of the first solid tumor TIC populations was identified in breast cancer. Al-Hajj *et al* isolated CD24^{-/low}/CD44⁺ cell populations from metastatic pleural effusions and from primary invasive breast tumor and showed that as few as 100 cells from this enriched population were capable of forming tumors in immunocompromised mice. [135]. CD44 expression has subsequently been used to isolate tumorigenic cell populations in many other solid tumors including head and neck, prostate, colon and pancreatic carcinomas [129, 130]. Other frequently used characteristics for the enrichment of TICs include high

expression of CD24 and Aldehyde Dehydrogenase 1 (ALDH1), as well as exclusion of Hoechst dye (dye excluding “side population” cells or SP) [130].

Epithelial Stem Cells and Tumor-initiating Cells in Skin and Head and Neck Squamous Cell Carcinoma

To date much of the work on identifying oral TICs has been performed using oral cancer cell lines. While the putative stem cell populations from these cell lines display many stem cell markers, such as CD44, CD133 and CD29 expression, as well as Hoechst dye exclusion [136] and glucose related protein 78 (GRP78) [137], these cell lines grow in an artificial environment devoid of an appropriate niche that may affect cell surface marker expression and proliferative capacity. The first study to identify TICs in primary human HNSCC came from Prince *et. al.*, who used the CD44^{high} cell population to successfully xenograft mice [138]. One problem with this work is that as many as 42% of the tumor cells expressed CD44, indicating that this population may be relatively impure. Subsequent studies have identified ALDH1 as a marker of HNSCC TICs either alone [139], or in combination with CD44⁺/CD24⁻ [140], greatly decreasing the number of cells needed to form tumors in immunocompromised mice. More studies are needed to identify TIC markers in HNSCC.

An analogous system to the head and neck epithelia is the skin. While these tissues are very different in many ways, they do possess common features. Normal epithelial stem cells have been well studied, and therefore a number of stem cell

markers are known. Other advantages to using skin as a model of SCC are the relative ease with which skin tumors can be produced in mouse models and the ability to generate much larger tumors than in the head and neck. The skin consists of two major groups of stem cells, the interfollicular epidermal stem cells and the hair follicle bulge stem cells. The interfollicular stem cells are thought to be the stem cells responsible for normal homeostasis of the skin, while hair follicle bulge stem cells can give rise to all layers of the hair follicle, during the hair follicle cycle. However, during times of injury, the hair follicle bulge stem cells can be recruited for repair of the epidermis [141]. The hair follicle bulge stem cells were first identified in label retaining assays based on their relative quiescence compared to more differentiated progenitor cells [142]. Based on these studies, a number of genes and cell surface markers have been identified as preferentially expressed in the hair follicle bulge, notably Keratin 15 [143] and CD34 [144]. Hair follicle bulge stem cells have been successfully isolated using combinations of the markers such as, $\alpha 6$ -integrin, $(CD49f)^{high}/CD71^{low}$ [145]; $CD34^{high}/\alpha 6$ -integrin high [146]; and the Hoechst dye excluding side population [147]. Based on the success of using normal hematopoietic stem cell markers to sort leukemic TICs, these stem cell markers represent good candidates for sorting skin SCC TICs.

Identification of the TIC populations in solid tumors has helped elucidate the process by which tumors are generated and provides a mechanism by which cellular heterogeneity is generated. In addition to *de novo* tumor formation, these TICs may

play a role in a number of other stages in tumor progression. Tumor recurrence and metastasis are two such processes that require a tumor-initiating step.

1.4. Metastasis and the Epithelial-to-Mesenchymal Transition

Overview of metastasis

Tumor metastasis is a complex, multistep process marking the final step in tumor progression and is the major factor influencing patient mortality associated with solid tumors [148]. In order for a tumor cell to metastasize it must detach itself from the primary tumor bulk and migrate towards blood vessels and lymphatics. This step requires loss of adhesion molecules, such as E-cadherin, binding the epithelial cells together. The cells then must be able to invade by traversing the basement membrane and intravasate in to the vasculature. The tumor microenvironment facilitates this process through increased angiogenesis as well as through mechanisms such as inflammation. Once in circulation the tumor cells may find their way to premetastatic niches, such as those in the bone marrow, or may form micrometastases that can lie dormant for years. Finally, the tumor cells must be able to initiate new tumor formation at the distant metastatic site [149]. One process that contributes to metastasis is an epithelial-to-mesenchymal transition, in which the tumor cell becomes more motile and invasive.

Epithelial-to-Mesenchymal Transition

EMT occurs when epithelial tumor cells lose epithelial characteristics, such as cell-cell adhesion, apical-basal polarity, and gain mesenchymal characteristics

such as migration, and invasion [150, 151] (Figure 4). To date, three major families of transcription factors have been shown to be involved in the process of EMT, the Snail, ZEB and bHLH families. The Snail family is a group of transcriptional repressors that acts by decreasing the expression of cell adhesion molecules. Notably, Snail1 and Snail2 both inhibit the expression of the adhesion molecules, E-cadherin and plakoglobin. Additionally, ectopic expression of Snail is sufficient to induce an EMT phenotype in many cell lines [152]. The ZEB family of transcription factors also acts to repress the expression of epithelial markers such as E-cadherin and is capable of activating mesenchymal markers, such as vimentin [153]. Finally, the bHLH family of transcription factors, includes Twist and Id proteins, all of which induce EMT. As an example, the Twist proteins, Twist 1 and Twist 2, can inhibit E-cadherin, occludin and claudin expression while increasing the expression of the mesenchymal markers vimentin and N-cadherin [154, 155].

TGF β signaling is the best characterized pathway involved in the regulation EMT. TGF β can induce EMT in Smad-dependent and -independent mechanisms. A number of studies have shown that Smad4 is required for TGF β induced EMT, and that inhibition of Smad4 leads to the maintenance of E-cadherin expression [156, 157]. Loss of Smad2, on the other hand, promotes EMT through increased binding of Smads 3/4 to the Snail promoter [95]. Smad independent TGF β -induced EMT occurs through activation of non-Smad signaling responses of TGF β signaling such as activation of Erk MAP kinases and the PI3K/AKT pathway.

Acquisition of Stem Cell Traits During Epithelial-to-Mesenchymal Transition

Recent studies have now shown a link between EMT and the acquisition of stem cell traits. Mani *et. al.* first showed this link by forcing EMT in breast cancer cell lines through treatment of the cells with TGF β or by ectopic expression of Twist and Snail [158]. This induced EMT resulted in an increase in the CD44^{high}, CD24^{low} cell population, which is a well-described breast TIC population [135]. An additional study has shown the cooperation of Bmi1, a stem cell associated gene, and Twist in the induction of EMT in HNSCC cell lines [159]. This study also showed an amplification of the CD44⁺, ALDH1⁺ and SP tumor-initiating cell populations, further providing evidence of a transition to a more stem like state after EMT. These stem cell characteristics likely contribute to metastasis in a number of ways including cell survival and tumor initiation (Figure 4).

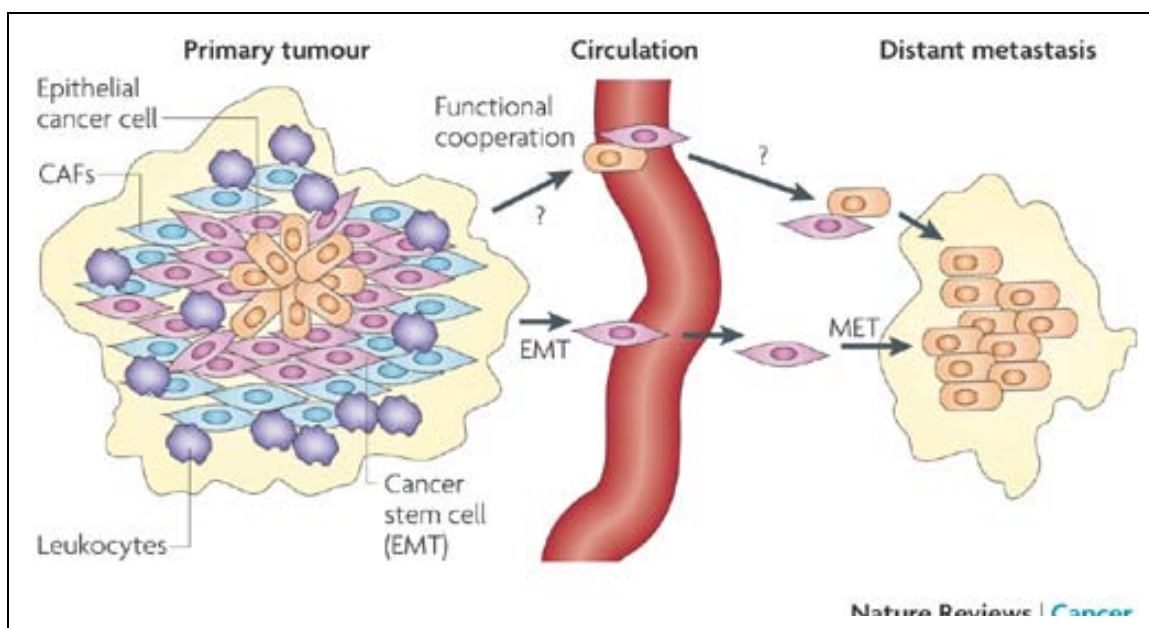


Figure 4. EMT and the acquisition of stem cell traits during cancer metastasis.

Tumor metastasis depends on the plasticity of the tumor cells. Epithelial-to-mesenchymal transition (EMT) may be induced by interactions of the tumor epithelial cells with the tumor stroma including carcinoma-associated fibroblasts (CAFs) and leukocytes. The acquisition of stem-like traits accompanies the EMT and may promote cell survival and initiation of metastasis at a distant site. Upon arrival at the metastatic site, the tumor cells may undergo a mesenchymal-to-epithelial transition (MET). Adapted by permission from Macmillan Publishers Ltd: Nature Reviews Cancer, 2009. 9(4): p. 265-73, Copyright 2009 [151].

1.5. ABC Transporters: Tumor-initiating Cell-Associated Regulators of Chemoresistance and Metastasis

Overview of the ABC Transporter Superfamily

Two of the major causes of treatment failure in cancer are chemoresistance and metastasis. A major cause of chemoresistance in tumor cells is increased expression of members of the ATP binding cassette (ABC) transporter superfamily, which actively transport chemotherapeutic agents from the tumor cells. The normal function of these transporters is the movement of a wide range of substrates, such as lipids and metabolic products, across cell membranes [160]. The ABC transporter superfamily consists of approximately 48 genes which are expressed in different tissues and have a variety of normal functions [161]. The best-characterized members of this family are, ABCB1 (MDR1/p-glycoprotein), ABCC1 (MRP1) and ABCG2 (BCRP), and have all been shown to play a role in chemoresistance. Mouse models have shown decreased intestinal tumor formation in Mdr1 (Abcb1a/b) deficient APC^{Min/+} mice indicating that Mdr1 expression may also play a role in tumor formation [162, 163].

ABC transporters are markers of tumor-initiating cells

ABC transporters were first identified as markers of stem cells by their co-expression on CD34⁺ hematopoietic stem cells. Utilizing the ability of these transporters to actively pump dyes such as Hoechst 33342 out of the cells, it was possible to flow sort a highly enriched hematopoietic stem cell population [164, 165]. This Hoechst dye excluding side population (SP) was later shown to select for

stem cell populations from other tissues, as well as TICs from solid tumors [166-168]. Animal models deficient in ABC transporters show an increased sensitivity to chemotherapeutic drugs; however, these mice did have normal stem cell function [169, 170], indicating that the ABC transporters are not essential for the maintenance of the stem cell characteristics. Overexpression of the ABC transporters may, however, contribute to the resistance of TICs to conventional therapy. This resistance may not only occur through efflux of chemotherapeutic agents. A number of reports have shown that the ABC transporters promote cell survival through anti-apoptotic mechanisms. One such study showed that the onset of apoptosis induced by colchicine or serum starvation in ABCB1 overexpressing cells is increased compared to control cells [171]. While, other studies have shown that MDR1 (ABCB1) protects cells from caspase-dependent, but not caspase-independent apoptosis [172, 173].

MDR1 (ABCB1) Plays a Role in Tumor Migration, Invasion and Metastasis

Expression of the ABC transporters in cancer is associated with malignant progression and tumor differentiation [160]. In colorectal carcinoma, expression levels of MDR1 (ABCB1) are increased at the invading edge of tumors. Further, tumors expressing MDR1, showed a greater incidence of vessel invasion and increased lymph node metastasis [174]. A number of *in vitro* studies have demonstrated the role of MDR1 in the regulation of invasion and migration of tumor cells. In breast cancer cell lines, siRNA knockdown of ABCB1, inhibited both invasion and migration in transwell assays [175]. Similar results were also seen in

chemoresistant melanoma cell lines [176]. The mechanism by which MDR1 regulated tumor cell migration and invasion appears to involve an interaction with the CD44 cell membrane receptor. CD44 is a well-described TIC cell marker that has been implicated in a number of cell functions such as cell adhesion, motility and metastasis [177], and in a number of multidrug resistant cell lines, including breast, oral and ovarian carcinoma lines, CD44 and MDR1 are co-expressed on the cell membrane [175]. The best studied mechanisms of ABCB1 transcriptional regulation involve transactivation by the T-Cell Factor 4/ β -Cateinin complex [178], and activation by the NF κ B pathway [179]. CD44 participates in the transcriptional regulation by these two pathways through interaction with p300 (acetyltransferase) and SIRT1 (deacetylase). CD44 upregulation of p300 leads to the acetylation of β -catenin and NF κ B, thereby activating these pathways and increasing MDR1 expression. Interaction of SIRT1 and p300, inhibits the acetyltransferase activity of p300 and subsequently inhibits MDR1 expression [180].

1.6. microRNAs: Small RNAs Playing a Large Role in Cancer and Metastasis

MicroRNA Overview

MicroRNAs (miRNAs) are emerging as important regulators of stem cells and tumorigenesis. These small regulatory RNAs are 20-24 nucleotide long RNAs that regulate gene expression post-transcriptionally, either by translational inhibition or exonucleolytic mRNA decay. Primary (pri)-miRNA genes often lie in introns and are transcribed by RNA polymerase II and occasionally RNA polymerase III. This stem and loop pri-miRNA is cleaved by a complex containing the RNase III, Drosha,

forming the precursor (pre)-miRNA. Another RNase III, Dicer, then further modifies the pre-miRNA to produce a 22 base-pair duplex RNA. One of the strands of this duplex is subsequently loaded in to RNA-induced silencing complexes (RISCs) and acts to suppress gene expression by binding to the mRNA and causing translational inhibition or mRNA degradation [181].

miRNAs in Cancer and Metastasis

MicroRNAs were first identified as tumor suppressors in B-cell chronic lymphocytic leukemia (CLL). This form of leukemia has frequent deletions at 13q14, and it was initially assumed that there must be a tumor suppressor gene in this region. It was later discovered that two miRNAs, miR-15a and miR-16-1, lie in an intron of a non-coding RNA in this region [182], and further studies identified the anti-apoptotic gene, BCL2, as a target of these miRNA [183]. Since then a number of miRNAs have been identified as both tumor suppressors and oncogenes. These miRNAs often interact with known oncogenes and tumor suppressors in affecting a tumorigenic response. For example, the let-7 family of miRNAs has been shown to regulate the expression of Ras, and is down regulated in human lung tumors with poor prognosis [184]. Moreover, when compared to normal lung tissue, squamous cell carcinoma of the lung shows inverse expression of Ras and let-7 [185].

The TGF β signaling pathway plays an important role in the regulation of miRNAs both at the transcriptional and processing level in cancer. At the transcriptional level, TGF β signaling regulates expression of the oncomiR, miR-155,

which regulates metastasis through inhibition of RhoA, a mediator of cell junctions [186]. TGF β and BMP signaling promotes processing of certain miRNAs through binding of the Smad proteins to components of the Drosha microprocessor complex [187]. Two oncogenic miRNAs regulated in this manner, are miR-21 and miR-199a. miR-21 is one of the most commonly overexpressed miRNAs in cancer cells and has been shown to target a number of tumor suppressors including PTEN [188], PDCD4 [189], and TGF β RII [190]. miR-199a targets the inhibitor of nuclear factor κ -B (NF κ B) signaling, inhibitor of nuclear factor kappa-B kinase subunit beta (IKK- β) [191]. This TGF β mediated regulation of miRNA processing occurs in a Smad4 independent manner. Therefore, the increased TGF β signaling seen upon loss of Smad4 in the skin and head and neck epithelia may lead to increased expression of these miRNAs contributing to tumor formation.

In addition to promoting tumor formation, a number of miRNAs have been shown to play important roles in tumor progression and metastasis (Figure 5). Studies of EMT and metastasis, have consistently shown a decrease in the miR-200 family in mesenchymal cells after EMT [192]. The miR-200 family consists of two clusters of miRNAs, miR-200b~200a~429 and miR-200c, that target the transcriptional repressors of E-cadherin, ZEB1 and ZEB2 [192]. Forced expression of miR-200 can inhibit TGF β mediated EMT [192, 193], while knockdown of miR-200 can induce an EMT [192, 194]. Other miRNAs are overexpressed during EMT and metastasis. For example, Twist activates the expression of miR-10b leading to increased invasion and increased metastasis [195]. Additionally, increased levels of

miR-9 seen in metastatic breast cancer [196] and colon cancer [197], can target E-cadherin, leading to EMT in a cell specific manner [196].

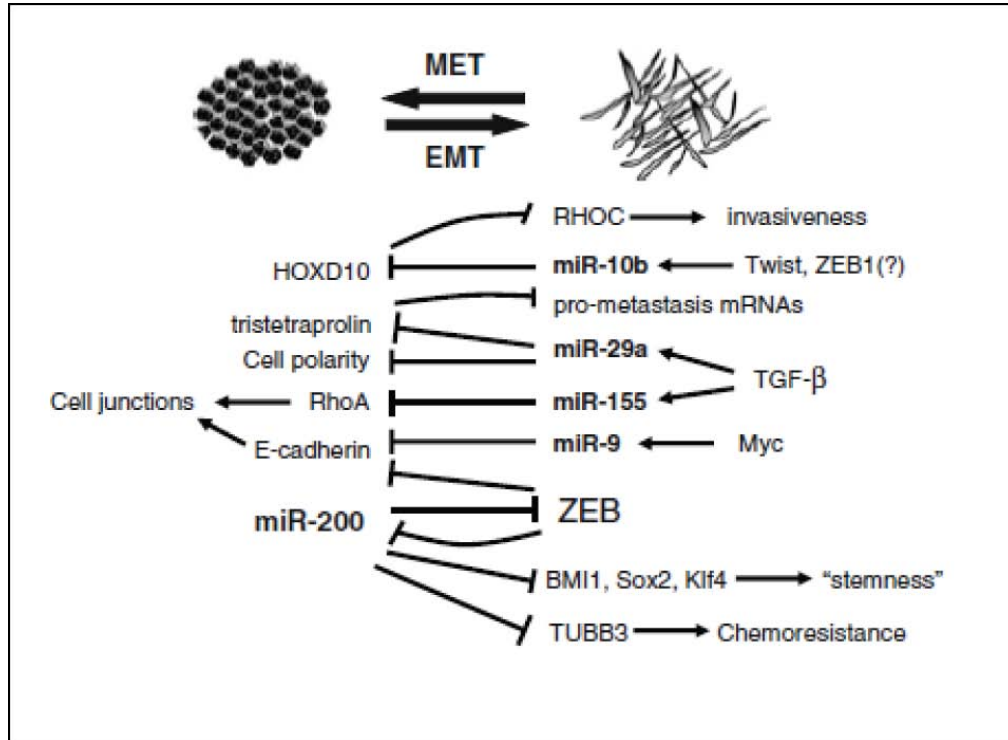


Figure 5. Overview of miRNAs involved in EMT. miRNAs contribute to metastasis either directly or indirectly by targeting cell junctions, stem cell genes and chemoresistance genes. Figure adapted with kind permission from Springer Science+Business Media: *Journal of Mammary Gland Biology and Neoplasia, microRNAs and EMT in Mammary Cells and Breast Cancer, Vol. 15(2):213-23, 2010, Wright J.A., Richer, J.K., and Goodall, J.G., figure 1, copyright 2010.*

miRNA Regulation of Epithelial Stem Cells and Tumor-initiating Cells

The first studies demonstrating the importance of miRNAs in stem cell regulation were carried out using Dicer deficient animal models. Loss of Dicer results in global defects in miRNA processing and severe defects in embryonic stem (ES) cell expansion and differentiation [198, 199]. Conditional deletion of Dicer in the epidermis, results in underdeveloped and hypoproliferative hair follicles and a loss of hair follicle bulge stem cell markers such as keratin 15 and CD34 [200]. These global studies demonstrate the importance of miRNAs in the maintenance of the stem cell pool in the epidermis. More specifically, miR-203 directly regulates the epithelial stem cells by repressing p63 and promoting stem cell differentiation [201, 202]. A number of miRNAs are expressed in unique compartments in the skin, for example, miR199a is highly expressed in the hair follicle, but not expressed in the epidermis. Conversely, the miR-200 family is expressed in the epidermis, but absent in the hair follicle [203]. This spatial expression of miRNAs in the different compartments of the skin indicates that the miRNAs have distinct roles in the regulation of the epithelium and its stem cells.

Since miRNAs play important roles in both stem cells and cancer it is understandable that miRNAs would be important regulators of tumor-initiating cells. Tumor-initiating cells have been shown to share similar miRNA expression patterns with normal tissue stem cells, for example, in breast cancer, decreased expression of the miR-200 family of miRNAs is seen in both normal and breast cancer stem cell populations [204]. Moreover, major regulators of stem cell self

renewal, Bmi1, Sox2 and Klf4, are inhibited by miR-200 [204], demonstrating the similar regulation of stem cell characteristics in normal tissue stem cells and tumor-initiating cells. The transcriptional activator of EMT, ZEB1, also acts to inhibit expression of miR-200 and miR-203, thereby further promoting a stem like state during EMT [205]. These studies support a clear link between miRNAs, stem cells and metastasis. However, further studies are needed to identify other miRNAs that regulate these processes, in order to better understand the mechanisms of metastasis and identify potential therapeutic targets.

Emergence of miR-9 as an Important Regulator of Cancer Progression

Recent studies have identified miR-9 to be an important regulator of both EMT and metastasis. Ma *et. al.* found that miR-9 targets the 3'UTR of E-cadherin, and in a context specific manner, can induce an EMT phenotype in breast cancer cell lines [196]. Additionally, as a result of miR-9 mediated degradation of E-cadherin, increased β -catenin signaling activity resulted in promoted VEGF expression and angiogenesis [196]. Not surprisingly, when overexpressed in non-metastatic breast cancer cell lines, miR-9 can promote lung metastasis in grafted tumors [196]. Interestingly, miR-9 is the only miRNA predicted to target E-cadherin, and as such plays an important role in the regulation of this adhesion molecule in the epithelium. Other confirmed targets of miR-9 include, SIRT1 [206], NF κ B1 [207], CDX2 [208] and FOXO1 [209]. The mature miR-9 miRNA is generated from three distinct transcripts, miR-9-1 on chromosome 1, miR-9-2 on chromosome 5, and miR-9-1 on chromosome 15 in humans. In mice the miR-9-1 through -3 transcripts

lie on chromosomes, 3, 13, and 7 respectively. miR-9 is highly expressed in neurons during differentiation and has been shown to be transcriptionally regulated by REST and CREB [210]. More recently Ma *et. al.* found that miR-9 expression is induced by direct binding of myc to the promoter of miR-9-3 [196]. Interestingly, miR-9 is also highly methylated on miR-9-1 and miR-9-3 in certain cancers resulting in decreased miR-9 expression [211, 212].

Currently, the role of miR-9 in human tumor growth and metastasis is controversial. To date, the *in vitro* studies of miR-9 in cancer cell lines points towards a pro-metastatic role through targeting E-cadherin, promoting angiogenesis and inducing metastasis in animal models [196]. On the other hand, studies of miR-9 in human tumors and the relationship of miR-9 expression with metastasis are divided. For example, methylation studies in clear cell renal cell carcinoma have shown that miR-9 methylation is associated with increased lymph node metastasis [211], while a recent study showed that increased miR-9 expression in the primary tumors was associated with distant metastasis in colorectal cancer [197]. Further studies are needed in other tumor types to better understand the role of miR-9 in tumor development and progression.

miRNAs in the Detection and Treatment of Cancer

miRNAs are attractive biomarkers in the detection of cancer because of their tissue specificity and relative resistance to degradation. Global studies in human cancers have found that miRNAs more accurately classify poorly differentiated

tumors than mRNA signatures, and that relatively few miRNAs are needed for this classification [213]. Based on these results a number of studies are now attempting to use miRNA signatures to identify cancer and predict outcomes [214]. For example, in HNSCC, lower levels of let-7d and miR-205 are associated with locoregional recurrence and poor outcome [215]. Since they target a number of genes and tend to be relatively tissue specific, manipulation of miRNAs is becoming an attractive option in the development of cancer therapeutics. Recent studies have shown the effective use of cholesterol conjugated anti-miRNAs in the inhibition of miRNAs in animal models [216], however, as with siRNA and gene targeting therapies, safe and effective methods of delivery still need to be developed.

1.7 MicroRNA Regulation of Tumor-Initiating Cells in Metastasis and Chemoresistance

Current therapeutic modalities for the treatment of epithelial tumors are often effective in prolonging patient survival, however, metastasis and local recurrence after treatment often occur despite this therapy resulting in patient mortality. Increasing evidence is pointing towards TICs as the mediators of therapeutic failure [128]. These pluripotent stem-like cells are thought to have the ability to initiate tumors *de novo* and give rise to tumor heterogeneity, and as such are thought to be responsible for tumor recurrence and metastasis, two processes that requiring these tumor-initiating capabilities [128]. TICs are believed to possess a number of properties that allow them to evade current therapeutic modalities such as chemotherapeutic drug efflux and resistance to DNA damage from

chemotherapeutic drugs and radiation [129]. Therefore, identification of the genetic pathways that are responsible for maintaining TICs will aid in the development of therapeutic modalities that can specifically target this resistant population and prevent tumor progression.

To start to identify some of these pathways and to better understand the origin of TICs, this dissertation work will make use of mouse models with conditional deletion of Smad4 in the epithelium. Previous work in the Wang lab has shown the dramatic role of Smad4 loss in the development of both skin SCC and HNSCC [64, 217]. In this work we used conditional mouse models to delete Smad4 and activate Kras in the hair follicle bulge stem cells to explore the **hypothesis that oncogenic mutations targeted to the epithelial stem cell population can give rise to tumors consisting of multiple hair follicle lineage cell types**, and using these tumors we further explore the **hypothesis that miRNAs and stem cell genes regulate functions of TICs including tumor recurrence, metastasis and chemoresistance**. The experimental plan followed during this dissertation work was based on the following specific aims:

Aim 1. Demonstrate that oncogenic mutations in the murine hair follicle stem cell pool can generate tumors consisting of cell types from multiple hair follicle lineages.

Aim 2. Demonstrate that the side population and SP⁻/CD34⁺/CD49f⁺ populations are tumor-initiating.

Aim 3. Identify miRNA profiles of TICs from metastatic tumors and the potential function of these miRNAs in tumor initiation, metastasis and chemoresistance.

Aim 4. Identify the role of stem cell genes in the TIC populations during tumor-initiation, metastasis and chemoresistance.

The work in this dissertation shows that deletion of Smad4 and activation of Kras in the mouse hair follicle stem cells leads to tumors consisting of multiple hair follicle cell types (K15.Kras^{G12D}.Smad4^{-/-} tumors). We further identify the SP and the SP⁻/CD34⁺/CD49f⁺ cell populations to be TICs in these tumors. Passaging (xenografting) the K15.Kras^{G12D}.Smad4^{-/-} tumors generates faster growing and more metastatic tumors. By miRNA profiling, we identify miR-9 as a miRNA overexpressed in the more metastatic passaged tumor SP cells, and show that this miRNA increases the invasive properties of tumor cells and my increase chemoresistance by indirectly promoting an increase in the expression of the ABC transporter Abcb1a. Finally, we show that the stem cell gene, Sox2, is increased in the SP⁻/CD34⁺/CD49f⁺ population from the more aggressive passaged tumors, and that increased Sox2 expression inhibits tumor cell invasion and migration. Taken together, this work begins to identify some of the genes and miRNAs involved in the regulation of tumor-initiating cells, and their function in tumor progression.

CHAPTER TWO

MICRORNA-9 REGULATES TUMOR-INITIATING CELL MIGRATION, INVASION AND CHEMORESISTANCE IN MURINE SKIN SQUAMOUS CELL CARCINOMA

MATERIALS AND METHODS

2.1 Mouse Strains

All animal experiments were conducted using protocols approved by the IACUC at Oregon Health and Science University and University of Colorado Health Sciences. All transgenic animals are on the C57Bl/6 background, and grafting and passaging experiments were conducted in athymic nude mice. *In vivo* tumor growth and metastasis assays were conducted in wild type C57Bl/6 and athymic nude mice.

DNA Extraction and Genotyping PCR

The transgenic mice were genotyped at 3 weeks of age. Tail snips were digested in using proteinase K and DNA precipitated using ethanol. Genotyping was conducted by PCR using primers that can identify the presence of the loxP sites in the transgene and thereby differentiate between the wild type and transgenic alleles (see appendix C for genotyping primers).

2.2 Targeting mutations to hair follicle bulge stem cells

The tissue specific, inducible transgenic mouse models consist of three different transgenes; an inducible Cre recombinase, an activating Kras^{G12D} mutation and a Smad4 deletion. The K15.CrePR1 transgene allows the Keratin 15 promoter to target Cre recombinase expression to the hair follicle bulge, the site of a subset of epithelial stem cells [218]. The CrePR1 fusion protein is activated by topical activation of the progesterone antagonist RU486, which binds to CrePR1 and

translocates the protein in to the nucleus. Once in the nucleus, the Cre recombinase functions to delete DNA flanked by loxP sites (floxed). The Smad4 transgene has a floxed exon 8; once exon 8 is recombined and deleted the resulting transcript is unstable and is rapidly degraded, leading to Smad4 deletion [219]. The constitutively active Kras^{G12D} mutation (LSL-Kras^{G12D}) is induced by removal of a floxed-stop codon upstream of exon 1 [220]. In order to induce the mutations, RU486 (100µl of 0.2µg/µl in ethanol) was applied to the shaved back skin of 4-week old transgenic mice for 5 consecutive days.

Mice were evaluated at least once per week for tumor development; once tumors became visible mice were monitored daily. Tumor-bearing mice were euthanized once the tumors reached 2cm in diameter, or if the mice were exhibiting signs of deteriorating health (e.g., huddled posture, difficulty breathing, vocalization, hypothermia, or ≥20% weight loss). Necropsy was performed on each euthanized mouse to identify primary tumors and lung metastasis. Tumor tissue was collected for histology, tumor cell isolation and passaging in to athymic nude mice.

Characterization of Epithelial-Specific Kras^{G12D} Activation and Smad4 Knockout Mice

To confirm the activation of the Kras^{G12D} allele and deletion of Smad4 in the epithelia of the transgenic mice, recombination PCRs were performed on the back skin of RU486 treated K15.CrePR1/LSL-Kras^{G12D}/Smad4^{f/f} mice and controls (see appendix C for recombination PCR primers).

2.3 Histology and Immunostaining

Paraffin Sections: Dissected tumors and transgenic epithelia were fixed in 10% neutral-buffered formalin overnight, embedded in paraffin and sectioned to 6 μ m thickness.

Frozen Sections: Dissected tumors and epithelia were embedded in Optimal Cutting Temperature (OCT, Fisher Scientific) and quickly frozen on dry ice. Frozen tissues were sectioned to 6 μ m thickness using a cryotome at the UC Denver Histology core.

Analysis of Tumor Histology Types

Tumor histology was classified by three independent observers into well-, moderately-, poorly-differentiated and spindle cell carcinoma (SPCC) based on basal cell hyperplasia, increased number of mitoses, abnormal mitoses, nuclear hyperchromatism, and increased nuclear/cytoplasmic ratio as previously described [221, 222]. SPCCs were characterized by a complete loss of tumor architecture and spindle-like morphology.

Paraffin Immunohistochemistry (IHC):

Tissue sections were deparaffinized by emersion in Xylene for 30 minutes followed by rehydration in 95%, 70%, and 50% ethanol for 5 minutes at each concentration. Slides were then heated in a pressure cooker for 10 minutes in 10mM Citric acid for antigen retrieval. Sections were blocked in PBS with 5% serum from the host animal used for the secondary antibody for 1-5 hours at room temperature.

Primary antibodies were incubated on the sections overnight at 4°C. The slides were then washed and incubated with secondary antibody for 20 minutes at room temperature. For list of antibodies used and relative concentrations see appendix A. Again the slides were washed and incubated with Avidin conjugated chromogen (M.O.M. Kit, Vector Laboratories) for 30 minutes at room temperature. DAB chromogen substrate (Dako Chemicals) was then added to the slides for 2 to 5 minutes. Sections were counterstained with Hematoxylin.

Paraffin Immunofluorescence (IF):

Deparaffinization was performed in the same manner as for IHC. After antigen retrieval, the sections were treated with Signal Enhancer (Invitrogen, Carlsbad CA) for 15 minutes at room temperature to further enhance antigen retrieval. The sections were then blocked using PBS containing 12% bovine serum albumin (BSA). Primary antibody was applied overnight at 4°C in the blocking medium. Sections were washed and incubated with fluorescence conjugated secondary antibodies in the dark for 20 minutes. Secondary antibodies were conjugated with Alexa Fluor 488 (green) or Alexa Fluor 594 (red). Slides were mounted with Fluormount G or with DAPI.

Frozen immunofluorescence (IF):

Slides were fixed in 4% paraformaldehyde for 40 minutes at room temperature. Alternatively the slides were fixed in cold methanol for 30 minutes. For IHC, sections were then blocked in PBS with 5% serum from the host animal used for the

secondary antibody for 1-5 hours at room temperature. The slides were then treated the same as the paraffin sections for the remaining steps. Slides used for frozen IF were fixed in the same manner as for frozen IHC. Following fixation the slides were treated with Signal Enhancer (Invitrogen, Carlsbad CA) for 15 minutes and then processed as for paraffin sections.

2.4 Tumor cell isolation and Fluorescence Activated Cell Sorting

Tumors were harvested from the mice and digested in a collagenase solution (250U/ml) (Worthington Biochemical, Lakewood, NJ) at 37°C for 30 minutes. After this time, the cells were manually dissociated by pipetting up and down approximately 10 times with a 10ml serological pipette. The cells were then incubated at 37°C for an additional 15 minutes. After a second round of manual dissociation the cells were filtered through a 70µm filter. The cells were then pelleted and resuspended in a solution of PBS 3% FBS at 1×10^6 cells/ml for Hoechst staining. The cells were stained at 25ng/ml Hoechst 33342 dye (Sigma-Aldrich, St. Louis, MO) in the dark in a 37°C water bath for 90 minutes [164]. Control cells were stained in the presence of 100µM verapamil to inhibit Hoechst dye efflux. After Hoechst staining the cells were pelleted and resuspended in 1ml PBS 3%FBS. The cells were then stained with FITC-CD31, FITC-CD45, Biotin-CD34 and PE-Cy5 CD49f for 20 minutes (for all antibodies and concentrations see Appendix A). In the case of sorting GFP positive cells, APC-CD31 and APC-CD45 were substituted for the FITC-conjugated antibodies. Secondary streptavidin-PE was then added to the cells to mark the CD34 positive cells and incubated for 20 minutes. Prior to flow sorting the

cells were washed, filtered (40µm filter) and propidium iodide (PI) (1µg/ml) was added to select for live cells at least 5 minutes prior to sorting.

Fluorescence Activated Cell Sorting (FACS) analysis was performed by the UC Denver Flow Cytometry Core on a Beckman Coulter MoFlo-XDP (Beckman Coulter, Brea CA) and data analysis was conducted using Summit Software V5.3 (Beckman Coulter, Brea CA). Single flurochrome stained Rat IgG control beads (BD Bioscience) were used for staining controls and setting compensation. Gating included forward/side scatter and dead cell exclusion with PI. Tumor cells were sorted for the Hoechst^{low} CD31⁻ CD45⁻ that was designated as the SP. A second cell population was sorted for Hoechst^{high} CD31⁻ CD45⁻ CD34⁺ CD49f⁺ and designated as the CD34⁺ CD49f⁺ population. The third cell population was sorted for Hoechst^{high} CD31⁻ CD45⁻ CD34⁻ CD49f⁻. Figure 6 outlines the cell populations sorted in this study.

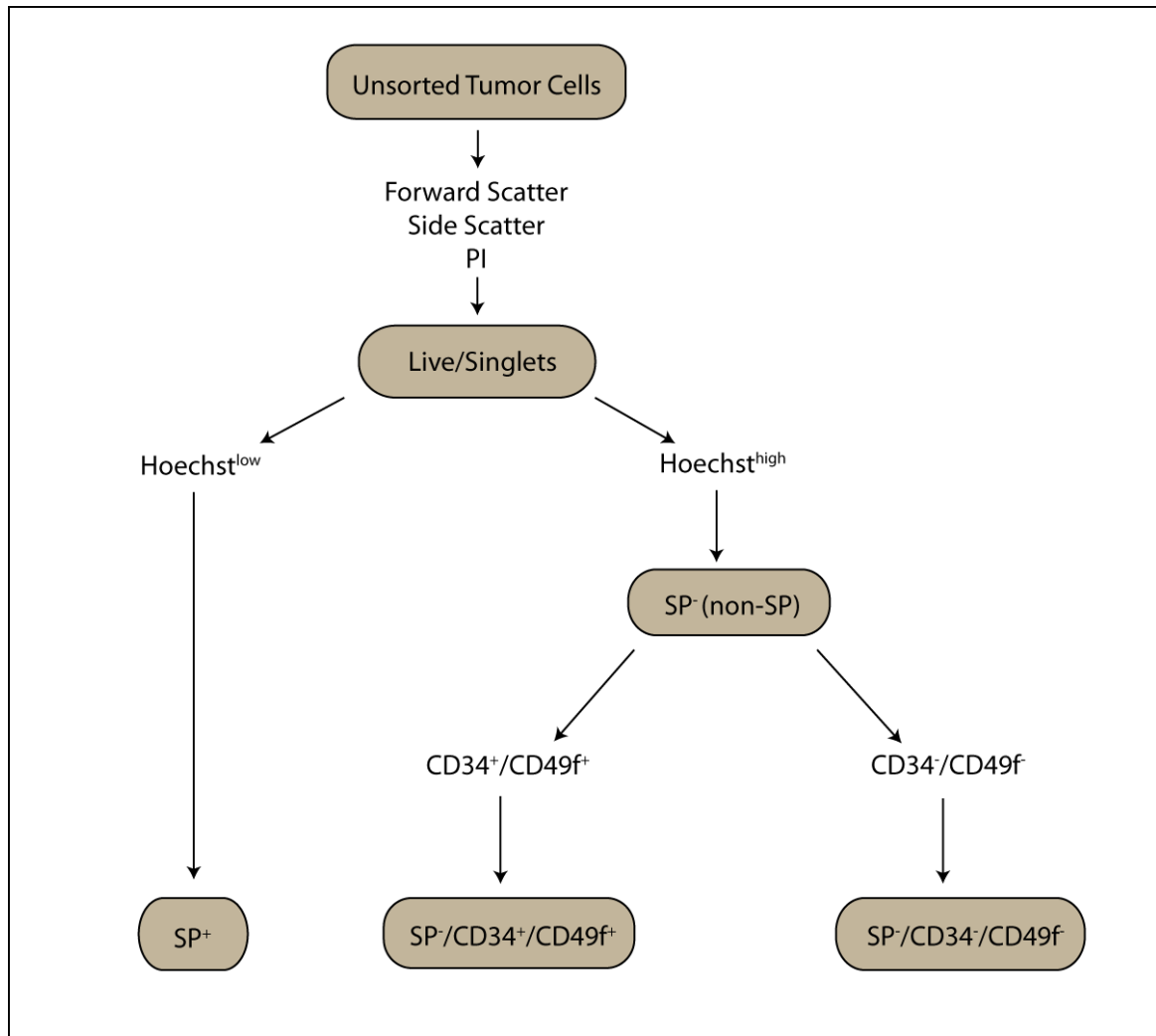


Figure 6. Schematic of FACS sorted tumor cell populations. Single cell suspensions of whole mouse tumors were sorted first for forward scatter, side scatter and propidium iodide (PI) uptake to select for singlets and live cells. The tumor cells were then sorted for the presence of Hoechst dye using the UV lasers. The Hoechst^{low} cells were collected as the side population (SP). The Hoechst^{high} cells were further sorted for CD34 and CD49f, the cells positive for CD34 and CD49f were collected as the SP⁻/CD34⁺/CD49f⁺ population and those negative for CD34 and CD49f were collected as

the SP-/CD34-/CD49f population. In the flow diagram, gray boxes represent different cell populations.

2.5 Tumor cell grafting and passaging of whole tumor cells

Tumor passaging: Tumors were maintained in nude mice by excising a small (2-4mm) piece of parent (primary) tumor from a K15.Kras^{G12D}.Smad4^{-/-} tumor-bearing mouse. A recipient athymic nude mouse was anesthetized and the back skin sterilized. Small incisions were made in the skin and the tumor piece was inserted subcutaneously. Once the tumor had grown these passaged tumors were subsequently serially passaged in to new athymic nude mice to maintain the tumor line.

Tumor cell grafting: Athymic nude mice were anesthetized and their back skins were disinfected with betadine and 70% ethanol. Scissors were used to cut small (~5mm) holes in the dermis and epidermis, and the underlying connective tissue was dissected away from the skin. Two silicone chambers (Renner, GMBH) containing a 2mm hole exposed to the air were placed such that the flanges of the chamber lay between the skin and the connective tissue, and the chamber extruded from the open hole. Primary fibroblasts and keratinocytes were isolated from wild type neonatal mouse back skins as previously described [223]. The sorted tumor cells (8×10^3 - 20×10^3) were injected in to the 2mm hole in the top of the grafting chamber along with a mixture of 1×10^6 keratinocytes and fibroblasts. The chamber was removed after one week and the mouse was observed for tumor formation. To

confirm the self-renewal ability of the TICs, grafted tumors were isolated and resorted for all TIC and non-TIC populations and each population was grafted to ensure tumor growth.

2.6 Analysis of Gene and miRNA Expression

RNA Isolation:

Total RNA, consisting of both the small and large RNA species, was isolated using the Qiagen miRNeasy mini kit (Qiagen, Valencia CA) as per the manufacturer's instructions. Briefly, 800-10x10⁶ pelleted cells were resuspended in 700µl of Qiazol lysis reagent. For sorted cells, where a small number of cells (<3x10⁶) were processed, homogenization was performed by vortexing the cells for 1 minute. For larger numbers of cells (>3x10⁶) and tissue samples, homogenization was performed using a bench top homogenizer. The total RNA was eluted from the column using 30µl of RNase free water.

Quantitative RT-PCR:

One-step qRT-PCR for gene expression: One-step qRT-PCR was used for gene expression when RNA samples were not limiting and amplification was not necessary. One-step qRT-PCR was performed using 100ng of RNA per reaction with the One-Step Brilliant II QRT-PCR system (Stratagene, Santa Clara CA). Expression of mRNA was measured using TaqMan® Assays-on-demand™ probes (Applied Biosystems, Carlsbad CA). All gene measurements were normalized to a GAPDH (human) or Gapdh (mouse) RNA probes. See appendix for TaqMan® probe details.

Each sample was run in triplicate and the data was analyzed using a standard relative quantification ($\Delta\Delta\text{Ct}$) method. Reactions were run on a Stratagene MX3000P qPCR machine (Stratagene, Santa Clara CA).

Two step qRT-PCR with pre-amplification for gene expression: For gene expression analysis on very small quantities of RNA, such as those generated from the sorted tumor cells, a two-step qRT-PCR reaction was performed with an amplification step. The first step involved an RT reaction starting with 2-200ng RNA. cDNA was generated using the High-Capacity cDNA Reverse Transcription kit (Applied Biosystems, Carlsbad CA), as per the manufacturers instructions. For the preamplification step, a pooled mix of TaqMan probes was made. Each of the probes were combined and diluted to 0.2x. The pooled assay mix was combined with 1-250ng cDNA and PreAmp Master Mix (Applied Biosystems, Carlsbad CA) as per the manufacturers instructions. The selected genes were amplified using 14 cycles to maintain amplification in the linear range. The qPCR reaction was performed using TaqMan Universal master mix (Applied Biosystems, Carlsbad CA) according to the manufacturers instructions. The results were analyzed using the $\Delta\Delta\text{Ct}$ method and normalized to Gapdh. Reactions were run on a Stratagene MX3000P qPCR machine (Stratagene, Santa Clara CA).

Two-step qRT-PCR for miRNA expression: All miRNA expression analysis by qRT-PCR was conducted using a two-step method. First miRNA specific cDNA was prepared using 10-300ng of starting RNA, and either individual miRNA specific RT primers, or

a pooled RT primer mix containing all of the miRNAs on the Applied Biosystems Rodent A v2.0 TaqMan Low Density Array card. The RT reaction was carried out using the High Capacity RT Kit from Applied Biosystems according to the manufacturers instructions. Once the miRNA specific cDNA was prepared, the qRT-PCR reaction was run using TaqMan miRNA probes and TaqMan Universal Master Mix (Applied Biosystems, Carlsbad CA).

Two-step qRT-PCR with pre-amplification for miRNA expression: Similar to the gene expression analysis, miRNA analysis on small quantities of RNA also requires an amplification step. In this case the miRNA specific cDNA was amplified using a pooled amplification primer mix containing all miRNAs on the Applied Biosystems (Carlsbad, CA) Rodent A v2.0 TaqMan Low Density Array card. The cDNA was amplified using 14 cycles, as for amplification of genes. Once the amplified cDNA was prepared, the qRT-PCR reaction was run as for samples with out amplification. All reactions were prepared according to the manufacturers instructions.

2.7 TaqMan Low Density miRNA Arrays

Preparation of miRNA-specific cDNA and preamplification were performed as described above for the two-step qRT-PCR and preamplification of miRNA expression analysis. cDNA synthesis and preamplification were performed in duplicate and combined prior to array analysis to help control for differences in amplification efficiencies between runs. Array reaction mixtures were set up according to the Applied Biosystems TaqMan Low Density Array protocol. Each of

the tumor cell population samples was run on the Rodent A v2.0 TaqMan Low Density Array card. This array card consists of the 335 most highly expressed rodent miRNAs identified in version 10 of the miRBase miRNA database. The cards contain a number of control probes including negative control probes that should not amplify mouse RNA and a number of endogenous small RNA probes for data analysis. The Mammalian U6 endogenous control probe is repeated in four wells of the card, and the average of Ct value from these probes was used as the endogenous control for this study. The array cards were run on an ABI 7900HT Fast qRT-PCR machine (Applied Biosystems, Carlsbad CA). TaqMan miRNA arrays were performed on the populations in Table 1. Each array was run on three distinct populations for each cell type.

	SP (Hoechst ^{low} /CD31 ⁻ /CD45 ⁻)	SP- /CD34⁺/CD49f⁺ (Hoechst ^{high} /CD31 ⁻ /CD45 ⁻ /CD34 ⁺ /CD49f ⁺)	Non-TIC (Hoechst ^{high} /CD31 ⁻ /CD45 ⁻ /CD34 ⁺ /CD49f ⁺)
Primary Tumor	□ □ □	□ □ □	□ □ □
Passage 1 Tumor	□ □ □	□ □ □	□ □ □

Table 1. Overview of TIC and non-TIC populations included in TaqMan miRNA Array study. For each array TIC cells from three separate tumors were combined. Each array for each TIC population was run in triplicate using three distinct combined TIC cell populations. In total, 9 primary tumors and 9 passage 1 tumors were assayed on the arrays.

Analysis of TaqMan miRNA Array Data

Array qRT-PCR data was analyzed using a standard relative quantification ($\Delta\Delta C_t$) method. Relative quantification analysis between samples was performed using the RQ Manager software from Applied Biosystems. For analysis of miRNA expression the ubiquitously expressed mammalian U6 small RNA was used for normalization and one array set was designated as the control sample to which the expression in the other samples was compared. Amplification curves of each miRNA represented on the plate were checked for adequate amplification. Samples, in which the C_t values were greater than 32 cycles in all samples, or those that did not amplify, were considered to be not expressed or expressed at very low levels in the tumor samples.

2.8 Bioinformatics and Statistical Analysis

Cluster Analysis of TaqMan miRNA Array Data

For cluster analysis of TaqMan miRNA array data, samples in which the C_t values were greater than 32 cycles in all samples, or those that did not amplify, were considered to be not expressed or expressed at very low levels in the tumor samples. These samples were set arbitrarily to 32 cycles for analysis. For each array set miRNA expression values were normalized to U6 expression for that replicate. The average ΔC_t value of expressed miRNAs (those with C_t values less than 32) for each array was calculated. Cluster analysis was conducted on this ΔC_t value. Cluster analysis was conducted for the array data using Cluster 3.0 software.

The data was filtered to include only those miRNAs that showed expression in 80% of samples and clustering was performed using Euclidian distance and complete linkage. Heat map images were generated using Java TreeView version 1.1.5r2 software.

Biostatistics of TaqMan miRNA Array Data

Biostatistical analysis of the TaqMan miRNA array data was conducted by the UC Denver Cancer Center Biostatistics Core. For each sample, miRNA readings that were labeled “Undetermined” or “flagged”, either because the sample did not amplify correctly or was not expressed, were removed from the analysis. For each sample the data was normalized to the average U6 RNA expression analysis averaged from four replicates on the array. Data was analyzed using the false discovery rate (FDR) approach to test the $\Delta\Delta C_t$ values based on the following comparisons:

1. Primary tumors: SP vs. SP⁻/CD34⁻/CD49f⁻
2. Primary tumors: SP⁻/CD34⁺/CD49f⁺ vs. SP⁻/CD34⁻/CD49f⁻
3. Passage 1 tumors: SP vs. SP⁻/CD34⁻/CD49f⁻
4. Passage 1 tumors: CD34⁺/CD49f⁺ vs. SP⁻/CD34⁻/CD49f⁻
5. SP cell type: Passage 1 vs. Primary
6. SP⁻/CD34⁺/CD49f⁺ cell type: Passage 1 vs. Primary
7. SP⁻/CD34⁻/CD49f⁻ cell type: Passage 1 vs. Primary

For each comparison, a t-test was conducted on each of the $\Delta\Delta Ct$ for the 335 individual miRNAs on each array. These “naïve p-values” were then ranked from lowest to highest. A q value was then calculated for each of the naïve p values defined as $q_1=335*p_1/1$, ..., $q_i=335*p_i/i$, etc. The minimum value in the series: $q_i, q_{i+1}, \dots, q_{335}$ was found and set as the FDR value for this miRNA. Samples were considered significant at an $FDR < 0.05$.

Statistical Analysis

For all qRT-PCR data, error bars are represented as the standard deviation between samples (triplicate), unless otherwise noted. In these cases, the standard error was used instead. In general standard error was used when there was wider variation between samples and larger numbers of samples were used, as in the case of tumor samples. Standard deviation was generally used with *in vitro* studies and studies with fewer replicates. In most cases significance was assessed using a standard student's t-test, however, analysis of significant differences between the percent of tumors with metastases was assessed using a χ^2 test. For qRT-PCR analysis, error was determined by calculating the standard deviation (std. dev.), or standard error from the ΔCt values. Upper and lower error limits for an expression value were then calculated using the standard $2^{-\Delta\Delta Ct}$ method as recommended by the manufacturer (Applied Biosystems, Carlsbad CA). For example the upper error limit was calculated as $2^{-(\Delta\Delta Ct - \text{std. dev } \Delta Ct)}$, and the lower error limit was calculated as $2^{-(\Delta\Delta Ct + \text{std. dev } \Delta Ct)}$. Finally, the upper error was calculated as the upper error limit – the

expression value, and the lower error was calculated as the expression value – lower error limit.

2.9 Cell culture

Generation of Primary Tumor Cultures:

Primary tumor cultures were generated from both primary and passaged tumors. Tumor tissue was harvested and the cells dissociated in collagenase (250U/ml) (Worthington Biochemical, Lakewood, NJ) for 45 minutes at 37°C. The cells were further dissociated manually by pipetting up and down. The cells were then filtered through a 40µm filter and washed in a culture medium of DMEM with 10% FBS. The cells were then plated in 10cm culture dishes and cultured at 5% CO₂ in a standard cell culture incubator. Prior to subculturing, the cells were treated with TrypLE (Invitrogen, Carlsbad CA) for 2 min and the floating cells discarded to select for epithelial cells. This selection was repeated prior to the subsequent 3-5 subcultures or as needed to remove fibroblast contamination. In total, 10 separate cell lines were generated from primary tumors and passaged tumors. However, three lines were used in this study all of which were generated from passaged tumors, B931, B911 and S4#8.

Generation of Stably Transduced Tumor Lines:

Lentivirus Production: Lentiviral particles were generated in the 293T packaging cell line. Prior to transfection the cells were changed in to Opti-MEM serum free media (Gibco, Carlsbad CA). Lentiviral vectors (see Appendix B for lentiviral vector

information) containing precursor miRNA sequences or miRNA antagonists were transfected in to the 293T cells along with the appropriate lentiviral packaging mix (see Appendix B for packaging mixes used with lentivirus) using Lipofectamine 2000 (Invitrogen, Carlsbad CA). Four hours after transfection the media was changed to DMEM containing 30%FBS and antibiotics. The virus containing media was harvested at 24, 32 and 48 hours. Virus was not concentrated for these studies.

Retrovirus production: Retroviruses (Appendix B) were produced in a similar manner to the lentivirus with the exception that the Θ nX-E packaging cell line was used and the pCL-ECO packaging vector was cotransfected with the retroviral vector. For human retroviruses, 293T packaging cells were used, and PUMVC, and pCMV-VSV-G were used for packaging (Appendix B). Virus harvesting was the same as for lentiviral particles.

Transduction and Selection of Transduced Cells: After harvesting from 293T cells, the cell culture medium containing virus was centrifuged at 3000rpm for 15 minutes to pellet any cellular debris. The 8nM polybrene was added to the media to aid in transduction. For a 10cm plate, 6ml of virus containing medium was added to the target cells. The cells were then incubated with the viral media for 24-48 hours for transduction. Selection of transduced cells was done by puromycin selection or FACS for GFP or RFP positive cells.

2.10 Luciferase Assays for miRNA activity

Functional activity of miRNAs *in vitro* was carried using a luciferase vector containing a miR-9 target sequence 3' to a luciferase gene. This pMIR-9-Luc reporter (Signosis, Sunnyvale CA) was transfected in to the miRNA transduced cells along with a Renilla control vector (pGL 4.74, Promega, Madison WI) using Lipofectamine 2000 as a transfection agent. After 48 hours the cells were washed with PBS then lysed using Passive Lysis Buffer (Promega, Madison WI). The luciferase and Renilla absorbance was read using the Dual Luciferase Kit (Promega, Madison WI) as per the manufacturers instructions using a GloMax®-96 Microplate Luminometer (Promega, Madison WI).

2.11 Invasion/Migration Assays

Invasion and migration assays were conducted using BD Bioscience Matrigel (Franklin Lakes, NJ) invasion chambers and transwell migration chambers. Prior to plating cells, the Matrigel layer was rehydrated in DMEM 10% FBS for 2 hours at 37°C. Once rehydrated 1×10^3 - 5×10^3 tumor cells transduced with miR-9 or miR-9 knockout vectors or controls were plated in the matrigel invasion chamber or transwell migration chamber in 500µl serum free medium. DMEM containing 10% FBS was used as a chemoattractant in the bottom well (750µl). The cells were then incubated at 37°C in a standard tissue culture incubator to allow for cell migration and invasion. After 24 hours the plates were removed from the incubator, and the cells that had not migrated or invaded were removed from the inside of the transwell by scrubbing the membrane with at cotton swab. The migrated/invaded

cells were stained fixed in Diff-Quick fixing medium for 2 minutes, then stained with 0.05% crystal violet for an additional 2 minutes. The membranes were washed well in water then left overnight to dry. Once dry the membranes were removed from the transwells and placed on slides with Fluormount G (Southern Biotech, Birmingham AL). To quantify the invading and migrating cells, 3 microscopic fields (10x) were imaged per membrane and the average number of cells per field was counted. Each assay was done in triplicate such that a total of 9 fields were counted for each condition.

2.12 Cell Growth Assays

In vitro cell proliferation was measured using a WST-8 [2-(2-methoxy-4-nitrophenyl)-3-(4-nitrophenyl)-5-(2, 4-disulfophenyl)-2H-tetrazolium, monosodium salt] Cell Count Reagent (Nacalai Tesque, Inc. Japan). Cell proliferation assays were performed on tumor cell lines transduced with miR-9 or GFP transduced control cell lines. For the cell growth assay, 50 cells were plated in a series of 96 well plates in triplicate. The proportion of viable cells was measured at 24, 48, and 72 hours by adding 10 μ l of WST-8 Cell Count Reagent to each well. The plates were incubated for at 37°C in a standard tissue culture incubator for 2 hours and then the absorbance of the reaction was measured at 450nm using a micro plate reader. At an absorbance 450nm the WST-8 reagent is proportional to the number of viable cells.

2.13 Cell Cycle Analysis

Control and miR-9 overexpressing of knockdown cells were harvested and washed with PBS. The cells were then pelleted by centrifugation and resuspended in 1ml Krishan Stain (produced as previously described [224]) at a concentration between $0.1-1 \times 10^6$ Cells/ml. The cells were vortexed to mix and incubated at 4°C overnight. Cell cycle analysis was performed with a FC500 flow cytometer and the data was analyzed using ModFit LT Software (Verity Software House, Topsham, ME).

2.14 Drug Resistance Assays

Control and miR-9 transduced cells were plated at a density of 1000 cells per well in duplicate 96 well plates. The next day the cells were treated with 0-260nM Docetaxel (Sigma-Aldrich, St. Louis, MO). A separate set of cells was treated with Docetaxel at the same concentrations in the presence of 0.05nM Verapamil. After 48 hours 10 μ l of WST-8 Cell Count Reagent was added to each well and the cells were incubated for 2 hours at 37°C. The absorbance at 450nm was measured on a plate reader to give a reading of the relative number of viable cells. Percent cell viability was calculated by setting the absorbance of untreated cells to 100% representing each Docetaxel treated sample as a percent of untreated.

2.15 *In Vivo* Tumor Growth Assay

In vivo tumor growth was assayed by subcutaneous injection of tumor cell lines in to the flank of athymic nude mice. Mice were injected with either miR-9

transduced, miR-9 knockdown, or control cells (GFP transduced or non-silencing control). The cells were prepared by washing the trypsinized cells in serum and antibiotic free EMEM medium, and then counted. A cell suspension of 1×10^3 cells per 100 μ l medium was made, and 100 μ l of cells (1×10^3 cells per mouse) were injected in to the flank of the mouse. A total of 8 mice were injected for each cell type. Tumor measurements were taken weekly by measuring the length and width of the tumor using calipers. The length and width measurements were then averaged to account for variations in tumor shape.

RESULTS

2.16 Metastatic Squamous Cell Carcinoma (SCC) Model Development

Generation and Characterization of K15.CrePR1/Kras^{G12D}/Smad4^{-/-} SCC

Previous inducible models of epithelial SCC have made use of keratin 5 and keratin 14 promoters targeting mutations to the entire basal cell layer [20, 64, 68, 82, 95, 225]. As the mutant basal cells grow and differentiate, the mutations are retained giving rise to mutant epithelia. In the skin, however, different tumor types are thought to arise from distinct subsets of epithelial progenitors [226], which reside in discrete compartments in the skin. One such region is the hair follicle bulge, the site of a set of multipotent epithelial stem cells that can give rise to all of the layers of the hair follicle in addition to the epithelium [141].

To generate mice with mutations targeted to the hair follicle bulge progenitor cells, we used a Keratin 15 promoter to drive Cre expression. Keratin 15 has been shown to be highly and specifically expressed in the hair follicle bulge [146]. Mice with the Keratin 15 (K15) CrePR1 fusion gene were crossed with mice with exon 8 of Smad4 flanked by loxP sites (floxed, Smad4^{f/f}) to target Smad4 deletion to the hair follicle bulge stem cells. To decrease tumor latency, an activating Kras mutation (Kras^{G12D}) was added (LSL- Kras^{G12D}) generating trigenic K15CrePR1/Kras^{G12D}/Smad4^{f/f} mice (hereafter referred to as K15.Kras^{G12D}.Smad4^{-/-}) (Figure 7A). Upon topical application of RU486 to the back skin, the CrePR1 fusion protein is shuttled to the nucleus where it activates recombination at the LoxP sites

in the transgenic $Smad4^{f/f}$ and $LSL-Kras^{G12D}$ constructs leading to deletion of $Smad4$ and constitutive activation of $Kras$. The floxed $Smad4$ allele (Figure 7B) and mutant $Kras$ (Figure 7C) were detected by genotyping PCR using primers specific for the presence of $LoxP$ sites (Appendix C). Recombination of the $Smad4^{f/f}$ and the $LSL-Kras^{G12D}$ constructs after RU486 application was verified by recombination PCR in the $K15.Kras^{G12D}$ papillomas and $K15.Kras^{G12D}.Smad4^{-/-}$ tumors (Figure 7D).

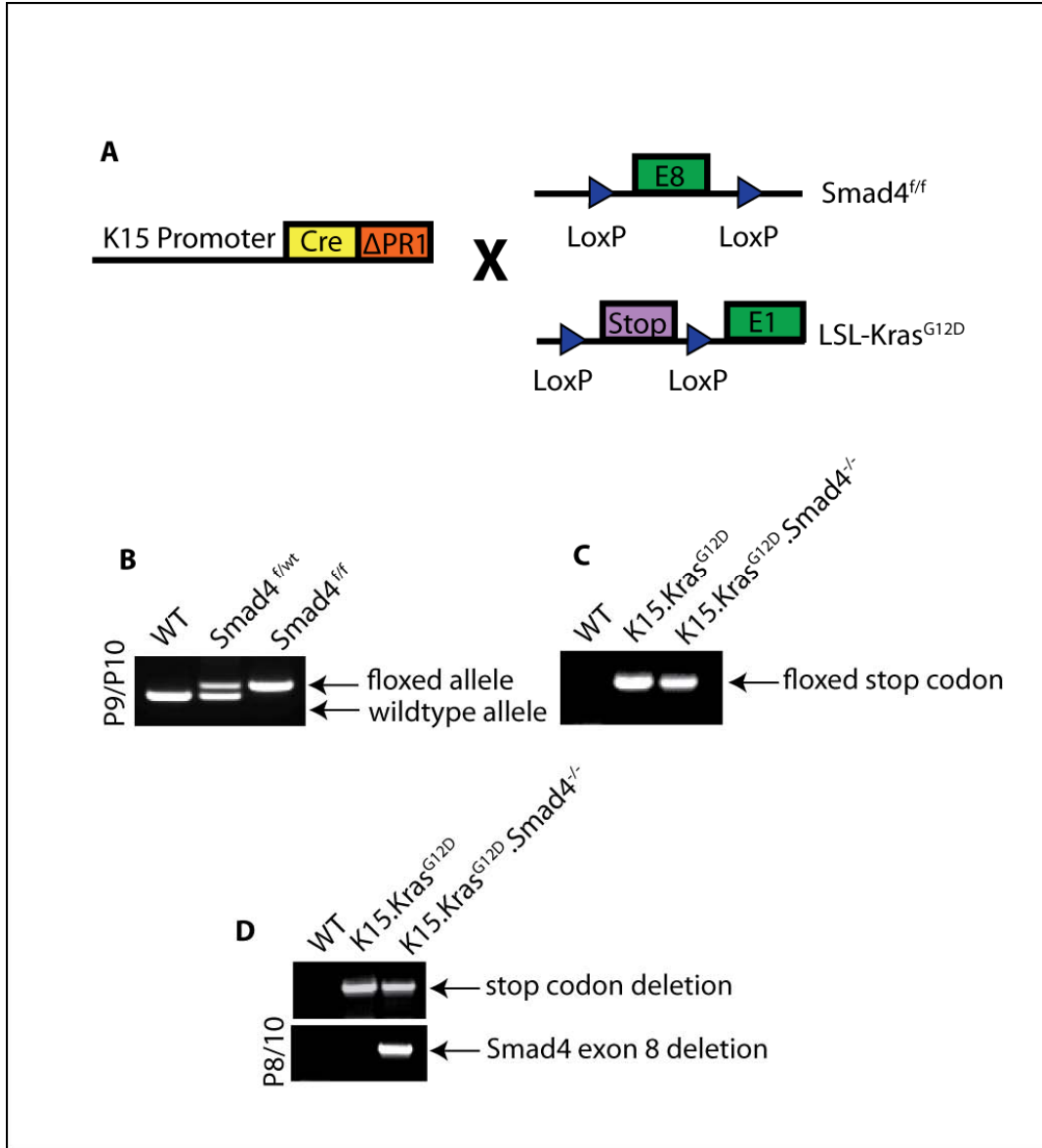


Figure 7. Generation of $K15.Kras^{G12D}.Smad4^{-/-}$ mice.

(A) Mating schematic for the $K15.Kras^{G12D}.Smad4^{-/-}$ mice. The Keratin 15 promoter targets the CrePR1 fusion protein expression to the hair follicle bulge. RU486 binds to the truncated progesterone receptor and activates shuttling of the Cre recombinase to the nucleus. The $K15CrePR1$ mice were mated with $Smad4^{f/f}$ mice and $LSL-Kras^{G12D}$ mice to generate trigenic $K15CrePR1/Kras^{G12D}/Smad4^{f/f}$ mice. (B) An example of

Smad4 genotyping using primers 9 and 10. (C) An example of *Kras* genotyping using primers specific for a *LoxP* site in the construct. (D) Recombination of the *LoxP* sites was confirmed by recombination PCR. *Kras* and *Smad4* recombination is confirmed using primers that span the floxed region and are too far apart to generate a PCR product. Upon deletion of the floxed region the primers are closer together and a PCR product is generated.

After treatment with RU486 the K15.Kras^{G12D}.Smad4^{-/-} mice developed well to moderately differentiated skin SCC (Figures 8A and 8B), with 25% developing lung metastasis (Figure 8C). In contrast K15.Kras^{G12D} mice developed benign papillomas that did not progress to malignant disease. Tumor development in the K15.Kras^{G12D}.Smad4^{-/-} mice occurred within 18 weeks after RU486 treatment with 100% penetrance (Figure 8D). To confirm that Smad4 was lost at the mRNA level in the K15.Kras^{G12D}.Smad4^{-/-} tumors, the relative expression of Smad4 transcripts was compared to the level in the K15.Kras^{G12D} papillomas by quantitative real-time PCR (qRT-PCR) (Figure 8E), and loss of Smad4 at the protein level was confirmed by IHC for Smad4 on the K15.Kras^{G12D}.Smad4^{-/-} tumors compared to the K15.Kras^{G12D} papillomas (Figure 8F). Residual expression of Smad4 in the tumors is likely due to the presence of cells that arose from other progenitor cell compartments such as the inter-follicular stem cells, or stromal cells.

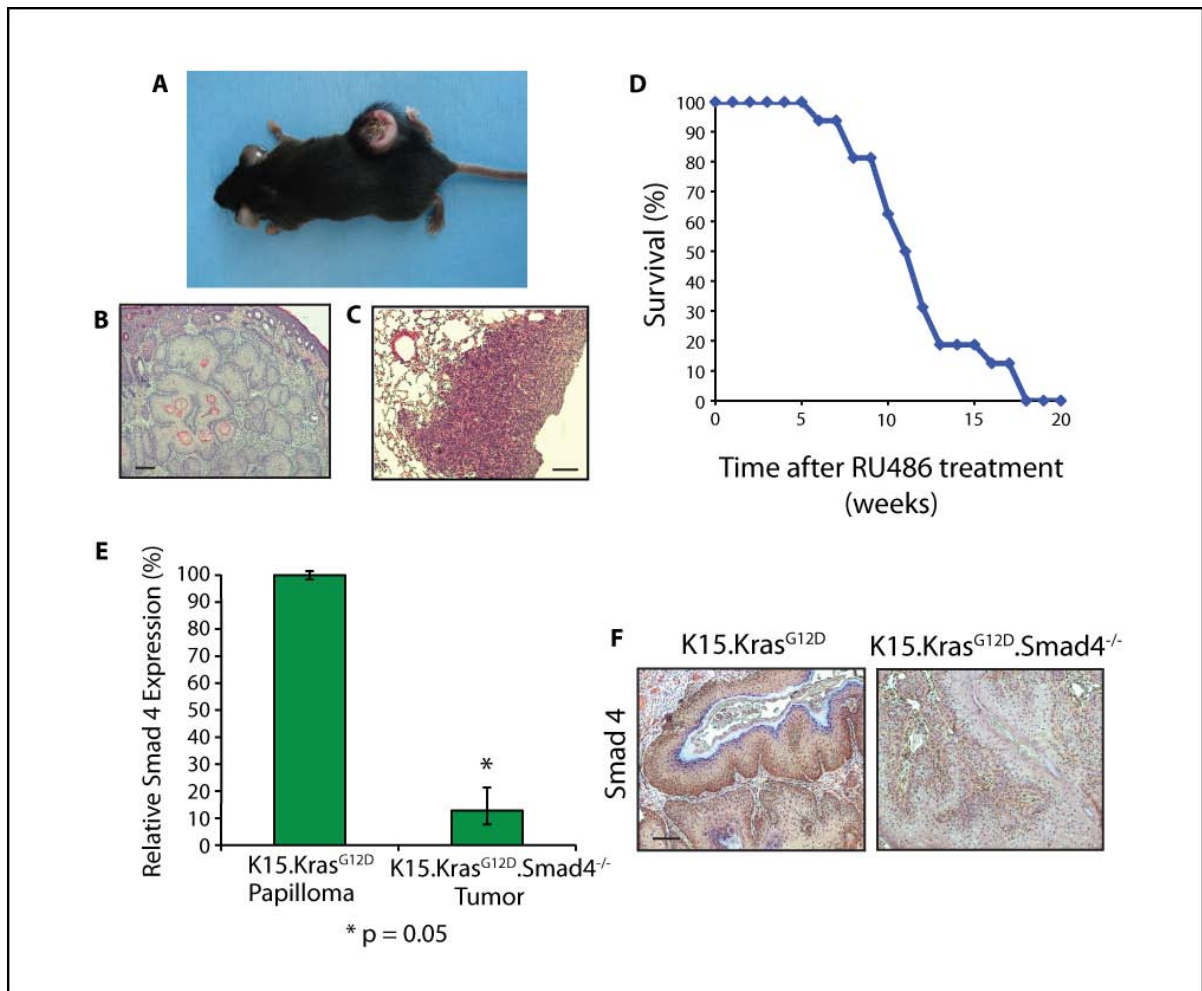


Figure 8. *K15.Kras^{G12D}.Smad4^{-/-}* mice develop metastatic Skin SCC with 100% penetrance. (A) Representative image of a *K15.Kras^{G12D}.Smad4^{-/-}* mouse with tumor. (B) H&E staining of a representative section from the SCCs showing well to moderately differentiated histology. Scale bar = 200µm. (C) H&E staining of an example lung metastasis. Scale bar = 50µm. (D) Survival curve of the *K15.Kras^{G12D}.Smad4^{-/-}* after RU486 treatment (n = 16). By 18 weeks, 100% of the mice had to be euthanized due to tumor burden. (E) qRT-PCR expression analysis of Smad4 in *K15.Kras^{G12D}.Smad4^{-/-}* tumor burden. (F) Immunohistochemistry for Smad4 in *K15.Kras^{G12D}* and *K15.Kras^{G12D}.Smad4^{-/-}* skin.

*SCCs compared to expression in K15.Kras^{G12D} papillomas. Smad4 expression in K15.Kras^{G12D} papillomas was arbitrarily set to 100%, and Smad4 levels in the K15.Kras^{G12D}.Smad4^{-/-} tumors were compared relative to expression in the K15.Kras^{G12D} papillomas. Error bars indicate standard error and significance was calculated using a Student's t-test: *p=0.05. (F) Immunohistochemistry of Smad4 in K15.Kras^{G12D}.Smad4^{-/-} tumors and K15.Kras^{G12D} papillomas. Scale bar = 100 μm.*

Passaged Tumors Have an EMT-like Phenotype and Increased Metastasis

The tumors from the K15.Kras^{G12D}.Smad4^{-/-} mice were xenografted (passaged) into athymic nude mice to amplify the working tumor mass and enrich for a tumor initiating cell population. The remaining K15.Kras^{G12D}.Smad4^{-/-} tumor mass was reserved for histology and cell sorting as discussed later. A small piece (~3mm³) of the primary tumor from the transgenic mouse was inserted subcutaneously into the flank of an athymic nude mouse (Figure 9A). Tumors in these mice developed within 40 weeks after transplanting and were denoted as Passage 1 (Figure 9B). Subsequent tumor passages grew within 8 weeks suggesting that enrichment for tumor initiating cells may occur during development of the Passage 1 tumor.

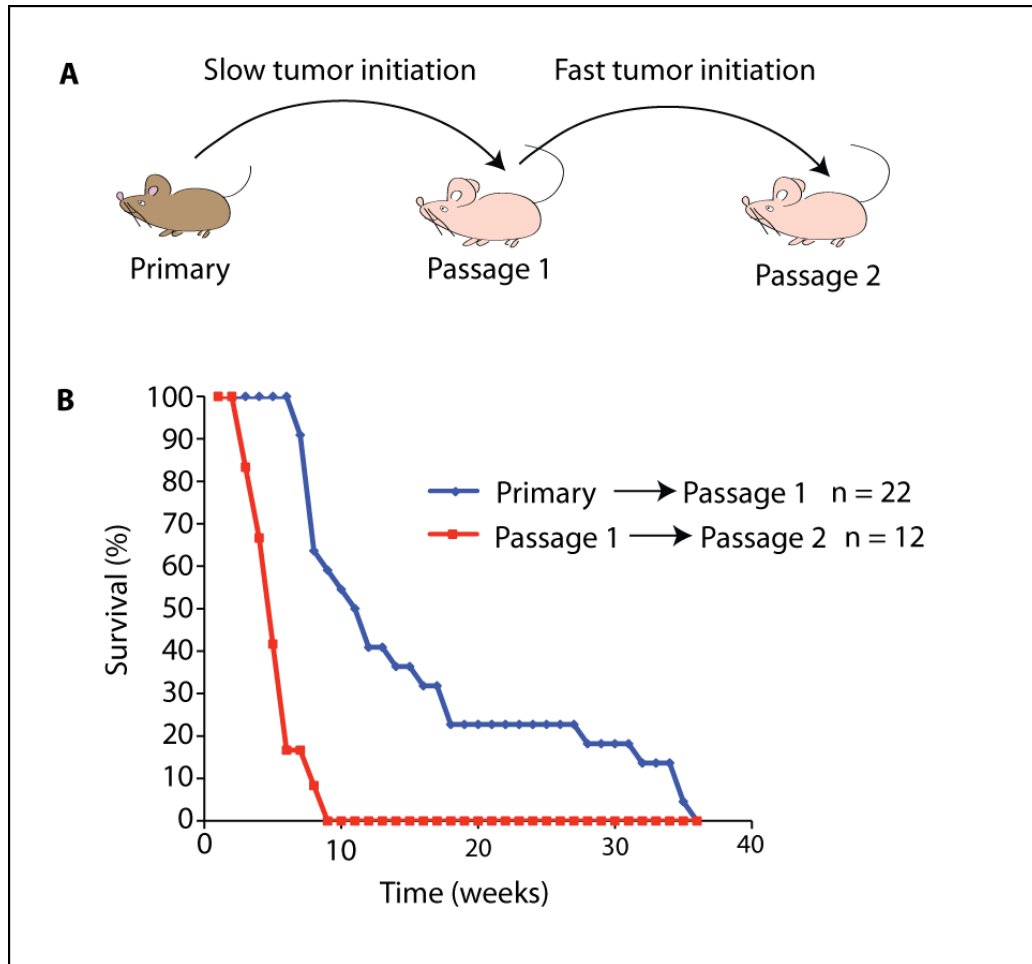


Figure 9. Passaging increases growth of grafted tumors. (A) Schematic of tumor passaging. Passaging of the primary tumor occurs slowly, while tumor growth in subsequent passages occurs more rapidly. (B) Survival curve of passage 1 (blue) and passage 2 (red) mice. Tumors were inserted subcutaneously at time = 0, and mice were euthanized when the tumors reached 20mm in diameter, or if there was a greater than 20% reduction in weight of the mouse.

The histology from the Primary and Passage 1 tumors varied in the level of differentiation and could be broadly categorized in to four histological groups; well

differentiated, moderately differentiated, poorly differentiated and spindle cell carcinoma (SPCC) (Figure 10B). The well-differentiated tumors exhibited keratin pearls that are pathognomonic for squamous cell carcinoma. Moderately differentiated tumor histology showed a loss of these keratin pearls, but retained eosinophilic staining and showed a lower density of nuclei. Conversely, the poorly differentiated tumors had lost the majority of the eosinophilic staining and were marked by tight nests of blue nuclei. Finally, the SPCCs showed a complete loss of tumor architecture and a spindle shape indicative of an epithelial-to-mesenchymal transition (EMT). Quantification of the tumor types showed that the majority of Primary tumors were well to moderately differentiated, whereas the Passage 1 tumors tended to have poorly differentiated and SPCC histology (Figure 10C).

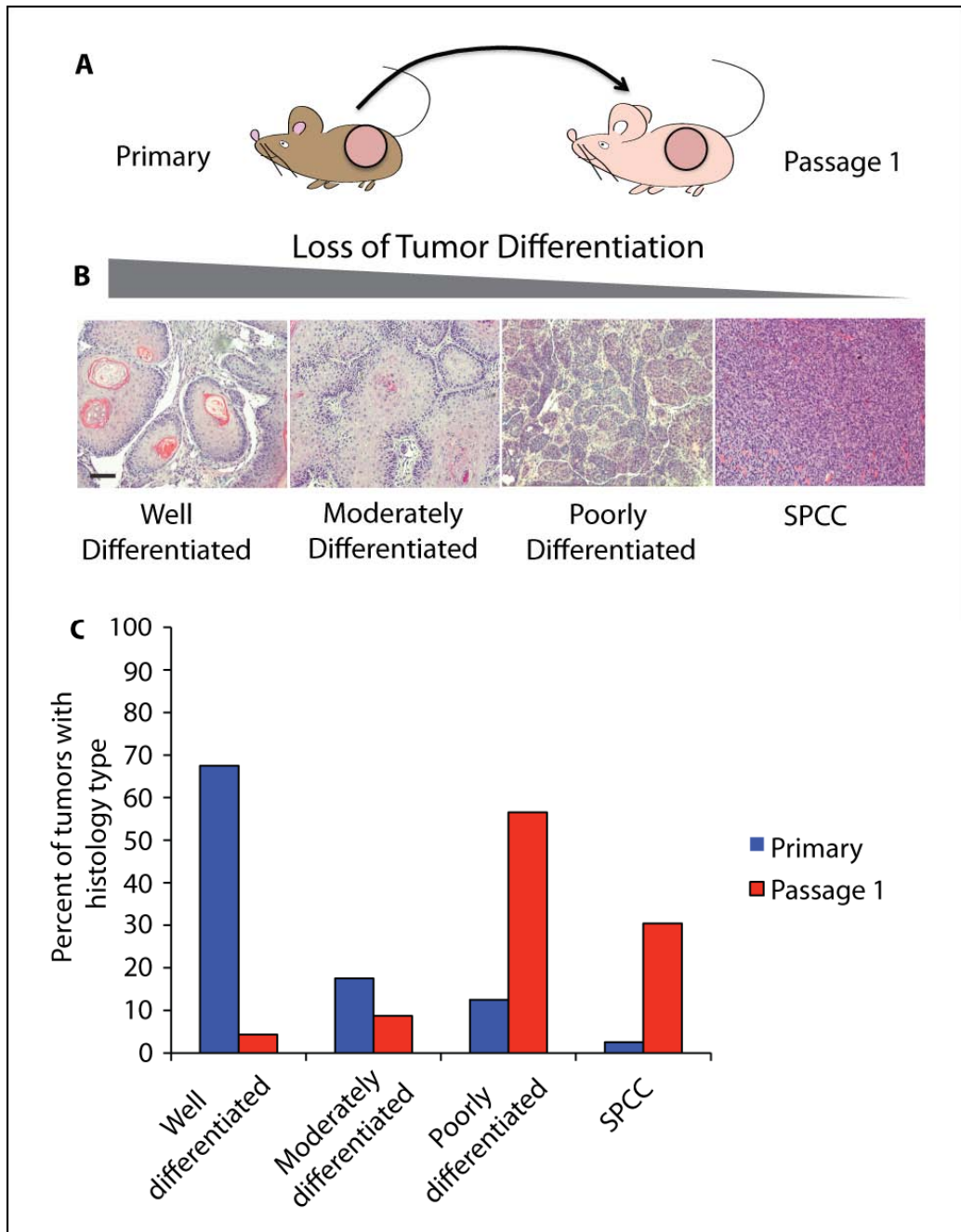


Figure 10. Passaging leads to loss of tumor differentiation. (A) Schematic showing Primary *K15.KrasG12D.Smad4^{-/-}* tumors and Passage 1 tumors studied for tumor differentiation. (B) Examples of the four histological tumor types seen in

Primary and Passage 1 tumors. (C) Quantification of tumor histology in Primary (blue bars) and Passage 1 (red bars) tumors. The tumors were grouped according to histology by three different investigators. Primary: n = 40 (well = 27, moderately = 7, poorly = 5, and SPCC = 1) and Passage 1: n = 23 (well = 1, moderately = 2, poorly = 13, and SPCC = 7).

Interestingly, some of the tumors showed regions of cellular heterogeneity. Analysis of tumor histology showed that the majority of the tumors were SCC (Figure 11A), however, a small subset (3/40) of the primary tumors displayed areas of sebaceous adenoma (SA), (Figure 11B), and 4/23 of the Passage 1 tumors had regions of basal cell carcinoma-like histology (Figure 11C), suggesting that the cells giving rise to these tumors may retain pluripotency – the capability to differentiate in to multiple hair follicle bulge cell types.

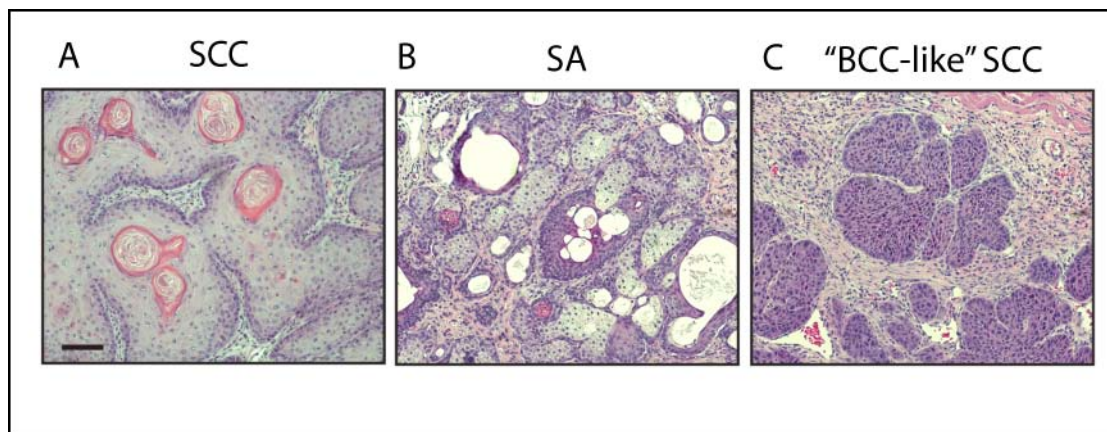


Figure 11. *K15.Kras^{G12D}.Smad4^{-/-}* tumors have regions of histological heterogeneity. H&E staining of *K15.Kras^{G12D}.Smad4^{-/-}* tumors showed that the majority of the tumors were SCC (A), however, 3/40 primary tumors had regions

characteristic of sebaceous adenoma (SA) (B), and after passaging 4/23 tumors had regions of basal cell carcinoma-like SCC ("BCC-like" SCC) (C). The scale bar in the left hand panel represents 100 μ m for all panels.

Loss of differentiation and development of an EMT-like phenotype in the Passage 1 tumors prompted us to look for molecular changes that occur during EMT. Therefore, we evaluated serial tumor sections for expression of E-cadherin and vimentin, markers of EMT, and found a loss of membrane specific E-cadherin (epithelial specific) staining and increased vimentin (marker of mesenchymal cells) staining in SPCC tumors compared to more differentiated tumors (Figure 12A). In addition, keratin 5 staining was decreased in the less differentiated tumors, indicating transition from an epithelial cell type to a more mesenchymal cell type (Figure 12A). Since tumor recurrence and metastasis have been associated with EMT, we also assessed the metastatic potential of each of the different histological tumor types (Figure 12B). Not, surprisingly this analysis clearly showed that the poorly-differentiated and SPCC tumor types were far more metastatic than the well- and moderately-differentiated tumor types. Since there were too few tumors for each histological group to find any statistical difference between the tumors, we compared the percent of mice with lung metastasis between the primary (mostly well- and moderately- differentiated) and passage 1 (mostly poorly-differentiated and SPCC) tumors. We observed that although the primary tumors were relatively metastatic to the lung, the incidence of lung metastasis in the mice with passaged tumors increased significantly ($p = 0.001$) from 25% to 80% (Figure 12C).

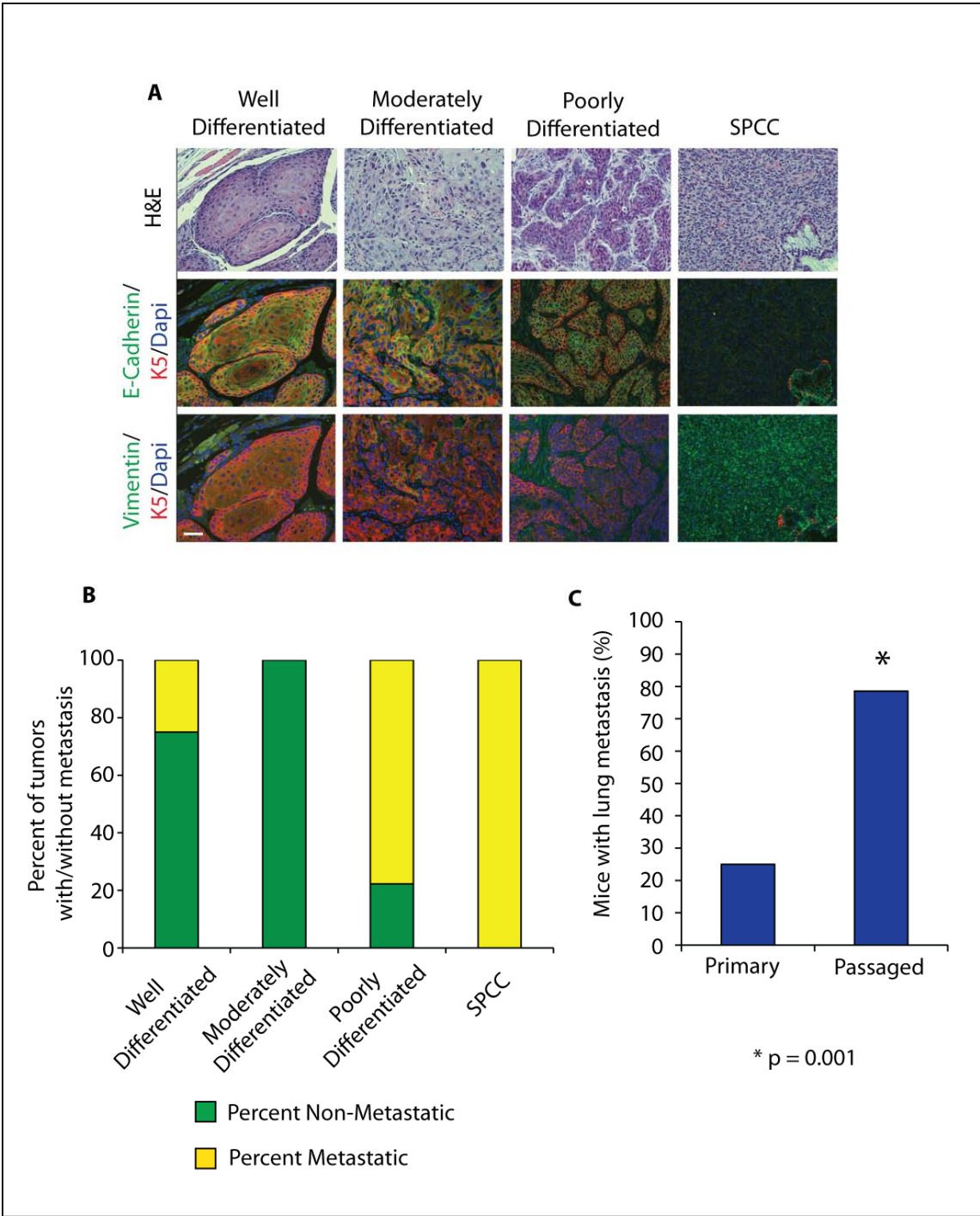


Figure 12. Passaging tumors induces an EMT-like phenotype and increases metastasis. (A) Serial section staining of EMT markers in the four histological tumor

types. The top row shows the H&E. The middle row shows E-cadherin staining (green) the cell membranes in the more differentiated tumors, but staining decreases in the less differentiated tumors and is completely absent in the SPCC tumors. In the bottom row more differentiated tumors do not show vimentin staining (green), while the SPCCs show strong vimentin staining. Each of the sections was counterstained with the keratinocyte marker, Keratin 5 (Red). Expression of Keratin 5 also decreases in the less differentiated tumors. Scale bar = 100 μ m. (B) Percent of mice from each histological tumor type with visible lung metastasis (yellow bars) compared to no metastasis (green bars). For well-differentiated n = 4, moderately-differentiated n = 2, poorly-differentiated n = 9 and SPCC n = 5. (C) The percent of mice with grossly visible lung tumors at necropsy was significantly increased in Passage 1 tumors. Significance was calculated using a χ^2 test: * p = 0.001. Primary tumors: n = 8, Passage 1 tumors: n = 14.

In summary, we have generated a model system for the study of metastasis. By passaging the tumors arising in K15.Kras^{G12D}.Smad4^{-/-} mice, the tumor-initiating capability is increased. There is a loss of differentiation in the Passage 1 tumors together with enhanced EMT-like characteristics and greatly increased metastatic potential. Therefore, we chose to use the Primary and Passage 1 tumors as a model in which to investigate the characteristics of tumor-initiating cells (TICs) in metastatic tumors in the following studies.

2.17 Identification and Characterization of Tumor-Initiating Cells in SCC

Identification of TICs in the K15.CrePR1/Kras^{G12D}/Smad4^{-/-} SCCs

To date, a number of different markers have been used to identify TICs in solid tumors. Since few studies have looked at the TICs in skin SCCs, we chose two approaches to identify TICs that have been used previously to identify normal epithelial stem cells. In the first approach, we defined the TIC population as the Hoechst dye excluding “side population”. These cells are flow sorted based on their ability to efflux certain dyes through members of the ABC transporter family. These transporters are often highly expressed on stem cells, and have been shown to mark the epithelial stem cells [147]. For the second approach, we isolated CD34 and CD49f expressing tumor cells, because both of these proteins are highly expressed on the membrane of cells in the hair follicle bulge, and have been used to isolate cell populations from normal skin that are enriched in multipotent stem cells that give rise to both hair follicle and epidermis upon grafting [146].

To enrich for the tumor epithelial cells, we first removed the leukocytes (CD45⁺) and endothelial (CD31⁺) cells from the population by flow sorting. The remaining cells were then sorted for the presence or absence of Hoechst staining. Cells that have the capability to pump out the Hoechst dye, give rise to a Hoechst dye negative side population (SP) (Figure 13A). Since high expression of ABC transporters is an accepted mechanism for Hoechst dye exclusion, we controlled for poor staining (false Hoechst negative cells) by treating a subset of the tumor cells with verapamil, a drug that blocks the ABC transporter functions. Verapamil

treatment eliminated the SP (Figure 13B), indicating that the SP population could be attributed to dye efflux, rather than poor staining. The SP⁻/CD34⁺/CD49f⁺ cells were subsequently isolated from the non-SP cells, as well as a control population that was negative for all TIC markers studied here (SP⁻/CD34⁻/CD49f⁻). Each of these tumor cell populations (SP, SP⁻/CD34⁺/CD49f⁺ and SP⁻/CD34⁻/CD49f⁻) was grafted in to athymic nude mice to assay for tumor initiating activity. As few as 1x10⁴ SP (Figure 13D) and SP⁻/CD34⁺/CD49f⁺ (Figure 13E) cells rapidly formed tumors upon grafting, while the same number of control SP⁻/CD34⁻/CD49f⁻ (Figure 13D) cells did not form tumors. These data show that we have identified two independent TIC populations in the K15.Kras^{G12D}.Smad4^{-/-} tumors with similar tumor-initiating capability. Finally, to determine if there was any overlap between the SP and the SP⁻/CD34⁺/CD49f⁺ populations we sorted the SP population for CD34 and CD49f expression. This analysis showed that there was no overlap and that the SP and SP⁻/CD34⁺/CD49f⁺ were distinct TIC populations.

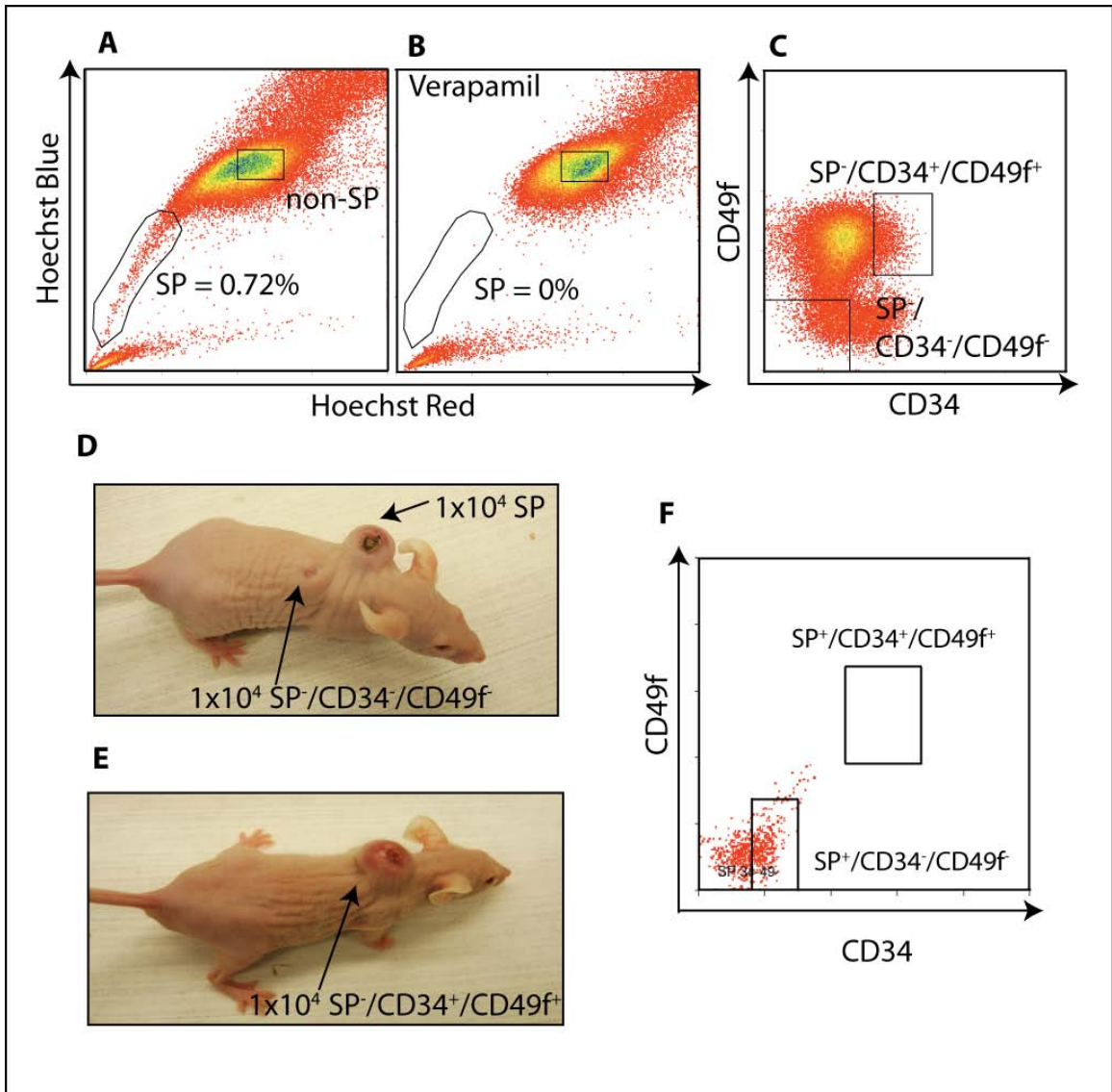


Figure 13. The SP and SP-/CD34+/CD49f+ cell populations are tumor initiating.

(A) Flow cytometry for the Hoechst dye effluxing side population (SP). The SP cells are gated as those cells negative for Hoechst dye. (B) The SP is completely removed by blocking the ABC transporter with verapamil treatment of the cells. (C) The non-SP

population was further sorted for the SP-/CD34+/CD49f⁺ population and a population that was negative for both TIC cells (SP-/CD34-/CD49f⁻). (D) Grafting of 1x10⁴ SP cells formed tumors 3 weeks after grafting, while 1x10⁴ of the SP-/CD34-/CD49f⁻ cells did not form tumors. (E) Grafting of 1x10⁴ SP-/CD34+/CD49f⁺ cells also formed tumors 3 weeks after grafting. (F) Analysis of CD34 and CD49f expression in the SP⁺ cells.

SP and SP-/CD34+/CD49f⁺ TICs are Distinct Populations That May Play Different Roles in the Growth, Progression and Recurrence of Tumors

After sorting a number of different tumors it became apparent that there were substantial differences in the size of the SP and SP-/CD34+/CD49f⁺ TIC populations. Figures 14 A and B demonstrate the variability in the SP size in two Passage 1 tumors sorted on the same day. In this example, Tumor A had a very small SP of only 0.15% of the viable cells (Figure 14A), while Tumor B had very large SP of 37.6% of the viable cells (Figure 14B). Treatment of the cells with verapamil completely removed the SP, indicating that the enlarged SP in Tumor B results from increased Hoechst dye efflux, rather than poorly stained cells (Figure 14C). A comparison of the histology from these tumors showed that Tumor A, with the small SP, was moderately differentiated (Figure 14D), while Tumor B, with the large SP, was a SPCC (Figure 14E). Comparing SP size across well, moderately, poorly differentiated and SPCC tumors, we found a significant increase in the size of the SP in SPCC tumors compared to all other histology types (p=0.003, Figure 14F). We note that, as discussed above, SPCC tumors are characterized by EMT, and that a number of studies have shown that inducing EMT in cultured cell lines can increase

the size of TIC populations [158, 159]. Therefore, we suggest that a similar phenomenon may be occurring in our model, an observation that, to our knowledge, has not previously been reported in an *in vivo* tumor model.

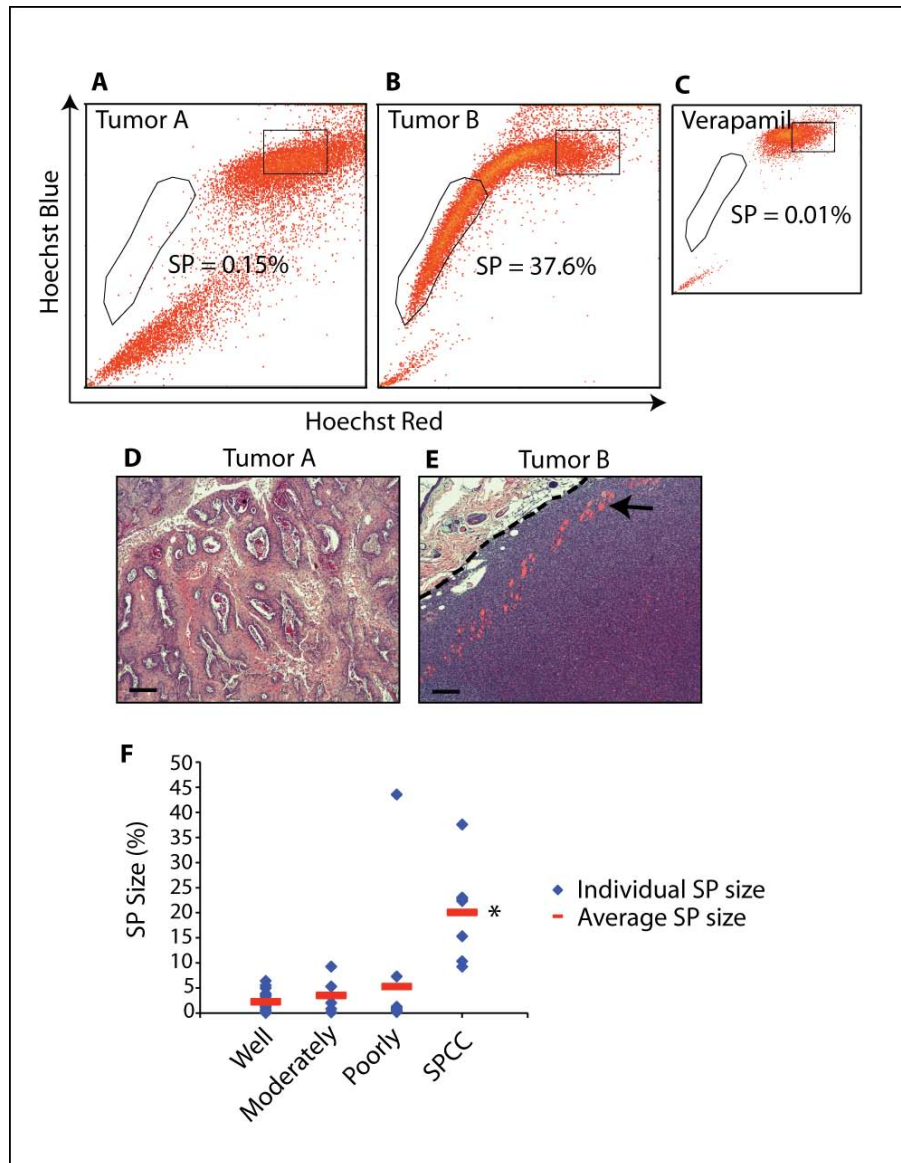


Figure 14. Variations in SP size correlates with tumor histology. Tumor A (A) and Tumor (B) are both Passage 1 tumors sorted on the same day showing the variation in

*SP size between tumors. (C) Verapamil treatment of tumor B demonstrates that blocking the ABC transporters with verapamil can inhibit the large SP. A comparison of the tumor histology from Tumor A (D) and Tumor B (E) shows that the tumor with the large SP has SPCC histology. In (D) the dashed line demarcates the tumor boarder and the overlying stroma and the arrow indicates an example of an area in the tissue that has separated during sectioning. (F) Graph showing the correlation between SPCC histology and SP size. Well-differentiated $n = 19$, moderately-differentiated $n = 5$, poorly-differentiated $n = 11$ and SPCC $n = 7$. Significance was determined by comparing SP size of the SPCCs with the SP size each of the other histology types using a Student's t -test: $*p = 0.003$.*

Since EMT is associated with metastasis [154], we also investigated whether the size of the TIC population in tumors may be related to metastasis in the K15.Kras^{G12D}.Smad4^{-/-} model. We sorted the SP and SP⁻/CD34⁺/CD49f⁺ populations from Primary ($n = 11$) and Passage 1 ($n = 15$) tumors and compared the size of the TIC cell populations with the presence of lung metastasis in the corresponding mouse. We found a significant increase in the size of the SP in metastatic tumors when we considered Primary or Passage 1 tumors together ($p = 0.009$, Figure 15A). When we considered the Primary and Passage 1 tumors separately, however, we found a significant increase in SP size only in Passage 1 metastatic tumors ($p = 0.02$), but not in the Primary tumors ($p = 0.2$), which may be due to the small number of metastatic tumors in this group ($n = 3/8$). By contrast, no significant difference in the size of the SP⁻/CD34⁺/CD49f⁺ population was observed in

metastatic and non-metastatic tumors ($p=0.74$, Figure 15B). We further noted a significant ($p < 0.05$) increase in SP size in the Passage 1 tumors, irrespective of metastatic state (Figure 15C).

The differences in the SP and SP⁻/CD34⁺/CD49f⁺ populations suggest that tumors contain distinct populations of TICs that may play different roles in the growth, progression and recurrence of tumors. Since we observed an increase in SP size with metastatic potential, this cell population may be involved in metastasis, consistent with the belief that the TIC capabilities of metastatic cells facilitate establishment of tumors at distant sites. On the other hand, the SP⁻/CD34⁺/CD49f⁺ populations do not appear to play such a role, as discussed further below.

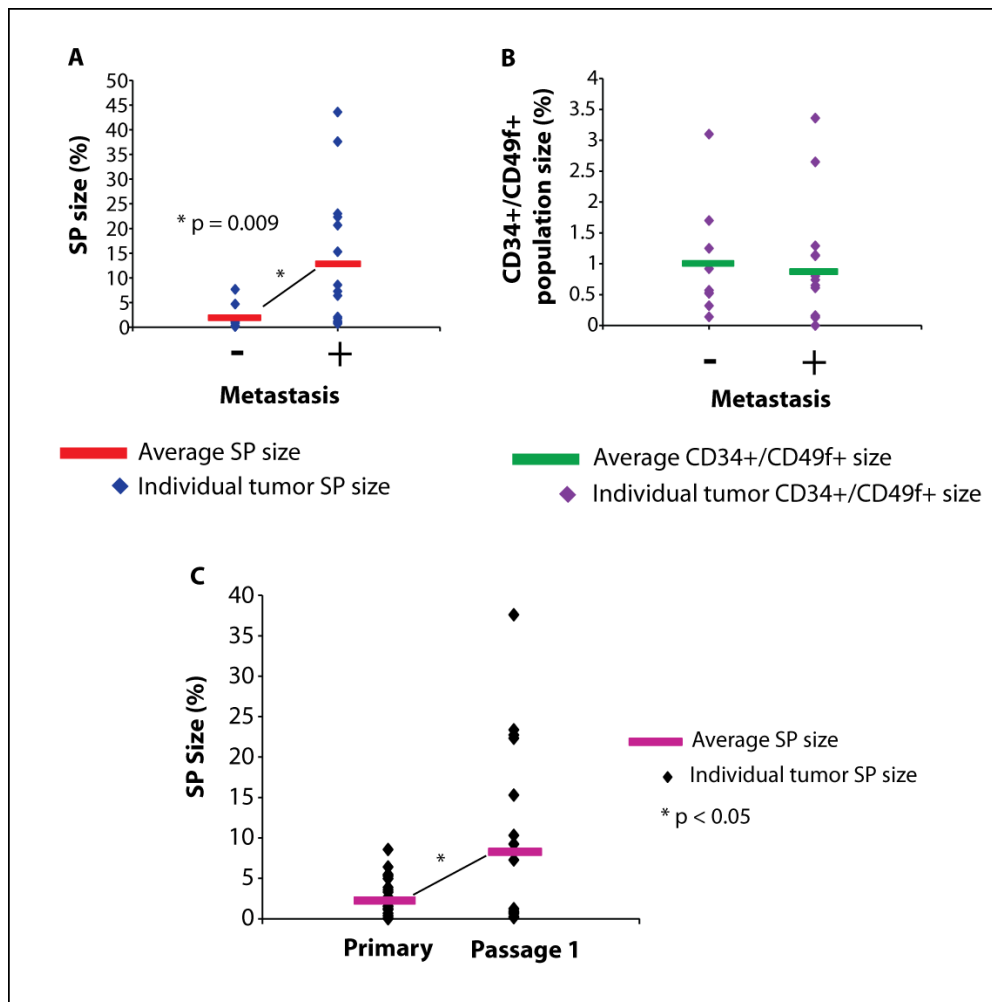


Figure 15. *SP size, but not SP/CD34⁺/CD49f⁺ size is increased in metastatic tumors.* (A) Graph comparing SP size (% of viable cells sorted) with presence of metastasis. Blue dots indicate SP size of individual tumors, and red bar indicates the average SP size. Significance was calculated using a Student's t-test: *p = 0.009. (B) Graph comparing SP/CD34⁺/CD49f⁺ size (% of viable cells sorted) with metastasis. Purple dots represent an individual tumor, and the green bar represents the average

*SP-/CD34+/CD49f⁺ size for that group. No significant difference was seen. For the non-metastatic tumors n = 9, and for the metastatic tumors n = 15. (C) Graph comparing SP size in Primary and Passage 1 tumors. Black dots represent individual tumors, and pink bars represent the average SP size for Primary or Passage 1 tumors. Primary tumors n = 11 and Passage 1 tumors n = 15. Significance was calculated using a Student's t-test: *p < 0.05.*

2.18 MicroRNAs as Potential Regulators of Stem Cells and Metastasis.

TaqMan Low Density Array Analysis of Differentially Expressed miRNAs in TICs From Primary and Passage 1 Tumors.

MicroRNAs have been shown to be important regulators of both metastasis and stem cells, however little is known about the role of miRNAs in the regulation of TICs. To identify miRNAs that may play a role in the regulation of TICs in metastasis, we set up an expression array screen to compare miRNA profiles of TICs from the primary and Passage 1 tumors (Figure 16).

SP and SP-/CD34+/CD49f⁺ cell populations were sorted from Primary and Passage 1 tumors. To generate samples for the expression analysis of Primary vs. Passage 1 tumors, TICs from three separate tumors were combined to reduce background variability. Three such samples of each TIC from both the Primary and Passage 1 tumors were then assayed for miRNA expression using the TaqMan Low Density Arrays (TLDA) (Figure 16). These assays are qRT-PCR based miRNA arrays that include probes for 335 of the most highly expressed miRNAs in the mouse.

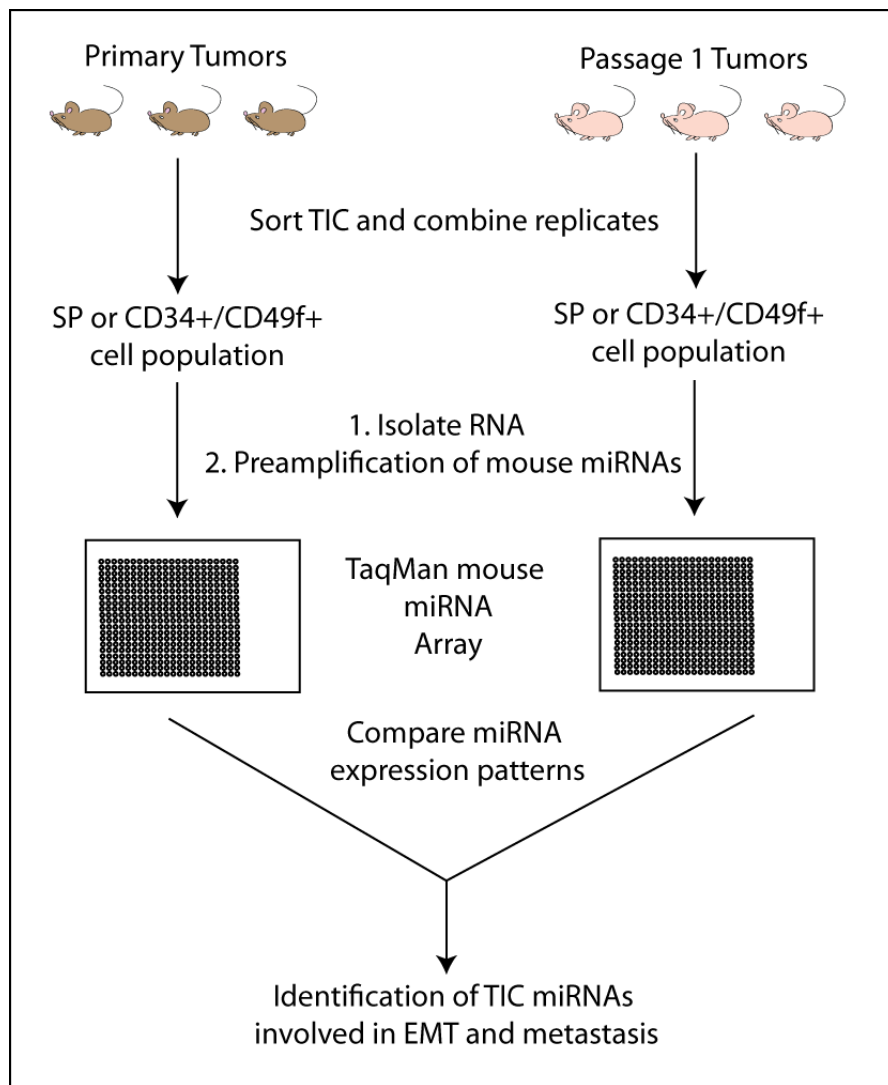


Figure 16. Schematic of miRNA expression analysis in Primary and Passage 1 TICs. Samples for analysis were comprised of TIC populations sorted from three separate mice. RNA was extracted from the TICs and preamplified for each of the miRNAs on the mouse TLDA. Three samples for each tumor type were generated in this way with different tumors. miRNA expression patterns were compared between

Primary and Passage 1 TICs to identify miRNAs that may play a role in EMT and metastasis.

To identify differentially expressed miRNAs between Primary and Passage 1 TICs, we initially utilized the standard $\Delta\Delta\text{CT}$ method, which involves normalizing the miRNA amplification data to that of the ubiquitous U6 small RNA and then determining the relative expression changes between the Primary and Passage 1 TIC populations. Due to the small sample size and variability in expression between samples, no significant differences in miRNA expression were found between Primary and Passage 1 TICs. Therefore, we used cluster analysis to identify miRNAs that may be differentially expressed in the TICs between the Primary and Passage 1 tumors. This analysis allowed us to visualize trends in miRNA expression changes as well as the consistency in expression differences between sample types. For this analysis the U6 normalized ΔCt values were averaged for each expressed miRNA ($\text{Ct} < 32$ cycles), and the expression of each individual miRNA was analyzed relative to this average miRNA expression. This analysis gives a value that shows whether the expression of a particular miRNA was higher or lower than the average expression for that sample. Cluster analysis was performed using complete linkage and Euclidean distance to generate a clustergram of miRNA expression in the SP (Figure 17A) and the SP⁻/CD34⁺/CD49f⁺ cells (Figure 18A). This analysis revealed two distinct clusters, one comprised of the Primary tumor SP samples and the other the Passage 1 tumor samples (Figure 17B). In contrast, the SP⁻/CD34⁺/CD49f⁺ Primary and Passage 1 samples did not cluster according to tumor type (Figure

18B). These observations suggest that the SP⁻/CD34⁺/CD49⁺ TIC populations are heterogeneous, whereas the TIC populations defined by the SP are reproducible and specific to tumor type. A number of miRNAs that were differentially expressed between the SP cells from the Primary and Passage 1 tumors (Figure 17B) have previously been shown to be involved in metastasis and/or EMT, consistent with the more metastatic and EMT-like phenotype of the Passage 1 tumors compared to the Primary tumors.

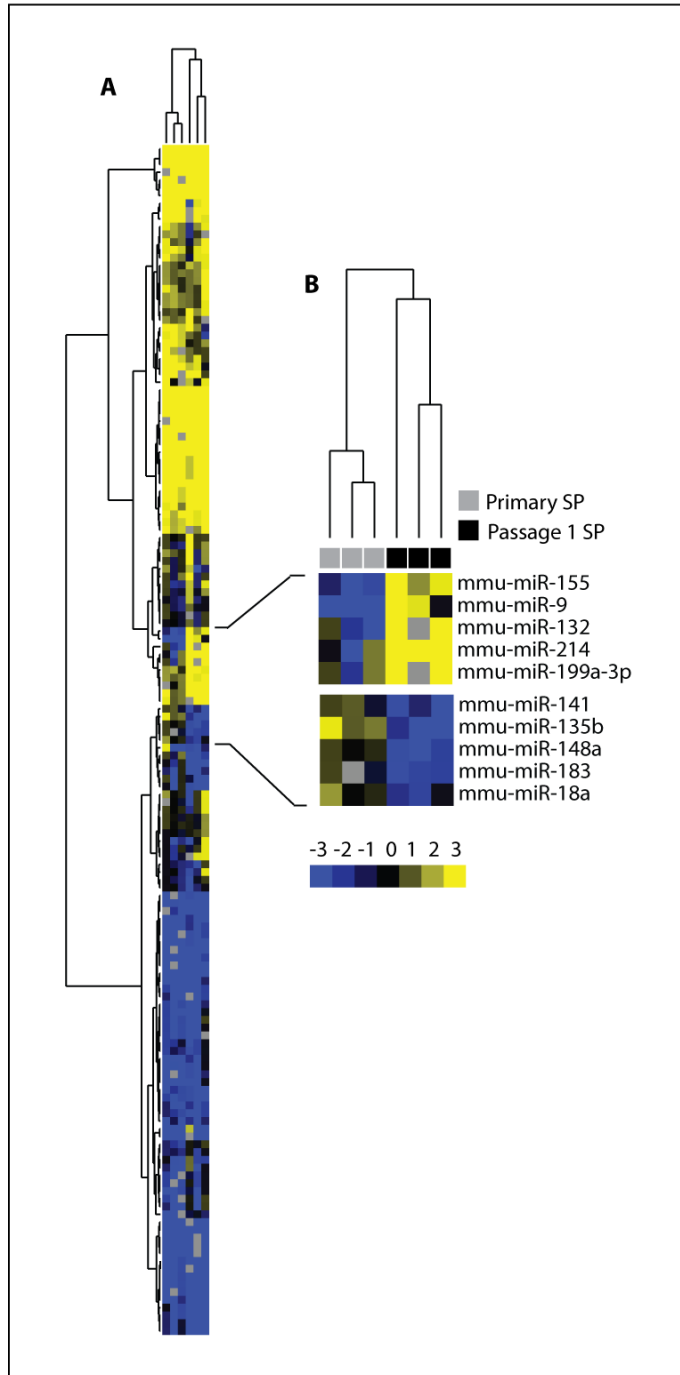


Figure 17. Cluster analysis of miRNA expression in Primary and Passage 1 SP cells.

(A) Cluster analysis of miRNA expression in Primary and Passage 1 tumor SP cells was performed on Ct values normalized to U6 expression. Analysis included only those miRNAs in which 80% of the samples showed expression. (B) Section of cluster showing miRNAs that were differentially expressed between Primary and Passage 1 tumors. The Primary and

Passage 1 SP samples cluster separately. Yellow boxes represent miRNAs that were

expressed at levels higher than the average of all expressed miRNAs, and blue boxes represent miRNAs that were expressed at levels lower than the average of all expressed miRNAs.

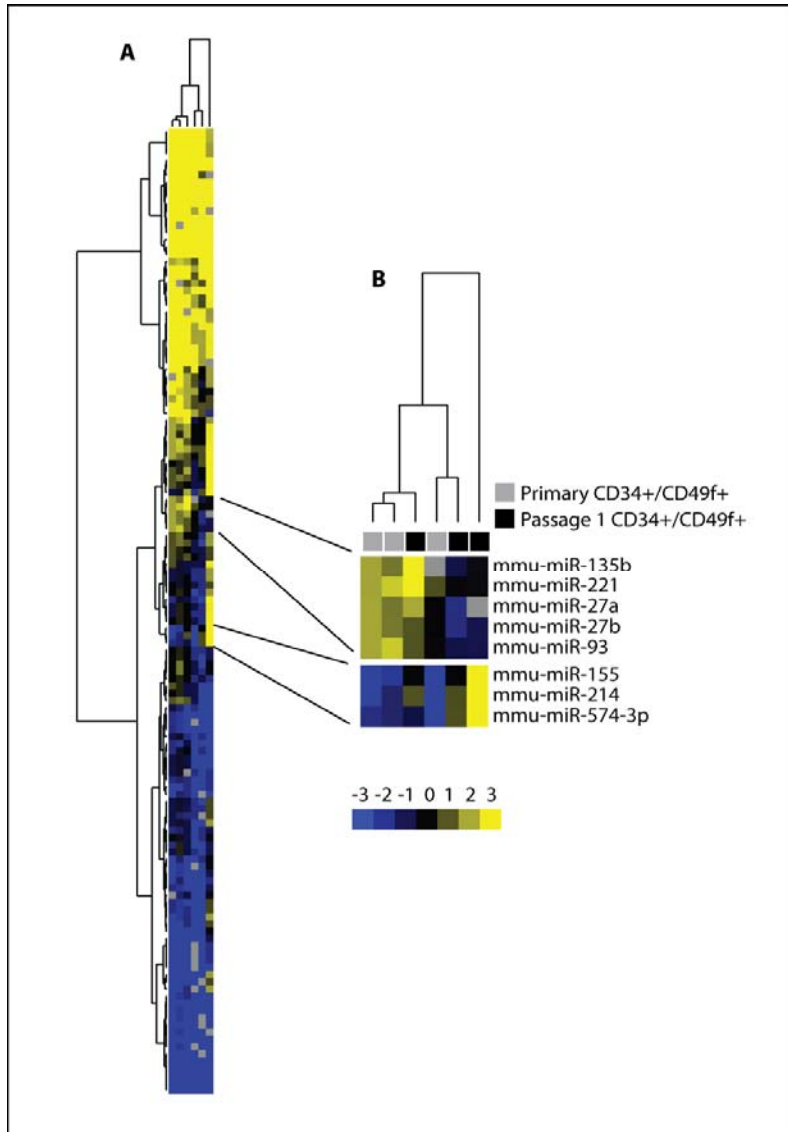
Figure 18. Cluster analysis of miRNA expression in Primary and Passage 1 SP

/CD34+/CD49f+ cells.

(A) Cluster analysis of miRNA expression in Primary and Passage 1 tumor SP- /CD34+/CD49f+ cells.

(B) Magnified region of miRNAs differentially expressed between the Primary and Passage 1 SP- /CD34+/CD49f+

cells. Unlike miRNA expression in the SP cells, Primary and Passage 1 SP- /CD34+/CD49f+ cell miRNA expression did



not cluster according to tumor type. Yellow boxes represent miRNAs expressed at

levels higher than the average of all expressed miRNAs, and blue boxes represent miRNAs that were expressed at levels lower than the average of all expressed miRNAs.

Identification of Differentially Expressed miRNAs

To select miRNAs for further study of their role in metastasis, we identified 10 miRNAs that are most likely to be reliably differentially expressed between the Primary and Passage 1 TIC populations based on raw p-value < 0.05 and the greatest relative fold change from the Primary tumor expression using the standard $\Delta\Delta C_t$ method for analyzing qRT-PCR data (Table 2). Included in the 10 miRNAs with $p < 0.05$ were each of the miRNAs identified as overexpressed in the Passage 1 SP by cluster analysis. These miRNAs also showed the greatest relative fold change from the Primary tumor expression (Table 2). We selected miR-9 and miR-132 from this list of miRNAs, because they were both overexpressed in the Passage 1 SP, but not differentially expressed in the Passage 1 SP⁻/CD34⁺/CD49F⁺ cells. In addition, miR-9 and miR-132, showed the greatest relative fold-change in expression from the Primary to the Passage 1 SP cells.

Detector	P1 SP Mean Δ Ct	Primary SP Mean Δ Ct	$\Delta\Delta$ Ct	Relative Fold Change	Naïve p-Value	q-Value	FDR Value
miR-667	32.82	34.99	-2.17	4.49	0.00209	0.36757	0.36757
miR-9	23.82	31.00	-7.17	144.02	0.00611	0.53772	0.53772
miR-140	21.47	26.46	-4.99	31.80	0.01782	1.04543	0.62484
miR-155	22.81	29.64	-6.82	113.35	0.02216	0.97516	0.62484
miR-132	17.32	29.31	-11.99	4072.50	0.02956	1.04067	0.62484
miR-214	21.51	27.33	-5.83	56.74	0.03193	0.93673	0.62484
miR-199a-3p	20.83	26.65	-5.82	56.50	0.03479	0.87484	0.62484
miR-434-5p	32.85	29.98	2.87	0.1364	0.03760	0.82709	0.62484
miR-125b-3p	29.18	32.67	-3.50	11.28	0.04692	0.91745	0.62484
miR-484	19.16	22.64	-3.48	11.17	0.04857	0.85475	0.62484

Table 2. Biostatistics analysis of miRNA expression changes in SP cells from Primary and Passage 1 tumors. Mean Δ Ct (normalized to U6) values from the three array samples were averaged for each miRNA. $\Delta\Delta$ Ct values were calculated by subtracting the mean Primary SP expression value from the Passage 1 expression value for each miRNA and then the relative fold change in miRNA expression from the Primary to the Passage 1 SP cells was calculated ($2^{-\Delta\Delta$ Ct}). p-values were generated by conducting individual Student's t-tests on the Δ Ct values for each miRNA. From these values, the q-values and FDR values were determined (see methods for details). miRNAs are ranked based on significance, and only those miRNAs with raw p-values <0.05 are displayed.

Validation of miRNA TLDA data for miR-9 and miR-132

To look more closely at how miR-9 and miR-132 are expressed in Primary and Passage 1 tumor SP populations, expression of these miRNAs was examined in a larger cohort of tumor samples. We used qRT-PCR to measure expression in five Primary and 10 Passage 1 SP cell populations. The expression data were again normalized to U6 expression and the miRNA expression in the Passage 1 SP cells was compared to the expression in the Primary SP cells. Validation in a larger sample set showed that although there was a wide variation in miR-9 and miR-132 expression between samples, there was a significant increase in miR-9 ($p=0.002$, Figure 19A) and miR-132 ($p=0.02$, Figure 19B) in the Passage 1 tumor SP cells compared to Primary tumor SP cells.

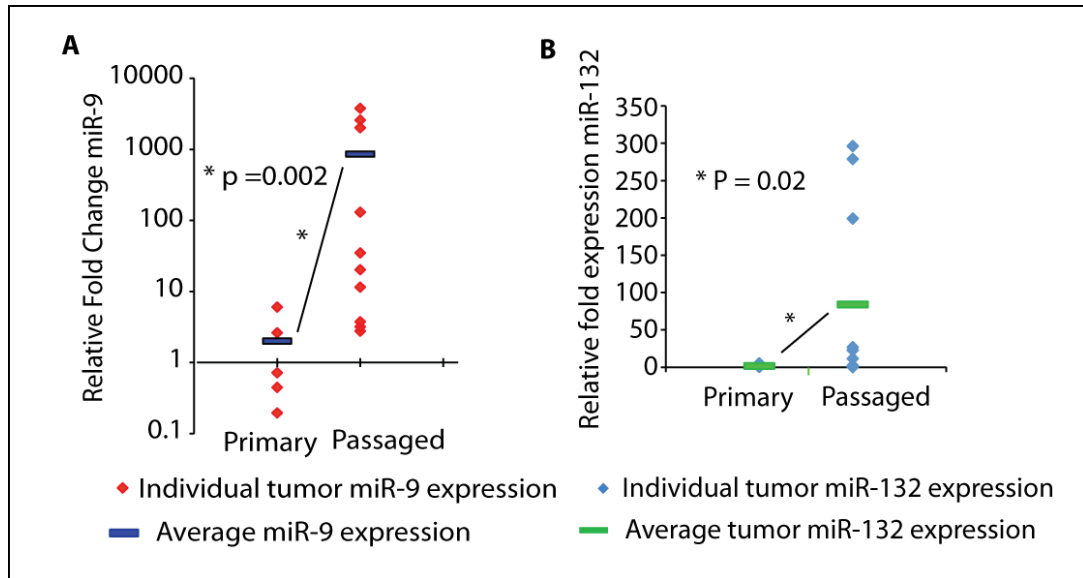


Figure 19. Validation of miR-9 and miR-132 expression in Primary and Passage 1 SP cells. (A) miR-9 expression was validated in 5 Primary and 10 Passage1 tumor SP populations. miR-9 in each individual tumor SP is shown by the red diamonds and the average miR-9 expression for that tumor type is shown by the blue bar. (B) miR-132 expression was also validated in the same tumor SP cells. The blue diamonds represents expression of miR-132 in individual tumor SP cells and the green bar shows the average miR-132 expression. For each miRNA significance was determined using a Student's t-test. miR-9: * $p = 0.002$, and miR-132: * $p = 0.02$.

2.19 Increased miR-9 expression in Kras mutant cells

Previous studies characterizing skin miRNA expression profiles did not identify miR-9 as a highly expressed miRNA in mouse skin [203]. To determine if the Smad4 and/or Kras mutations generated in the hair follicles of the K15.Kras^{G12D}.Smad4^{-/-} mice resulted in increased miR-9 expression, we recreated

these mutations in the HaCaT human epithelial cell line [227] that has normal levels of both Smad4 and Kras. These cells were transduced with a control expression vector, an shRNA against Smad4, an activating Kras-G12V mutation, or both mutations. Efficacy of the Smad4 shRNA was determined using qRT-PCR. Those cells that contained the Smad4 shRNA had a significant reduction in Smad4 expression ($p < 0.001$, Figure 20A). miR-9 expression in these cell lines was then determined using qRT-PCR (Figure 20B). Surprisingly, the Smad4 shRNA cells showed a significant ($p < 0.01$) decrease in miR-9 expression compared to control HaCaT cells. Activation of Kras in the HaCaT cells, on the other hand, significantly increased the expression of miR-9 ($p < 0.001$), although this increase was modest. The combination of Smad4 loss and Kras activation returned miR-9 expression to control levels. By contrast, in mouse epithelial tumor cell lines with Smad4 loss and Kras activation (K15.Kras^{G12D}.Smad4^{-/-} tumor cell lines B911, S4#8 and B931) mir-9 expression was highly and significantly increased (Figure 20C) relative to expression in a K15.Smad4^{-/-} mouse epithelial tumor cell line that does not have an activating Kras mutation (K15.S4^{-/-}). These results suggest that Kras may regulate miR-9 expression, however, since Kras activation in non-tumorigenic cell lines only modestly increased miR-9 expression, this regulation might be modulated by the relative contribution of these mutations in epithelial cells in a context dependent manner.

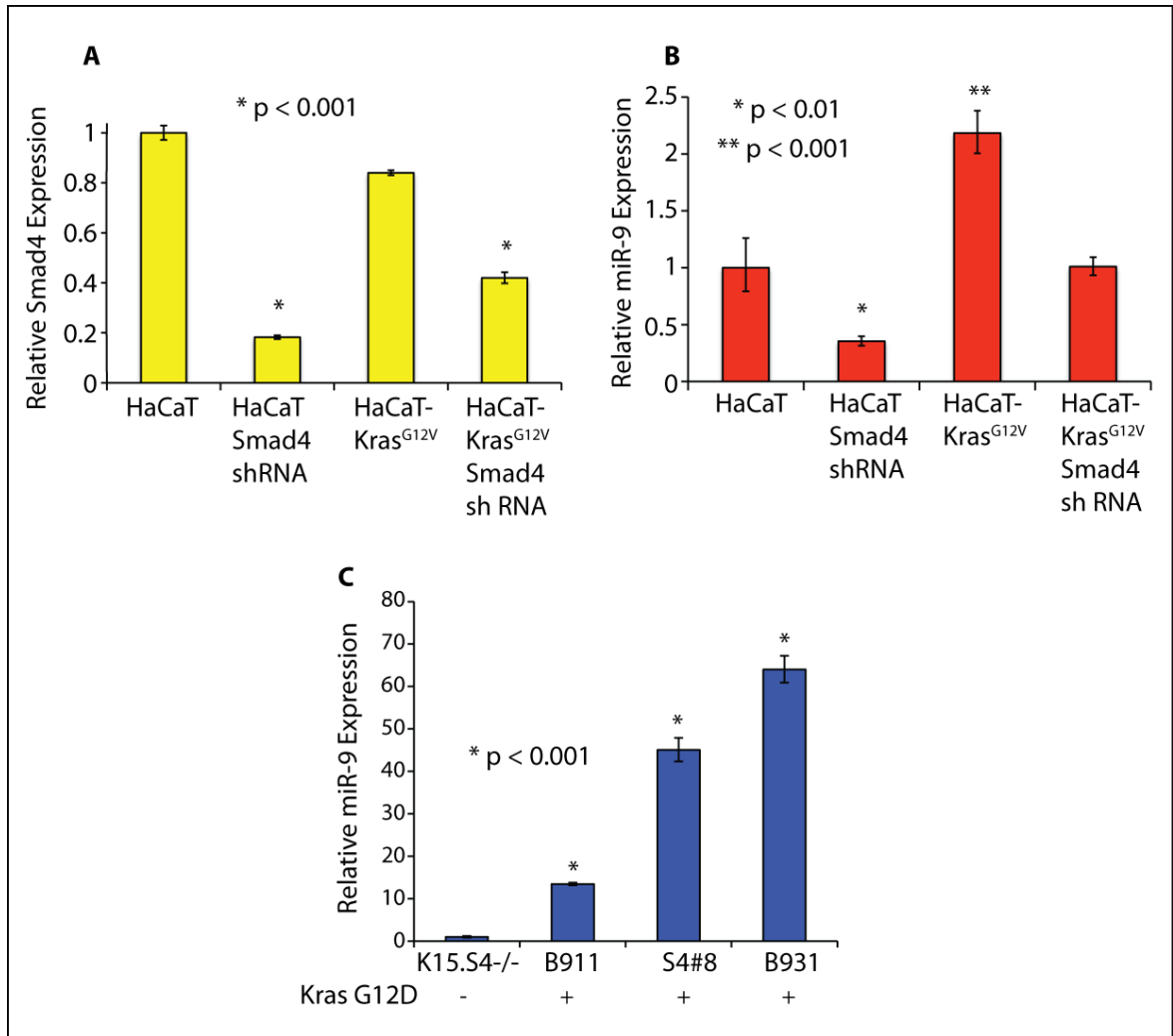


Figure 20. Activation of Kras increases miR-9 expression. (A) Expression of Smad4 in HaCaT human epithelial cells or HaCaT-Kras^{G12V} cells transduced with Smad4 shRNA. (B) Decreased miR-9 expression in HaCaT cells with Smad4 shRNA, and increased miR-9 in HaCaT cells with activated Kras. (C) Increased miR-9 expression in mouse epithelial tumor cell lines with activated Kras. In each Figure, error bars represent standard deviation and significance was determined using a Student's t-test.

2.20 Increased miR-9 in the Passaged Tumor SP is not a Result of Increased c-Myc Expression

In their study of miR-9 in breast cancer metastasis, Ma *et. al.* found that both N- and -Myc could bind to the promoter of two miR-9 primary transcripts (miR-9-1 and miR-9-3) and regulate miR-9 transcription [196]. Interestingly, the TGF β signaling pathway targets and represses the expression of c-myc [228], thus a disruption of TGF β signaling should increase the levels of c-myc in the K15.Kras^{G12D}.Smad4^{-/-} mouse model and subsequently increase miR-9 levels. To determine if an increase in c-myc may be contributing to the increase in miR-9 in the Passage 1 tumor SP cells we used qRT-PCR analysis to determine if c-myc levels were increased at the mRNA level. While there appears to be a very slight increase in c-myc expression in the Passage 1 tumors compared to the Primary tumors, this increase was not significant (p = 0.1) (Figure 21A). To further determine if there was a correlation between c-myc expression and miR-9 expression in the entire tumor set (Primary and Passage 1), we compared the expression of c-myc and miR-9 in each individual tumor (Figure 21B). Again, we saw no significant correlation between the expression of c-myc and miR-9 in the K15.Kras^{G12D}.Smad4^{-/-} tumors.

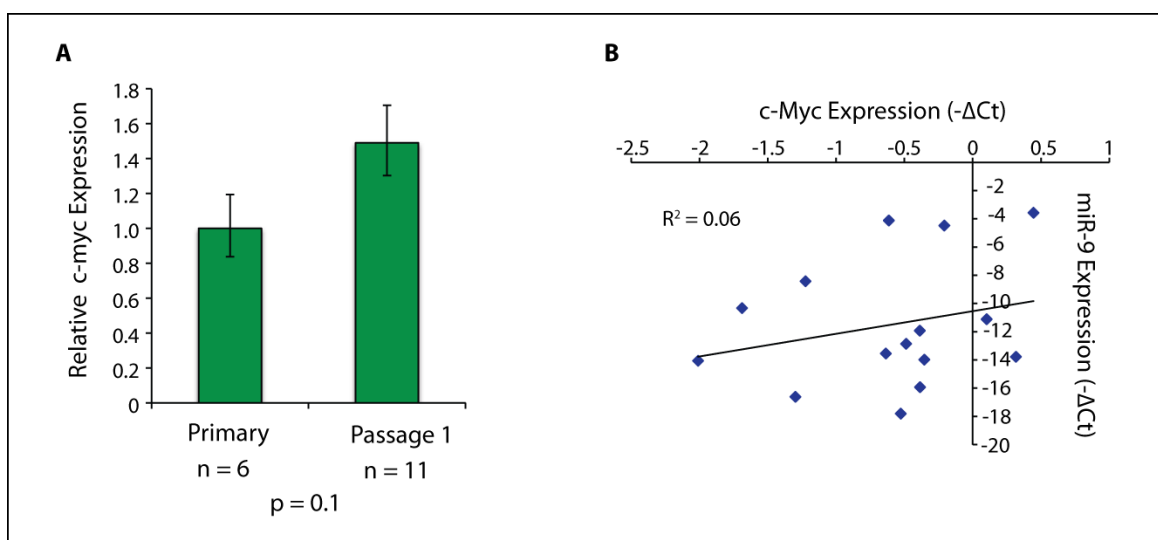


Figure 21. *c-Myc* expression does not correlate with increased *miR-9* expression in the *K15.Kras^{G12D}.Smad4^{-/-}* tumors. (A) qRT-PCR expression analysis of *c-myc* expression in primary and Passage 1 tumor SP cells. Primary tumor SP n = 6, and Passage 1 tumors SP n = 11. Error was calculated using standard error and significance was determined using a Student's t-test (p = 0.1). (B) Correlation between *c-myc* expression and *miR-9* expression in primary and passage 1 tumor SP. Expression was measured using qRT-PCR, and expression values are represented as $-\Delta Ct$.

2.21 *miR-9* regulation of tumor cell growth *in vitro* and *in vivo*

Generation of Tumor Cell Lines with Stable miR-9 Overexpression or Knockdown

To study the role of *miR-9* in the *K15.Kras^{G12D}.Smad4^{-/-}* tumors *in vitro*, we generated cell lines from the passaged tumors (Figure 22). Since these cell lines often exhibited a spindle-like morphology (Figure 22B), *Smad4* expression was measured to ensure the cells were of epithelial origin, rather than fibroblasts, which

would not be expected to show Smad4 loss (Figure 22A). The qRT-PCR analysis of the cell lines compared to wild type (WT) keratinocytes showed a significant loss ($p < 0.005$) of Smad4 mRNA in each of three cell lines isolated from different mice (Figure 22A). miR-9 expression in these cell lines was also evaluated by qRT-PCR. Each of the cell lines tested showed a significant increase in miR-9 expression compared to WT keratinocytes (Figure 22C), although there was a wide range of miR-9 expression.

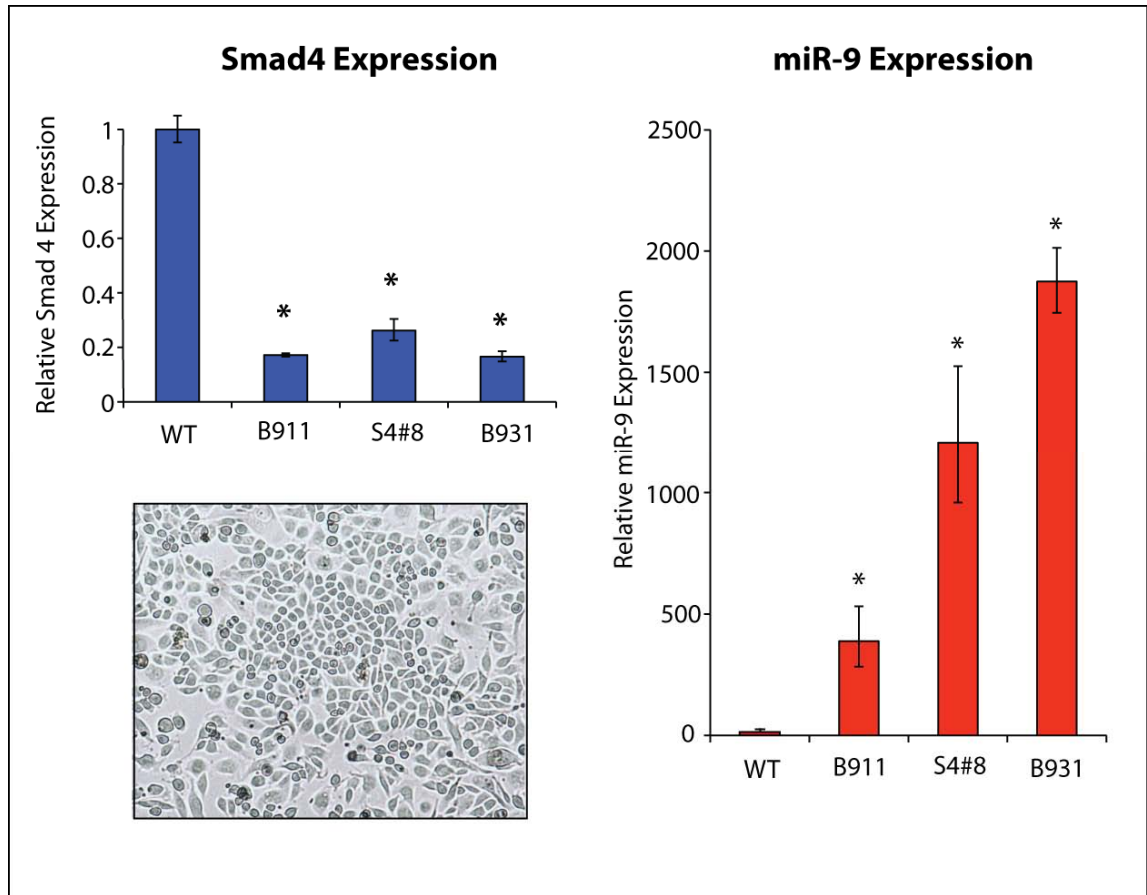


Figure 22. Generation of *K15.Kras^{G12D}.Smad4^{-/-}* tumor cell lines. (A) Loss of *Smad4* expression in *K15.Kras^{G12D}.Smad4^{-/-}* tumor cell lines compared to WT Keratinocytes. Expression was measured by qRT-PCR and analyzed using a standard $\Delta\Delta C_t$ analysis. Significance was determined using a student's t-test: * $p < 0.005$. (B) Representative image of *K15.Kras^{G12D}.Smad4^{-/-}* tumor cell line morphology. (C) miR-9 expression in *K15.Kras^{G12D}.Smad4^{-/-}* tumor cell lines compared to WT Keratinocytes. Expression was measured by qRT-PCR and the data were normalized to U6 expression. miR-9 expression in tumor cell lines is expressed relative to expression in WT

*keratinocytes. Significance of miR-9 overexpression in tumor lines was determined using a Student's t-test: * p < 0.01.*

To study the effect of miR-9 overexpression in tumor cells, we utilized a lentiviral vector containing the pre-miRNA, miR-9-1. Transduction of pre-miR-9 in to the cell lines with the lowest intrinsic miR-9 expression (B911) led to increased mature miR-9 expression, as determined by qRT-PCR (Figure 23A). Functional activity of miR-9 in these cells was determined using a reporter assay in which the miR-9 target site was positioned in the 3'UTR of a luciferase reporter gene. This miR-9 luc reporter (Signosis) was introduced into either a GFP transduced control cell line, or the miR-9 transduced cell line. The increased activity of miR-9 in the pre-miR-9 transduced cell lines resulted in a decrease in luciferase activity (Figure 23B), indicating that the transduced pre-miR-9 was giving rise to functional mature miR-9 in the tumor cell lines. To further assess miR-9 function, we examined the expression of a reported miR-9 target gene, Nfkb1, whose expression is altered at the miRNA level [207, 229]. The miR-9 transduced cells showed a 40% reduction of Nfkb1 mRNA levels compared to the control cell line by qRT-PCR, further demonstrating functional activity of the transduced miR-9 (Figure 23C).

To knockdown miR-9 expression in the tumor lines we used a lentiviral anti-miR approach. This "miR-Zip" (System Bioscience) vector produces shRNAs that are processed in to short single stranded anti-miRNAs that competitively bind the miRNA of interest. To generate the stable line we chose the K15.Kras^{G12D}.Smad4^{-/-}

cell line with the highest intrinsic miR-9 expression (B931). Since the miR-Zip anti-miRNAs do not consistently alter mature miR-9 expression by qRT-PCR, we measured the activity of miR-9 in the control (non-silencing GFP vector) and Zip-9 stable cell lines by luciferase reporter assay (Figure 23D). The B931 Zip-9 cell line showed a significant increase in luciferase activity ($p = 9 \times 10^{-5}$) compared to the control cell line, indicating that the line has reduced levels of functional miR-9. To further test the activity of the Zip-9 knockdown in the B931 cells, we measured the Nfkb1 mRNA levels in the Zip-9 cells compared to controls (Figure 23E). The B931 Zip-9 cells showed a small but significant ($p = 0.001$) increase in Nfkb1 levels compared to the control line supporting the miR-9 luciferase activity data.

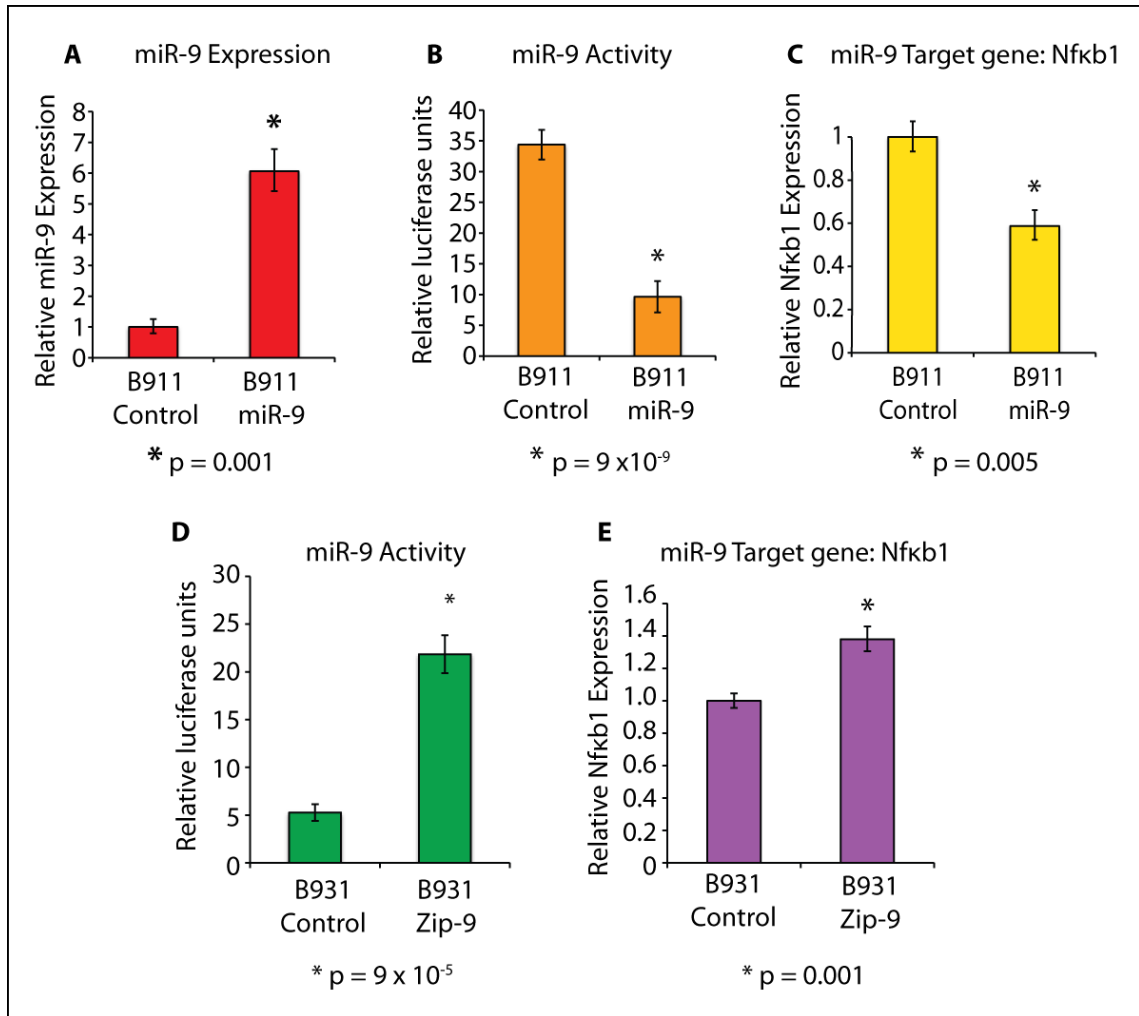


Figure 23. Generation of mouse tumor cell lines with stable overexpression or knockdown of miR-9. (A) Increased expression of mature miR-9 in pre-miR-9 stably transduced B911 cell line. Expression was measured by miRNA specific qRT-PCR. (B) Increased miR-9 activity in the stably transduced B911 cell line. Activity was measured using a luciferase construct containing a miR-9 target sequence 3' to the luciferase gene. miR-9 binds to the target and causes a reduction of luciferase protein levels. (C) Reduced expression of a known miR-9 target gene, *Nfkb1*, in pre-miR-9

stably transduced B911 cell line. (D) Increased miR-9 activity in B931 cells containing the Zip-9 miR-9 knockdown vector. (E) Increased expression of *Nfkb1* in B931 Zip-9 cells compared to control. In each Figure, error bars represent standard deviation and significance was determined using a Student's *t*-test.

The effect of miR-9 on tumor cell growth and proliferation

To determine how miR-9 overexpression affects the behavior of the tumor cells we looked at cell growth and proliferation in the miR-9 overexpressing and knockdown cells compared to control cells. Cell cycle analysis of the high miR-9 expressing cells, B911-miR-9 (Figure 24A) showed a significant increase in the percent of cells in G1 phase of the cell cycle compared to controls ($p < 0.005$), and conversely, the low miR-9 expressing B931-Zip-9 cells showed a significant decrease in the percent of cells in G1 ($p < 0.005$, Figure 24B). While the differences in the percent of cells in G1 between lines with high miR-9 and low miR-9 are not overly striking, the consistency of the data indicates that miR-9 inhibits cell proliferation *in vitro*.

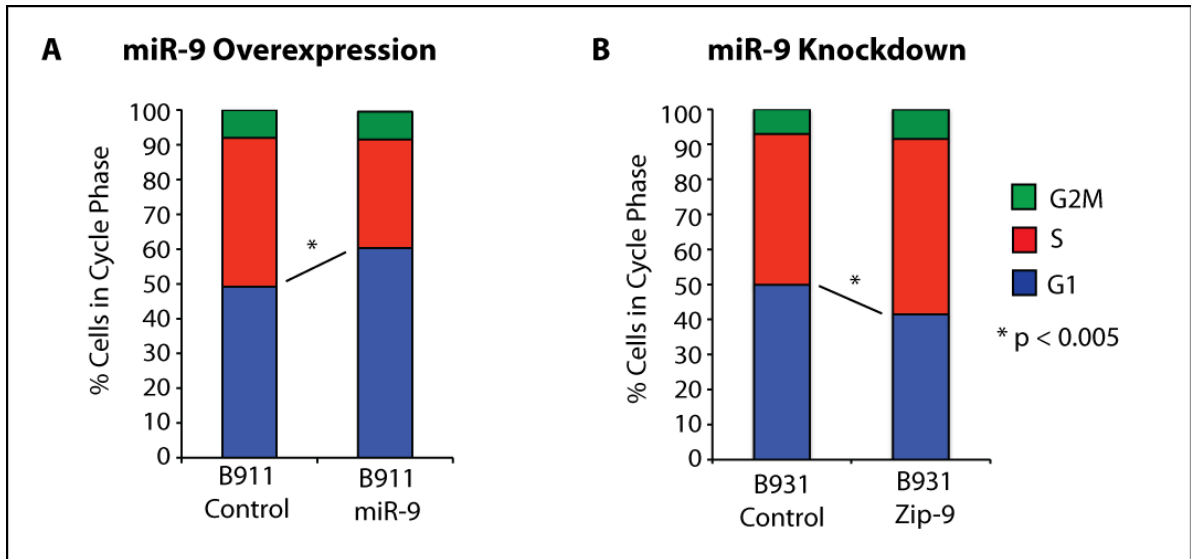


Figure 24. miR-9 slows cell cycling. (A) miR-9 overexpression increases the percent of cells in G1 compared to control in B911 mouse tumor cell lines. (B) Knockdown of miR-9 in the B931 mouse tumor line decreases the percent of cells in G1 and increases the percent in S phase. Each cell cycle assay was done in triplicate. Significance was assessed using a Student's t-test, $p < 0.005$ in each case.

We further examined the effect of miR-9 overexpression on cell proliferation *in vitro*. Proliferation of B911-miR-9 cells compared to control was measured using a WST-8 colorimetric proliferation assay. Consistent with the cell cycle data, the miR-9 overexpressing cells showed decreased proliferation compared to control (Figure 25A). Since a number of factors in the microenvironment may affect the growth of tumor cells *in vivo*, we wanted to determine if miR-9 also inhibited the growth of tumors after subcutaneous injection of the B911-miR-9 tumor cell lines. First, we injected 1×10^3 cells in to the flank of immunocompromised athymic nude

mice and followed tumor growth over 35 days. Interestingly, there was no clear difference in tumor growth between the control and mir-9 overexpressing cells (Figure 25B). The aggressive growth of these tumor lines in the immunocompromised mice prompted us to repeat the *in vivo* growth assay in immunocompetent C57Bl/6 (B6) wild type mice. Since injections of small numbers of cells in these mice produced varying results with low tumor initiation rates, we chose to inject a much larger number of tumor cells (5×10^5 cells per mouse) in combination with matrigel. Tumor kinetics assays were done with both the high miR-9 expressing B911-miR-9 (Figure 25C) and low miR-9 expressing B931-Zip9 (Figure 25D) cell lines and compared to their respective control lines. Each of these tumor types shows an initial rapid growth phase, which is likely due to the matrigel medium. Interestingly, at around three weeks it appears as if the miR-9 overexpressing line started to show an increase in tumor growth compared to the control line (Figure 25C), and the B931-Zip-9 showed a decrease at this same time point (Figure 25D). While these experiments need to be carried out further, these preliminary results indicate that in an immunocompetent system, miR-9 may support tumor initiation. The difference in tumor cell growth between immunocompetent and immunocompromised mice indicates that the tumor microenvironment plays an important role in the regulation of tumor kinetics *in vivo*, and that miR-9 may regulate the interaction of the tumor cells with the microenvironment.

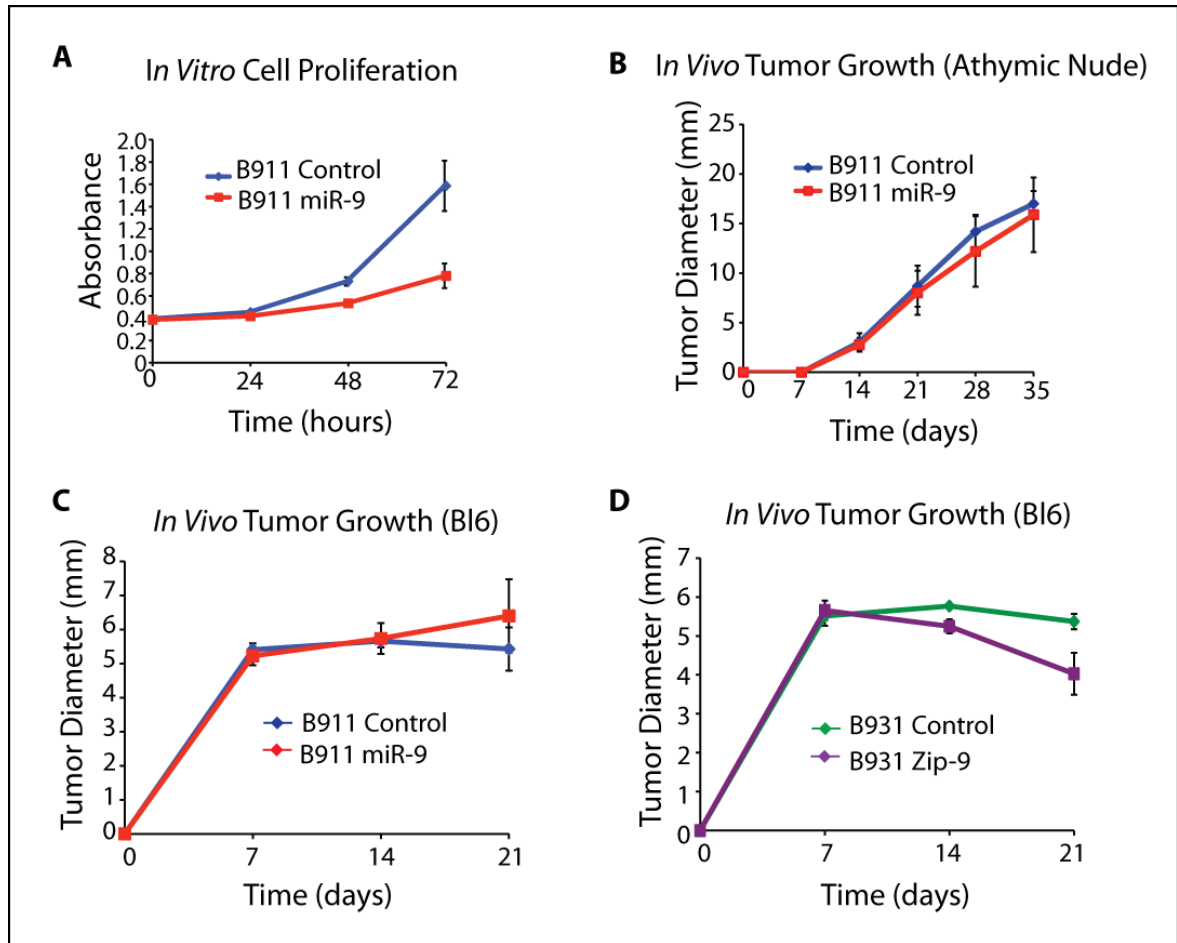


Figure 25. Context dependent effect of miR-9 on tumor cell growth. (A) miR-9 overexpression inhibits B911 tumor cell growth in vitro. Cell proliferation was measured using a WST-8 colorimetric assay. Error bars represent standard deviation between replicate wells. (B) miR-9 overexpression in B911 tumor cells does not alter tumor growth in immunosuppressed athymic nude mice. 1×10^3 control or miR-9 overexpressing cells were subcutaneously injected into athymic nude mice and tumor growth was measured weekly. Error bars represent standard deviation. (C) miR-9 overexpression may increase tumor growth in immunocompetent mice. 5×10^5 control ($n = 6$) or miR-9 overexpressing B911 tumor cells ($n = 6$) were injected subcutaneously

in to C57Bl/6 (B6) mice. Error bars represent standard error. (D) Inhibition of miR-9 may inhibit tumor growth in immunocompetent mice. 5×10^5 control ($n = 6$) or miR-9 knockdown (Zip-9) cells ($n = 6$) were injected subcutaneously in to Bl6 mice and tumor size was measured weekly. Error bars represent standard error.

2.22 miR-9 expression is associated with increased SP size and chemoresistance.

miR-9 and miR-132 expression correlates with SP size and SPCC tumor histology.

Since SP size was significantly larger in metastatic tumors, we wanted to determine if miR-9 might play a role in the regulation of the SP and metastasis. To determine if the expression of the miRNAs identified in the array screen were correlated with SP size we plotted miR-9 and miR-132 expression against SP size for each tumor (Figures 26 A and B). These plots show that miR-9 and miR-132 expression and SP size fall in to two groups; those with high miR-9 and miR-132 expression and large SP fractions, and those with low miR-9 and miR-132 expression and small SP fractions. Since SP size is much larger in SPCC tumors compared to more differentiated tumors, we then further compared miR-9 and miR-132 expression with tumor type, which revealed an increase in miR-9 and miR-132 expression in the less differentiated tumors (Figures 26 C and D). In the SPCC tumors, the expression of miR-9 and miR-132 was significantly increased compared to each of the more differentiated tumor types ($p < 0.01$). These data, which show a clear increase in SP size and mir-9 and miR-132 expression in the EMT-like and

metastatic SPCC tumors suggest that miR-9 and miR-132 may play a role in regulating the SP fraction during EMT and metastasis.

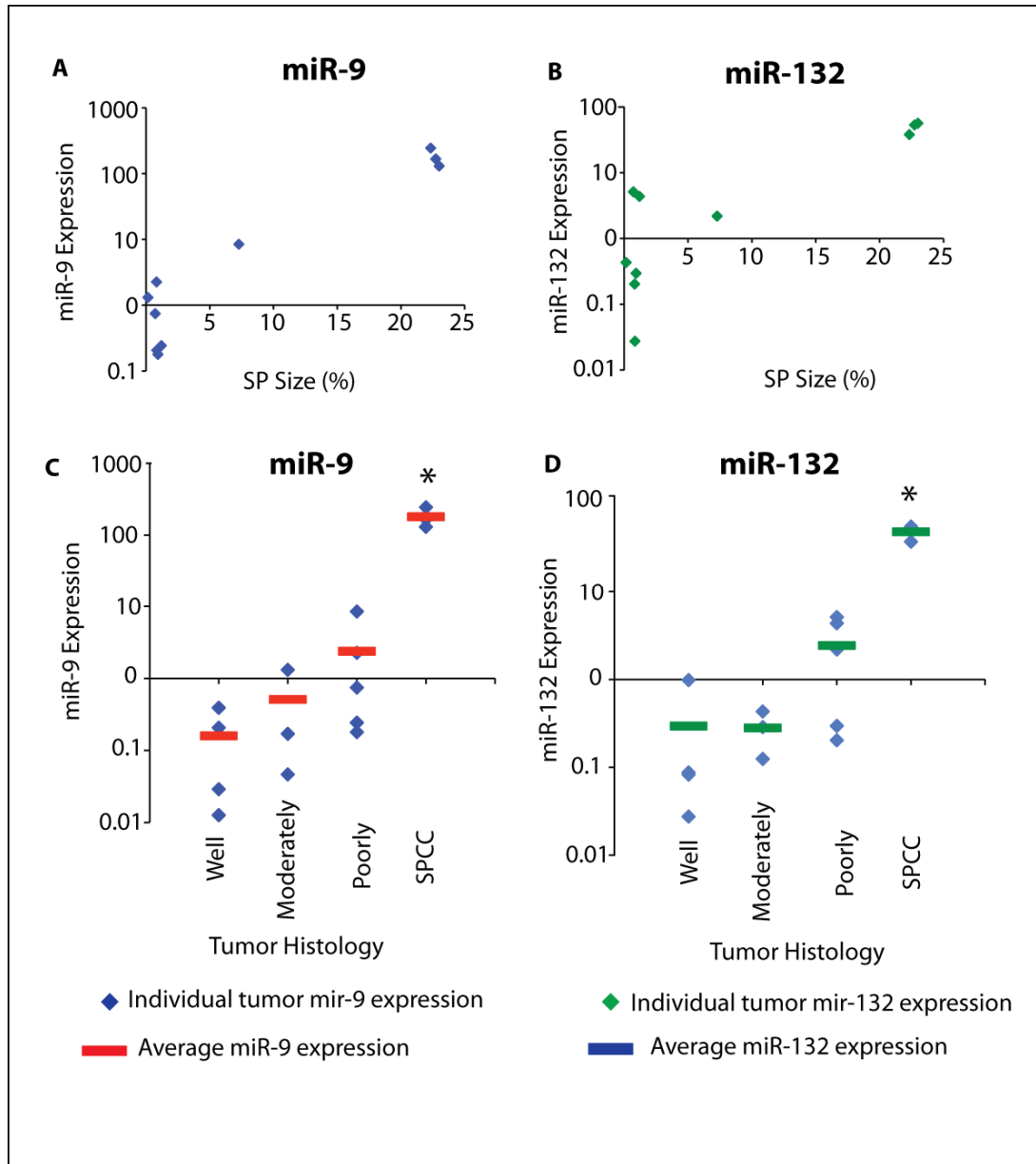


Figure 26. miR-9 and miR-132 expression correlates with SP size and tumor histology. (A) Correlation between SP size and miR-9 expression. (B) Correlation between SP size and miR-132 expression. (C) miR-9 expression in the SP cells from

*each tissue type. (D) miR-132 expression in the SP cells from each tissue type. miR-9 and miR-132 expression was measured using qRT-PCR. The data were analyzed by normalizing to the U6 small RNA and relative miRNA expression calculated using the standard $\Delta\Delta Ct$ method comparing the expression of each miRNA to the average miRNA expression in all of the samples. In Figures C and D, miR-9 and miR-132 expression was significantly increased in SPCCs relative to each of the other tumor histology types. Significance determined using a Student's t-test: * $p < 0.01$.*

The multidrug resistance gene Abcb1a is increased in Passage 1 SP cells

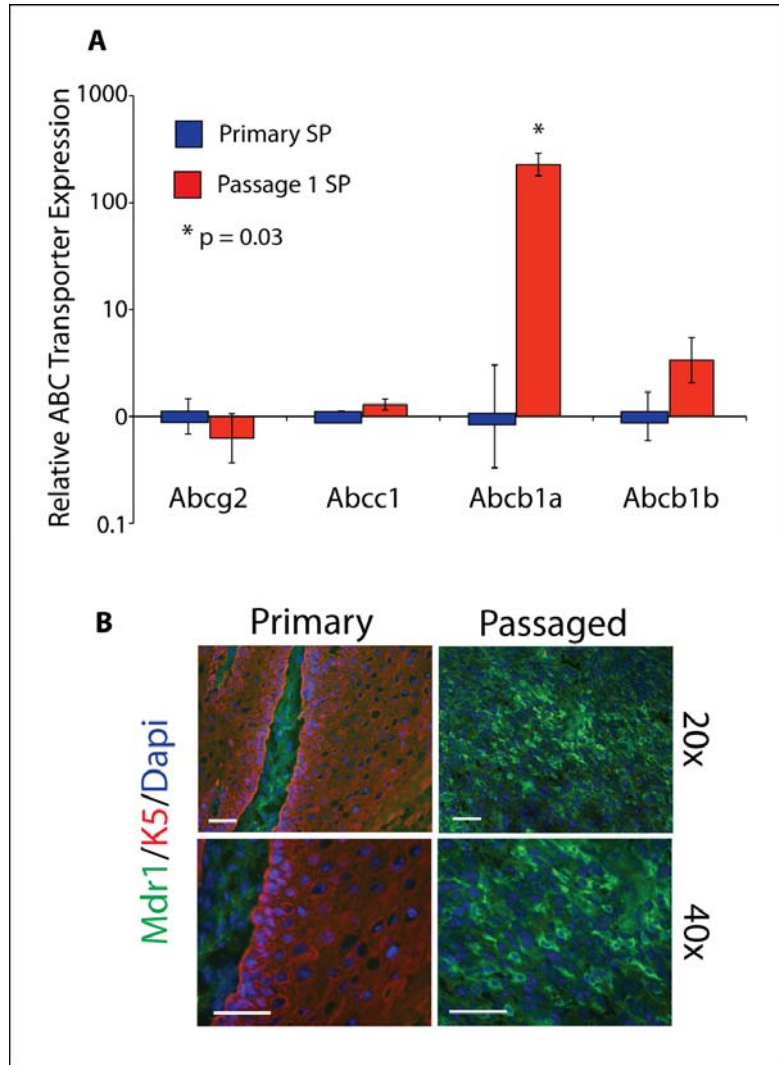
The side population phenotype is due to the presence of ABC transporters on the cell surface. This family of transporters consists of upwards of 40 distinct members [161]. In order to determine which of these transporters may be responsible for the increase in the SP size in the Passage 1 tumors, we screened four of the transporters that are most commonly associated with chemoresistance in tumors, Abcg2 (BCRP), Abcc1 (MRP) and Abcb1a and Abcb1b which both encode for the protein Mdr1 (p-glycoprotein). Expression analysis of these genes in the SP cells from the primary and Passage 1 tumors by qRT-PCR showed that only Abcb1a was significantly increased in the SP cells from the Passage 1 tumors (Figure 27A).

In mice, the genes for Abcb1a and Abcb1b code for a single protein, Mdr1/p-glycoprotein. To determine whether the Mdr1 protein expression was increased in the mouse tumors with larger SPs, we stained well differentiated (lowest miR-9 levels) and SPCC (highest miR-9 levels) tumors for Mdr1 (Figure 27B). The Passage

1 SPCC tumors showed a clear increase in Mdr1 staining (green), correlating with a loss of Keratin staining (red).

Figure 27. Increased Abcb1a (Mdr1) in the Passage 1 Side population. (A)

Abcb1a is increased at the mRNA level in Passage 1 tumor SP cells. qRT-PCR expression analysis was conducted on the SP cell fractions from ten Passage 1 and five Primary tumors for the four best studied ABC transporters in tumors.



Expression of the transporter in the Passage 1 tumor SPs was compared to the expression in the Primary tumor SPs. Error bars represent standard error and significance was determined using a Student's t-test. (B) Immunofluorescence staining for Mdr1 in tumors. Mdr1 expression (green) is increased in Passage 1, SPCC tumors compared to primary, well-differentiated tumors. Sections were counter stained with

Keratin 5 (red) and Dapi (blue). Top panels show sections magnified to 20x and lower panels show sections magnified to 40x. Scale bar represents 50 μ m in each panel.

Because Abcb1a expression is increased in the Passage 1 tumors, particularly in SPCC tumors, we investigated whether Abcb1a expression levels varied with SP size, tumor histology or miR-9 expression. Surprisingly, when we plotted Abcb1a expression against SP size in individual tumors, there was no association ($R^2 = 0.20$) (Figure 28A). We did, however, find an increase in Abcb1a in both poorly differentiated and SPCC tumors, but these data were not significant due to low numbers of well- and moderately-differentiated tumors included in the analysis (Figure 28B). We also found a slight correlation of Abcb1a expression with miR-9 expression ($R^2 = 0.45$) (Figure 28C). Taken together these data suggest that while Abcb1a may be up-regulated in less-differentiated Passage 1 tumors, which generally have larger SP populations, other mechanisms, including regulation via miR-9 and miR-132 determine SP size in these tumors.

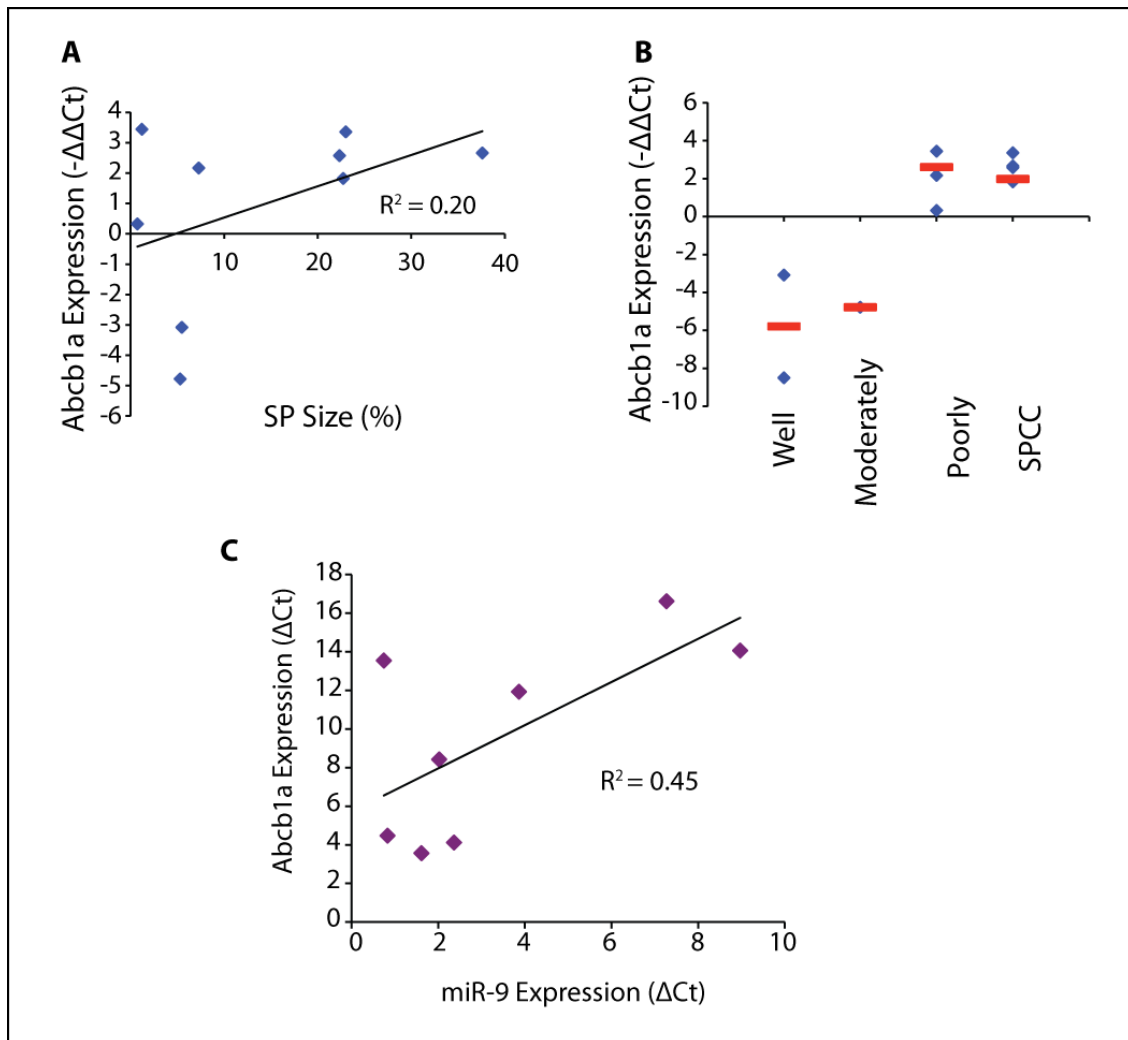


Figure 28. Variable association between *Abcb1a* expression and SP size, tumor histology and *miR-9* expression. (A) *Abcb1a* expression does not correlate with SP size in all tumors. *Abcb1a* expression, displayed as the inverse $\Delta\Delta\text{Ct}$ value relative to the average *Abcb1a* expression, was plotted against SP size for the corresponding tumor. $R^2 = 0.20$ indicating that there is no correlation between *Abcb1a* expression and SP size. (B) *Abcb1a* expression is increased in poorly differentiated and SPCC tumors. *Abcb1a* expression ($-\Delta\Delta\text{Ct}$) was plotted against tumor histology for each

tumor. Blue diamonds represent individual tumors and red bars represent the average *Abcb1a* expression for each tumor type. (C) Slight correlation between miR-9 and *Abcb1a* expression. ΔCt values for miR-9 and *Abcb1a* were plotted against each other for each tumor. $R^2 = 0.45$ indicating a low level of correlation between the two variables.

Context dependent increase in Abcb1a after miR-9 overexpression

To determine if miR-9 may regulate the expression of the ABC transporters, we generated a number of cell lines overexpressing miR-9. First we used the lentivirally transduced B911 cells to screen for any transporters that may be altered after miR-9 overexpression. The B911 miR-9 cell line has only a modest increase in miR-9 expression over the control cells (Figure 29A); however, when we screened this line for expression of the ABC transporters, we saw a very large increase in the expression of *Abcb1a* (Figure 29B). There was also a small, but significant increase in *Abcb1b* expression in the B911 miR-9 cells compared to control. The expression of *Abcg2* and *Abcc1* was also slightly decreased in this line compared to control. The dramatic increase in *Abcb1a* was somewhat surprising since the miR-9 levels were not dramatically increased in this line. To further determine if miR-9 may be responsible for the increase in *Abcb1a* expression, we transiently transfected a pre-miR-9 small RNA in to three K15.Kras^{G12D}.Smad4^{-/-} cell lines, B911, S4#8, and B931. Each of these lines showed a dramatic increase in the expression of mature miR-9 after transfection (Figure 29C). In each of these lines there was an increase in *Abcb1a* expression; however, only S4#8 and B931, showed a significant increase in

Abcb1a expression (Figure 29D). Interestingly, these lines also have the highest intrinsic levels of miR-9.

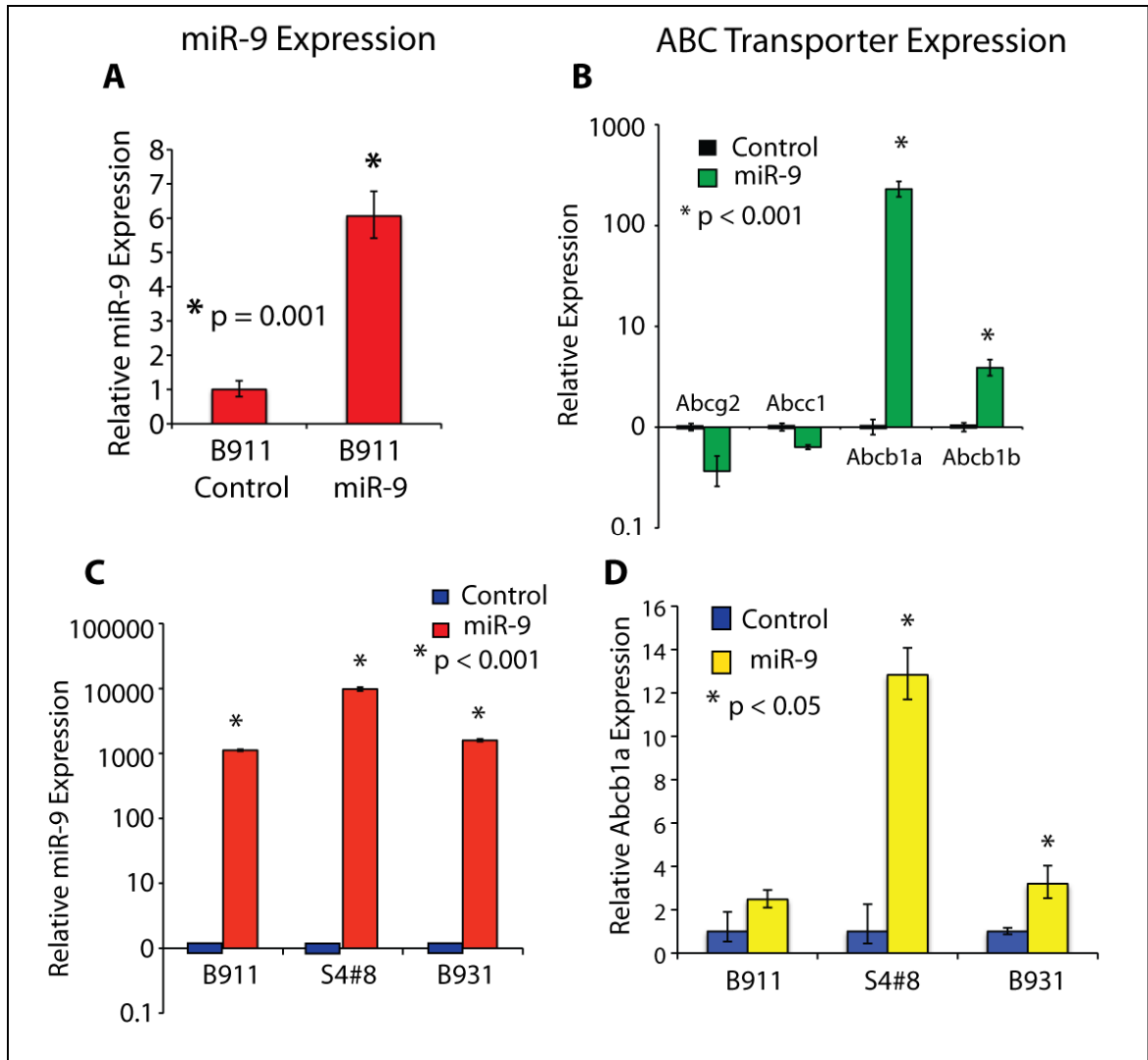


Figure 29. Context dependent increase in Abcb1a after miR-9 overexpression.

(A) miR-9 expression level in lentivirally transduced B911 tumor cell lines compared to control. (B) Screen for ABC transporter expression in the B911 lentiviral miR-9 cells compared to control shows an increase in Abcb1a expression. (C) Transient

transfection of miR-9 in to three different mouse tumor lines shows large increases in mature miR-9 expression compared to controls. (D) Abcb1a expression in transiently transfected miR-9 tumor lines compared to controls shows varying degrees of increases in Abcb1a. In each Figure, error bars represent standard deviation and significance was determined using a Student's t-test.

To further determine if miR-9 may regulate the expression of Abcb1a, we knocked out miR-9 expression in two K15.Kras^{G12D}.Smad4^{-/-} cell lines, B911 and B931. Knockdown efficiency was analyzed by miR-9 knockdown of a luciferase target (Figure 30A). Each of the knockdowns showed a significant decrease in miR-9 activity, by increased expression of the luciferase target ($p < 0.001$). However, neither of the lines showed a significant change in Abcb1a expression (Figure 30B). This disparity between the effect of miR-9 overexpression and miR-9 knockdown in the K15.Kras^{G12D}.Smad4^{-/-} cell lines suggests that any role miR-9 may play in regulation of Abcb1a is unlikely to be direct.

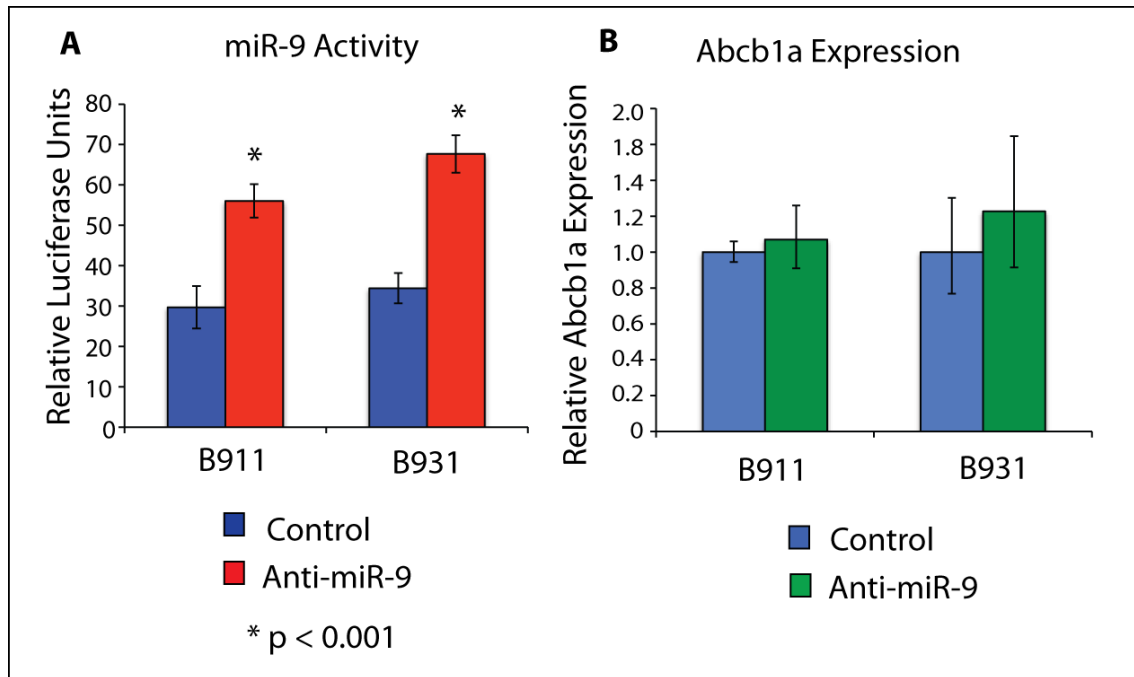


Figure 30. miR-9 knockdown does not alter Abcb1a expression. (A) Increased luciferase expression in mouse cell lines with miR-9 knockdown. (B) No change in Abcb1a expression in mouse cell lines after miR-9 knockdown. Error bars represent standard deviation and significance was determined using a Student's t-test.

Abcb1a overexpression increases the SP size and chemoresistance

While it is not clear if miR-9 regulates the expression of Abcb1a in the K15.Kras^{G12D}.Smad4^{-/-} tumors and cell lines, we wanted to confirm whether Abcb1a was contributing to the side population. To accomplish this goal, we made use of the B911 miR-9 lentivirally transduced line that expressed Abcb1a at levels greater than 100 fold higher than control lines. B911 control cells with low Abcb1a expression and B911 miR-9 cells with high Abcb1a expression were stained with

Hoechst dye then analyzed by flow sorting for the effluxing population. To compare the two cell lines, the gating on the Flow analysis was kept the same between samples. While the SP was generally quite small (~0.7%) in the B911 control cell lines (Figure 31A), the increase in *Abcb1a* in the B911 miR-9 cells dramatically increased the SP size to 30% or greater of the viable cells (Figure 31B). In addition, the gated fraction of the non-SP cells decreased from ~23% in the control cell line to ~0.23% in the B911 miR-9 cells. To ensure that the large SP in the *Abcb1a* overexpressing cells was a true SP, and not an artifact from poorly stained cells, we treated the cells with verapamil to block the ABC transporters. Verapamil treatment in these cells completely inhibited the SP fraction and restored the size of the non-SP (Figure 31C). These results were consistent between samples and showed a significant difference ($p < 0.05$) in the SP size between control and *Abcb1a* overexpressing cells (Figure 31D).

To determine whether the increase in SP size was maintained *in vivo*, we injected 1×10^3 B911 control or B911 miR-9 tumor cells into the flanks of athymic nude mice. Once the tumors grew, they were harvested and analyzed by flow cytometry for the SP. While the *in vivo* tumor environment supported a larger SP fraction in the control cells (Figure 31E), an enlarged SP fraction was still detected in the *Abcb1a* overexpressing tumors (Figure 31F). Again, verapamil treatment of these tumor cells completely inhibited the SP fraction and increased the size of the non-SP fraction (Figure 31G). These results were reproducible between tumors and

showed a significant difference ($p = 0.003$) in the SP size between control and miR-9 overexpressing cells (Figure 31H).

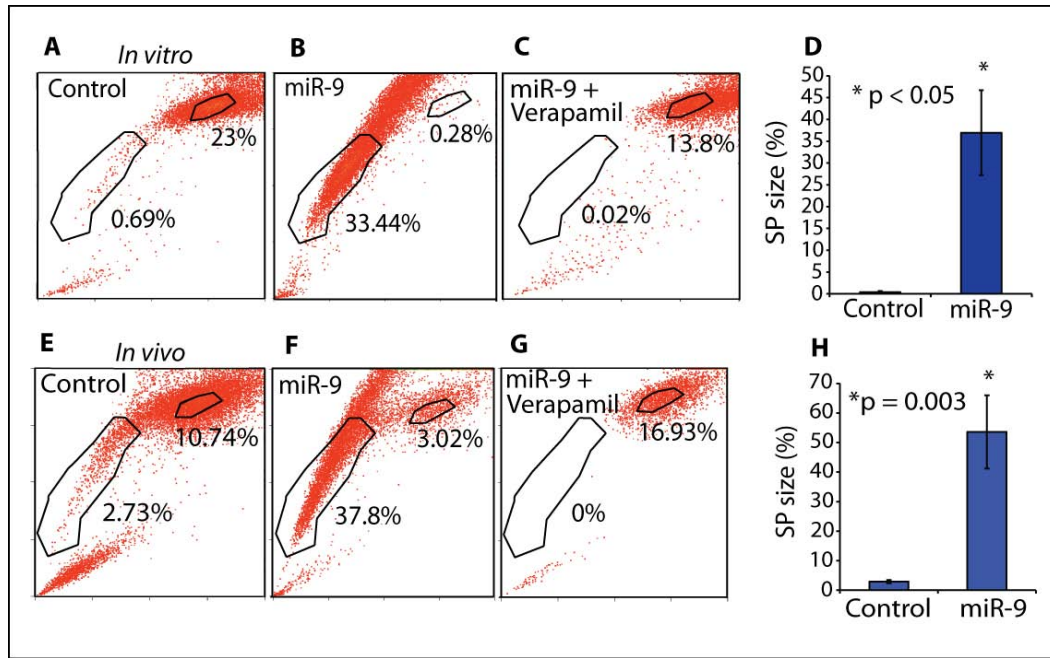


Figure 31. *Abcb1a* overexpression increases the size of the Side Population.

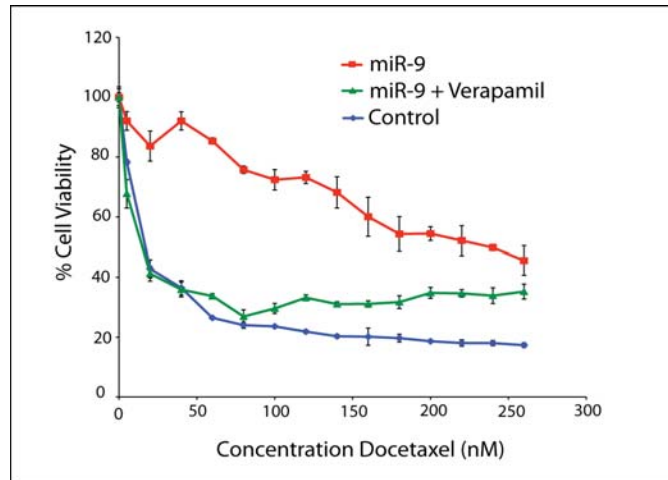
Control B911 cells (low *Abcb1a*) (A) and the lentivirally transduced miR-9 overexpressing B911 cells (high *Abcb1a*) (B) were sorted for the Hoechst dye excluding side population. miR-9 overexpressing, *Abcb1a* high, cells exhibited extremely large SP cell fractions, upwards of 30% (B). Verapamil treatment completely removes the SP from these cells (C). Overall the increase in *Abcb1a* shifts the SP size from approximately 0.7% to 35% of the viable cells in vitro. Tumor cells were sorted in triplicate and significance was determined using a Student's t-test: $*p < 0.05$ (D). SP size of the low *Abcb1a* control (E) and high *Abcb1a*, miR-9 overexpressing (F) cells after subcutaneous injection and tumor growth in vivo. The enlarged SP fraction in the cells with high levels of *Abcb1a* was completely removed by treatment of the cells

*with verapamil (G). Tumors analyzed in triplicate showed an increase in SP size from 3% to 50% of the viable cells. Significance was determined using a Student's t-test: * p = 0.003.*

Since the ABC transporters function in part by effluxing chemotherapeutic drugs from tumor cells, we wanted to determine if the increase in Abcb1a in the B911 miR-9 cell line contributed to chemoresistance. We treated the B911 miR-9 cells and B911 control cells with increasing doses of the microtubule stabilizing agent, Docetaxel. After treating the cells for 48 hours we used a WST-8 assay to determine the percent of live cells remaining after Docetaxel treatment. The control cells quickly responded to the Docetaxel treatment with a LD₅₀ of ~20nM, however, the Abcb1a overexpressing B911 miR-9 cells showed a clear resistance to Docetaxel treatment with a LD₅₀ of ~240nM Docetaxel (Figure 32). Since miRNAs have many targets we wanted to be sure that the chemoresistance seen in the B911 miR-9 cells was due to the increased expression of Abcb1a rather than some other miR-9 mediated mechanism. Treatment of the cells with Verapamil to block the transporters in the miR-9 cells increased the sensitivity of the cells to similar levels as the control cells.

Figure 32. Increased *Abcb1a* expression results in increased chemoresistance.

Control B911 cells expressing low levels of *Abcb1a* (blue) and B911 miR-9 overexpressing cells



expressing high levels of *Abcb1a* (red) were treated with increasing concentrations of Docetaxel. The B911 miR-9 overexpressing cells were also treated with Verapamil in addition to Docetaxel (green). Cell viability was determined using a WST-8 assay 48 hours after treatment with the drug.

Taken together these observations support a role for *Abcb1a* in mediating dye efflux *in vitro* and *in vivo* in K15.Kras^{G12D}.Smad4^{-/-} tumors and cell lines, as well as chemoresistance when highly expressed. The role of miR-9, however, remains unclear due to the variability of induction of *Abcb1a* expression in miR-9 overexpressing cells.

2.23 miR-9 Regulation of Tumor Cell Invasion and Migration

Studies have shown SP cells to be a more invasive and migratory population than the non-SP cells, indicating that this TIC may be involved in metastasis [230]. Since the more metastatic Passage 1 tumors had larger SP fractions and increased

levels of miR-9, we wanted to see if miR-9 overexpression may regulate invasion and migration in the SP. Using a trans-well migration assay, we plated either miR-9 overexpressing cells or control cells in the trans-well in serum free medium, the bottom well was filled with medium containing serum as a chemoattractant. The B911 K15.Kras^{G12D}.Smad4^{-/-} tumor cells showed an increase in migration upon miR-9 overexpression (Figure 33A). To determine the invasive abilities of these cells, we used trans-wells coated with a matrigel basement membrane. The miR-9 overexpressing cell lines showed significantly increased invasion through the matrigel membrane compared to the controls (Figures 33B). Interestingly, the increase in invasion after miR-9 overexpression was far more pronounced than the increase in migration, suggesting that miR-9 may be more important for the invasive properties of the SP cells. Knockdown of miR-9 in the B931 K15.Kras^{G12D}.Smad4^{-/-} tumor cells showed a slight decrease in migration (Figure 33C), and a decrease in invasion (Figure 33D), further supporting a role for miR-9 in invasion and migration of tumor cells.

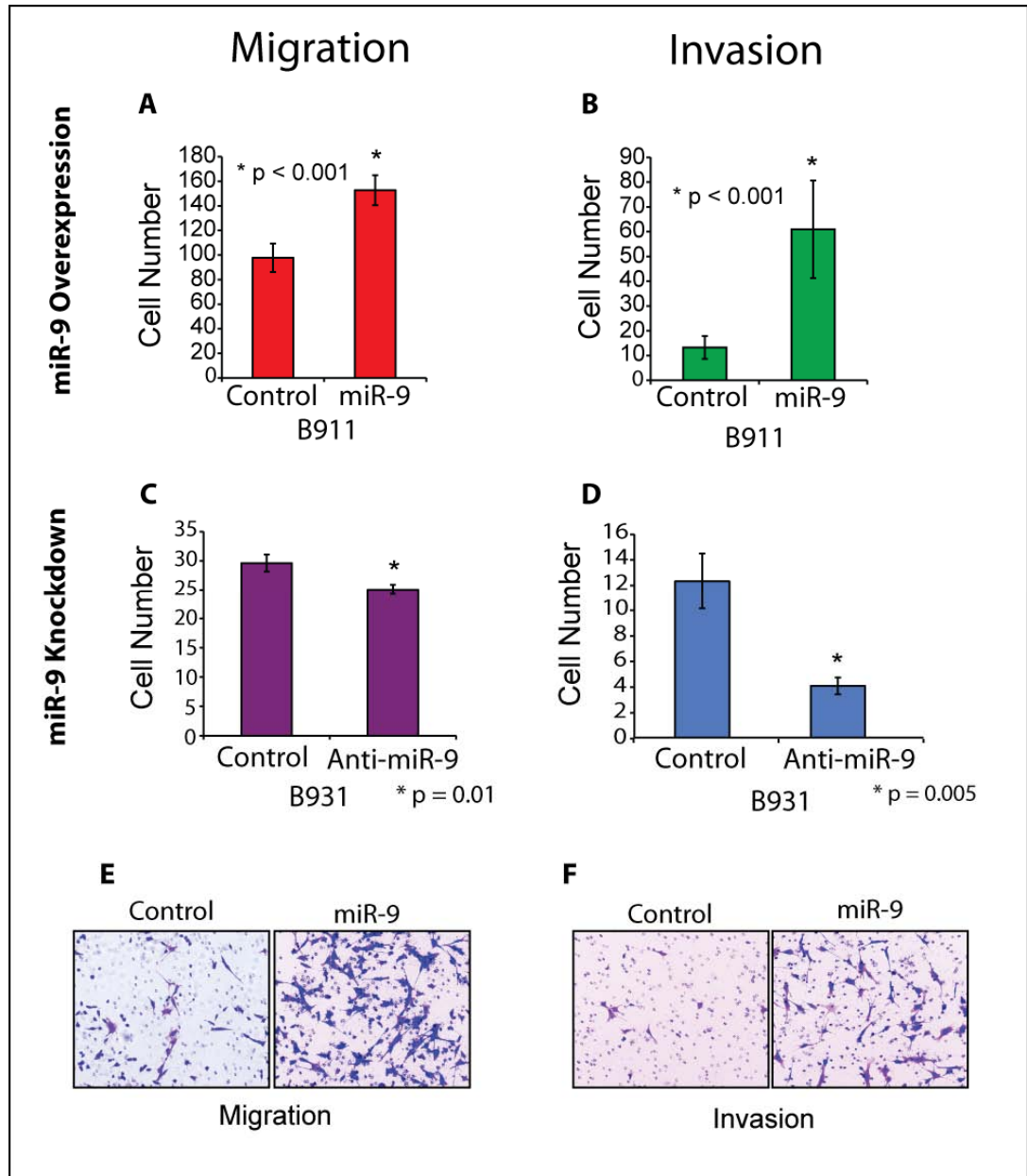


Figure 33. miR-9 regulates tumor cell invasion and migration. (A) Migration of control and miR-9 overexpressing tumor cells through 8 μ m pores. miR-9 overexpression increases the migration of B911 K15.KrasG12D.Smad4^{-/-} tumor cells. (B) Invasion of control and miR-9 overexpressing tumor cells through a matrigel basement membrane layer. miR-9 overexpression significantly increases the invasion of B911 tumor cells (* p \leq 0.001). Knockdown of miR-9 in B911 K15.KrasG12D.Smad4^{-/-}

/- tumor cells significantly decreases both migration ($p = 0.01$) (C), and invasion (* $p = 0.005$) (D). Representative images of control and miR-9 overexpressing tumor cells after migration (E) and invasion (F). Each migration and invasion assay was performed in triplicate. For each replicate three microscopic fields were taken in different regions of the membrane, and the number of cells per field were counted. Significance was determined using a Student's t-test.*

DISCUSSION

2.24 Smad4 loss and Kras activation targeted to the murine hair follicle bulge stem cells generates metastatic SCC.

Previous mouse models of inducible epithelial mutations made use of keratin promoters targeting mutations to the basal epithelial layer [20, 64, 68, 82, 95, 217]. These models effectively generate a mutant epithelial layer by targeting early progenitor cells that then differentiate to generate the mutant epithelium. In this work, we have developed a mouse model that specifically targets gene mutations to the hair follicle bulge stem cells. Since the skin is continuously proliferating and regenerating the epithelium, it is more likely that oncogenic mutations accumulate in the stem cell populations. The more mature progenitors have a much shorter lifespan, and as such may not have time to acquire sufficient mutations to generate tumors. Therefore, by targeting the epithelial stem cell pool, the K15.Kras^{G12D}.Smad4^{-/-} mouse better models epithelial tumorigenesis than previous models targeting mutations to the entire basal epithelial layer. Unlike other mouse models [64, 68], Smad4 loss in this model was not sufficient to generate spontaneous tumors in the skin. This is potentially because the Smad4 loss was limited to a smaller population of epithelial cells. Because of this, it is likely that tumor formation would be seen in a larger cohort of K15.Smad4^{-/-} mice.

Addition of an activating Kras^{G12D} mutation to the K15.Smad4^{-/-} mouse, resulted in the development of spontaneous and aggressive tumors within 18 weeks

with 100% penetrance. About a quarter of the transgenic animals also developed lung metastases. In this case activation of Kras may be acting as an initiating mutation for tumorigenesis. Cooperation between mutations in the TGF β signaling pathway and Kras has been shown previously in both the oral cavity [20] and pancreas [108]. In the absence of transgenic Kras activation, we also found that, while not mutated, Ras signaling is amplified in Smad4^{-/-} mouse models of HNSCC further demonstrating the cooperation between these pathways in epithelial tumorigenesis. Activation of the Ras pathway in these tumors may also be promoting lung metastasis, since previous studies of skin SCC in Smad4^{-/-} models do not show metastasis to the lung [68].

While the K15.Kras^{G12D}.Smad4^{-/-} tumors were primarily SCC, a small subset of the tumors had regions of sebaceous adenoma and basal-like SCC. These regions of tumor heterogeneity suggest that the targeted stem cells maintain their pluripotency and the capability to differentiate down distinct hair follicle cell lineages.

2.25 Tumor Passaging Induces EMT and Increases Metastasis.

The primary transgenic tumors were passaged in to nude mice to amplify the working tumor mass for sorting and grafting experiments and to select for the tumor-initiating population. We found that the transgenic tumors initially grew relatively slowly in the transplanted mice, however once that tumor grew, all subsequent passages grew rapidly. This change in tumor kinetics suggests that

passaging enriches for TIC populations during the growth of the Passage 1 tumor. This enrichment occurs as the transplanted progenitor cells terminally differentiate and die. TICs are predicted to be resistant to DNA damage and apoptosis [128], these properties likely also contribute to increased survival and selection of these cells in the transplanted mice.

The differences in tumor initiation provided us with two mouse models with which to study the properties of TICs, the Primary tumors with poor tumor-initiating capability, and the Passage 1 tumors with enhanced tumor-initiating capability. When the histology of these two tumor types were compared, the majority of the Primary tumors were well- to moderately-differentiated, while the more aggressive Passage 1 tumors tended to be poorly-differentiated. These differences in histology are again consistent with a selection for the more primitive tumor cell populations in the passaged tumors.

Interestingly, a subset of the Passage 1 tumors also had spindle cell carcinoma morphology, a rare, but aggressive form of epithelial carcinoma that is thought to result from an epithelial-to-mesenchymal transition. Staining of the Primary and Passage 1 tumors for markers of EMT showed greater loss of E-cadherin staining and increased vimentin staining in less differentiated tumors. This EMT-like phenotype in the Passage 1 tumors also correlated with a large increase in the frequency of metastasis (up to 80% of the Passage 1 tumors). In many ways passaging the tumors acts as an artificial model of metastasis. By forcing

the tumor cells to a new location, those cells that have the ability to reform tumors and potentially metastases are selected for. The increase in metastasis seen in these passaged tumors suggests that metastatic cells are selected for in this model.

2.26 The Side Population and SP⁻/CD34⁺/CD49f⁺ Population are Tumor-Initiating

To date, few people have studied TICs in skin SCC. One of the major challenges to studying TICs is the identification of cell surface markers with which to purify these populations. Fortunately in the skin, the epithelial stem cell populations have been well-studied. We chose two sets of these markers, the Hoechst dye excluding side population (SP), and the SP⁻/CD34⁺/CD49f⁺ cell population. Both the SP and SP⁻/CD34⁺/CD49f⁺ purified cell populations had an increased ability to form tumors after grafting in to nude mice compared to cell populations negative for each of the markers. Interestingly, none of the SP cells were also positive for either CD34 or CD49f suggesting that these are two distinct cell populations.

In each case, we found that 1×10^4 cells were sufficient to generate tumors after grafting. While the Passage 1 tumors initiate tumors more rapidly after grafting compared to the Primary tumors, it is not known whether this increased tumor initiation is due to increased numbers of TICs within the tumors, or if the TICs have acquired additional alterations that improve their capability to initiate

tumors. Further studies are needed to determine the lowest number of TICs needed to successfully generate tumor grafts from both the Primary and Passage 1 tumors.

2.27 The Side Population, but not the SP⁻/CD34⁺/CD49f⁺ Size, Correlates with Metastasis

After isolating TIC populations from a number of tumors, it became clear that there was a wide variation in the size of these populations from tumor to tumor. This variation in TIC size was most pronounced in the SP cells. Interestingly, the tumors with the largest SP fractions were those that had SPCC tumor histology. This finding was intriguing since, SPCC tumors are often more aggressive tumors that have undergone an EMT and as such are more metastatic. Further investigation of the association of SP size and the metastasis status of the tumors showed a clear correlation between the SP size and metastasis. This correlation was limited to the SP cell population and was not seen in the SP⁻/CD34⁺/CD49f⁺ population. This difference indicates that there may be multiple TIC populations within tumors that play distinct roles in tumor growth, progression and recurrence. The correlation between the SP size and metastasis in the K15.Kras^{G12D}.Smad4^{-/-} mice suggests that this population may be a metastatic cell population. This idea is supported by studies in human HNSCC cell lines that have shown the SP to be increased in more metastatic lines. This same study also showed that the SP cells were more invasive than the non-SP cells from the same cell line further suggesting that this population may be involved in metastasis [230].

Since the Passage 1 tumors were more metastatic than the Primary tumors, we looked at the relative SP sizes between these two types of tumors and found that there was a significant increase in the SP size in the Passage 1 tumors. Increased TIC population size has recently been documented in *in vitro* cell culture systems that have been stimulated to undergo EMT [158, 159]. To our knowledge, this animal model represents the first *in vivo* system to show the correlation between EMT and increased TIC populations.

2.28 Oncogenic and Metastatic miRNA Profile of the Passage 1 Tumor Side population

Array profiling of the differentially expressed miRNAs between Primary and Passage 1 tumor SP cells identified a number of differentially expressed miRNAs that are known oncomiRs and tumor suppressors. Additionally, miRNAs with known roles in EMT were also found to be differentially expressed between the two populations. Of the miRNAs with decreased expression in the passage 1 SP cells, two, miR-141 and miR-183, are associated with EMT and regulation of stem cell genes (figure 34). miR-141 is a member of the miR-200 family of miRNAs, which target ZEB1 and ZEB2. This family, along with the miR-183-96-182 miRNA cluster is both downregulated in breast tumor-initiating cells as well as normal tissue stem cells compared to normal differentiated breast tissue [204]. Furthermore, miR-141 and miR-183, have both been shown to target the stemness-associated gene, Bmi1 [204, 205]. While Bmi1 was not expressed in the K15.Kras^{G12D}.Smad4^{-/-} cell

populations, these miRNAs may have other stem cell associated targets and may participate in the acquisition of stem cell characteristics during EMT.

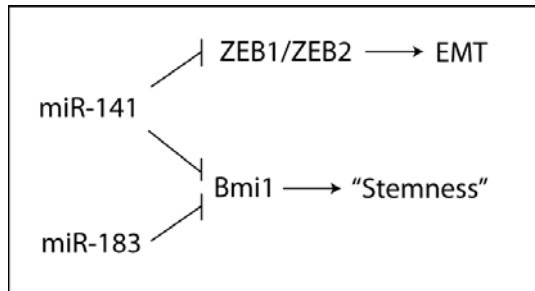


Figure 34. Summary of downregulated miRNAs and their potential contribution to metastasis. miR-141 is a member of the miR-200 family of miRNAs that

target the inducers of EMT, ZEB1 and ZEB2. Loss of these miRNAs can induce an EMT in vitro. miR-141 and miR-183 both target the stem cell gene Bmi1.

One of the most highly overexpressed miRNAs in the Passage 1 SP cells was miR-155 (Figure 35A). This miRNA is highly expressed in a number of tumors including lung [231], and breast cancer [186, 195, 232, 233]. The role of miR-155 in EMT and metastasis is somewhat controversial. On one hand miR-155 has been shown to play a role in TGF β induced EMT, in part through regulation of RhoA and dissolution of tight junctions [186]. On the other hand, miR-155 has been shown to target TCF4, a transcription factor that forms complexes with β -catenin and promotes EMT [234]. Interestingly, this same group also showed that miR-155 promoted lung colonization of tumor cells injected in to the tail vein of mice [234], indicating that miR-155 may play a role in mesenchymal-to-epithelial transition (MET).

Two miRNAs, miR-199a and miR-214, both overexpressed in the Passage 1 SP, are transcriptionally activated by the EMT associated transcription factor Twist 1 [235, 236] (Figure 35C). miR-199a has been generally reported as a tumor suppressor miRNA, through regulation of $I\kappa\kappa\beta$ and inhibition of NF κ B signaling [191]. Interestingly, miR-199a is also mediated by BMP2, and targets Smad1, inhibiting chondrogenesis [237]. In the K15.Kras^{G12D}.Smad4^{-/-} tumors, miR-199a inhibition of Smad1 may lead to increased deregulation of BMP mediated stem cell maintenance, and subsequently affect the tumor-initiating capabilities of the tumor cells. The other Twist regulated miRNA, miR-214, targets PTEN and protects cancer cells from cisplatin-induced apoptosis, through increased activation of the AKT pathway [238], indicating that miR-214 may contribute to increased oncogenic Akt signaling and chemoresistance in the K15.Kras^{G12D}.Smad4^{-/-} tumors.

In this study, miR-132 expression mirrored miR-9 expression in the passaged tumor SP as well as in the different tumor histologies. miR-132, is an important regulator of neuronal morphogenesis and dendritic plasticity [239, 240] (Figure 35D). While less is known about miR-132 in cancer, a few recent studies have shown that miR-132 may play a role in regulating tumor cell proliferation and regulation of the microenvironment. In pancreatic cancer, miR-132 inhibits the retinoblastoma (Rb) tumor suppressor leading to increased cell proliferation and tumor promotion [241]. Other studies have shown that miR-132 may be important in regulating the tumor microenvironment. For example, miR-132 targets p120RasGAP in the endothelium, resulting in increased Ras activity and

angiogenesis [242]. Since these studies were carried out in endothelial cells, it is not known whether increased miR-132 would have the same effect in the tumor epithelial cells. miRNAs, however, can be found in the circulation, often in cell derived exosomes, which could provide a potential mechanism whereby the tumor derived miR-132 could be released and act upon local endothelial cells to promote angiogenesis. While we focused on the function of miR-9 alone in this study, further studies are needed to examine any cooperative roles between miR-9 and miR-132 in tumor development and/or metastasis.

In this study we focused on miR-9. This miRNA was one of the most significantly differentially expressed miRNAs between the primary and passage 1 SP cells. miR-9, has been shown to play a role in EMT by targeting E-cadherin [196] (Figure 35B). Interestingly, it has been reported that miR-9 inhibition of E-cadherin results in an increase in nuclear and cytoplasmic β -catenin and subsequently increases in vascular endothelial growth factor (VEGF) expression [196]. Additionally, miR-9 was shown to be transcriptionally regulated by myc, and as such was increased in tumors that have myc amplifications [196]. Interestingly, miR-9 could only induce an EMT in certain cell lines, indicating that the effects of miR-9 overexpression may depend on other active pathways within the tumor cells [196]. The role of miR-9 in metastasis is controversial. In clear cell renal cell carcinoma (ccRCC), increased methylation and decreased expression of miR-9 was associated with tumor recurrence and worse prognosis [211]. Additionally, miR-9 was found to be highly methylated in colorectal cancer (CRC), and this methylation was

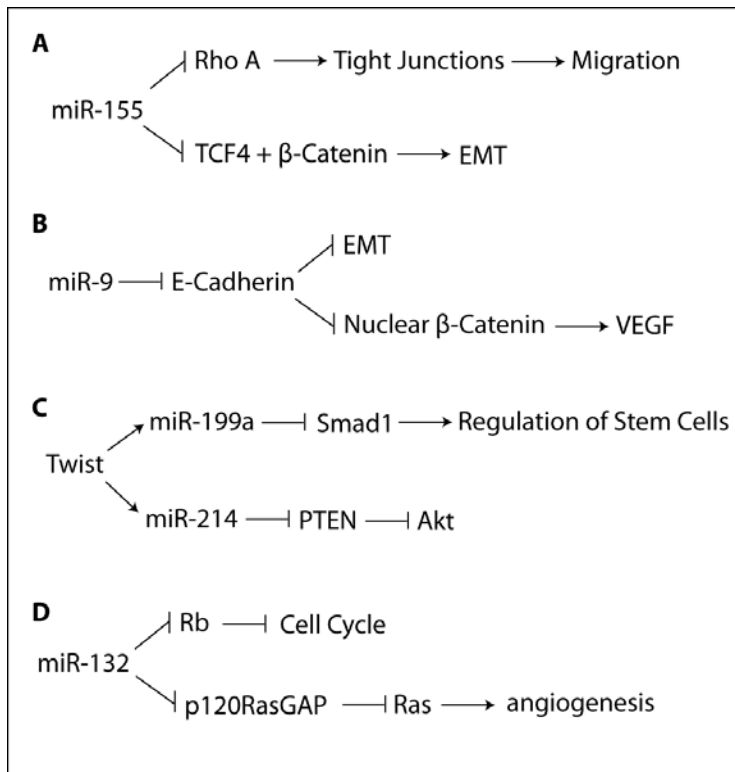
correlated with lymph node metastasis [212]. Conversely, high miR-9 expression has been correlated with distant metastasis in CRC [197]. Our studies suggest, however, that miR-9 likely plays an important role in squamous cell carcinoma metastasis.

Figure 35. Summary of overexpressed miRNAs and their potential contributions to tumor progression.

(A) miR-155 may promote metastasis through inhibition of RhoA and dissolution of tight junctions.

Conversely, miR-155

may inhibit EMT by regulating levels of TCF4. (B) miR-9 inhibits E-cadherin resulting in EMT. Loss of E-cadherin also results in increased nuclear β -catenin mediated VEGF expression. (C) Twist increases the expression of miR-199a and miR-214. miR-199a targets Smad1 and may affect BMP mediated stem cell regulation. miR-214 targets PTEN resulting in increased Akt signaling. (D) miR-132 targets Rb resulting in



increased cell proliferation. miR-132 also increases angiogenesis by targeting p120RasGAP and activating Ras.

2.29 Regulation of miR-9 Expression in the K15.Kras^{G12D}.Smad4^{-/-} Tumors

MicroRNA expression analysis of the different compartments of the skin has shown that the skin and hair follicles express a unique miRNA profile [203]. Interestingly, miR-9 was not detected in any of the subpopulations within normal mouse skin. Because of this observation, we predicted that the increased miR-9 seen in the K15.Kras^{G12D}.Smad4^{-/-} mice resulted from the Smad4 and Kras mutations introduced in to the stem cells. When we recreated these mutations in the non-tumorigenic human epithelial cell line, HaCaT, we were surprised to find that Smad4 loss reduced the expression of miR-9. In their study of miR-9 in breast cancer, Ma *et al* showed that myc binds to the miR-9 promoter and increases its expression [196]. The TGF β pathway normally transcriptionally represses c-myc [228], thus disruption of the pathway by loss of Smad4 should result in increased c-myc expression and subsequently increase miR-9 expression. The discrepancy we saw in the HaCaT cell line with Smad4 loss may be a result of other aberrant signaling pathways in these cells. For example, the NF κ B signaling and upstream mediators of this pathway have been shown to be dysfunctional in this cell line [243]. Further studies are needed in other systems such as primary mouse or human keratinocytes to determine the effect of Smad4 loss on miR-9 expression.

In the HaCaT cells Kras activation seemed to increase the expression of miR-9, however this increase was only a two-fold increase over the control. This minimal change could also be a result of aberrant signaling in the HaCaT cells. When we looked at miR-9 expression in Smad4^{-/-} cell lines with and without Kras activation, there was a greater increase in miR-9 expression in the cells with mutant Kras compared to those with WT Kras. These results indicate that Kras activation increases the expression of miR-9; however, this effect may be dependent on other pathways activated in tumor cells that are not activated in the non-tumorigenic HaCaT cells. Other studies have identified both myc [196] and Creb [210] as transcriptional activators of miR-9. When we looked at c-myc expression in the primary and passage 1 tumor SP cells, we found no significant increase in myc expression (Figure 21B). Moreover, we found no correlation between c-myc expression and miR-9 expression in these populations (Figure 21B). While the mRNA expression analysis does not tell us anything about c-myc activation in these tumor cells, the expression data does suggest that c-myc is not the primary regulator of increased miR-9 in the passaged tumor SP cells. Further studies are needed to determine if Kras is the primary regulator of miR-9 expression in the K15.Kras^{G12D}.Smad4^{-/-} tumors.

2.30 miR-9 Slows Cell Proliferation *in vitro*, but may Promote Tumor Growth *in vivo*.

Cell cycle analysis of miR-9 overexpressing cells showed that forced expression of miR-9 slows cell cycling and increases the percent of cells in G1.

Knockdown experiments showed the opposite result, indicating that miR-9 directly affects the cell cycle. This reduction in cell cycling might be expected in metastatic cells in which it might be advantageous to direct metabolic resources to other functions such as invasion and migration. Initial *in vivo* tumor growth assays were performed in immunocompromised nude mice and showed no difference in tumor growth rates between miR-9 overexpressing and control cells. A similar phenomenon was observed by Ma *et al* in breast tumor cells [196]. An explanation for this difference is the interaction of miR-9 with the microenvironment. One observation from Ma *et al* [196] was an increase in VEGF expression in the breast tumor cells, resulting from increased β -catenin/TCF signaling after miR-9 targeting of E-cadherin. This increase in VEGF may promote a supportive environment for the growth of miR-9 overexpressing tumors that would not have been seen *in vitro*. Alternatively, miR-9 may have anti-apoptotic effects that may support tumor growth in the transplanted mice. The effect of miR-9 on apoptosis has yet to be studied.

Since the K15.Kras^{G12D}.Smad4^{-/-} tumor lines grew so quickly in the athymic nude mice, we injected the cells into WT B6 mice to slow tumor growth. Although the transgenic K15.Kras^{G12D}.Smad4^{-/-} tumors were developed on the B6 background, the immunocompetent WT B6 mice required more cells injected with matrigel to support consistent tumor growth. Interestingly, at three weeks after injection it appeared as if the miR-9 overexpressing tumors might be growing at an increased rate compared to controls. Similarly the miR-9 knockdown tumors appeared to be regressing compared to controls. While these studies clearly need to be followed

out for a longer period of time, the current results indicate that miR-9 may provide a growth advantage for tumor cells in an immunocompetent environment. If these data hold true, future studies should address the potential role of miR-9 on the microenvironment and evasion of the immune system.

2.31 miR-9 Expression is Associated with SP size and Chemoresistance in a Context Dependent Manner

One striking finding was the correlation of miR-9 and miR-132 expression with both the size of the SP and the SPCC tumor histology. By screening for the four ABC transporters most commonly associated with expression in tumor cells, we identified Abcb1a as being increased in the Passage 1 tumor SP cells compared to Primary tumors. Surprisingly, expression of Abcb1a did not correlate with the SP size indicating that more than one ABC transporter may be responsible for the SP in these cells. Other explanations for this discrepancy may be due to posttranscriptional regulation of Abcb1a or other mechanisms affecting the activity of the ABC transporters. Further studies are needed to screen for the expression of other members of the ABC transporter family.

Although Abcb1a expression did not correlate with SP size, there was an increase in Abcb1a expression in the poorly differentiated and SPCC tumors. We also found a slight correlation between Abcb1a expression and miR-9 expression. This observation prompted us to determine whether miR-9 might regulate Abcb1a expression. Overexpression of miR-9 in different cell lines resulted in varying levels

of increased Abcb1a expression, however, knockdown of miR-9 had no effect on Abcb1a expression. These inconsistent results suggest that while miR-9 may support an increase in Abcb1a expression, any regulation of Abcb1a is not a direct effect of miR-9.

Although any regulation of Abcb1a by miR-9 is inconclusive, we wanted to determine whether the increase in Abcb1a in the Passage 1 tumors could be contributing to the increase in SP size and promoting chemoresistance in these tumors. Using the stably transduced miR-9 cell line that expressed very high levels of Abcb1a, we saw that the increase in Abcb1a did dramatically increase the size of the SP and led to chemoresistance. However, it should be noted that the cell lines expressing high levels of Abcb1a also had slightly higher expression of miR-9, because of this other targets or effects of miR-9 overexpression should be considered in the regulation of chemoresistance in these cells. Since the large SP sizes in the K15.Kras^{G12D}.Smad4^{-/-} did not correlate with Abcb1a expression, further studies in human cell lines that overexpress miR-9 are needed to determine if these cells have increased SP sizes as a result of increased expression of another ABC transporter. Similarly, drug treatment assays in these cells will also determine if miR-9 promotes chemoresistance either through increased expression of other ABC transporter family members, or by other means such as anti-apoptotic mechanisms.

2.32 miR-9 Increases Invasion and Migration of Tumor Cells

The role of miR-9 in metastasis is controversial. A number of studies have associated increased levels of miR-9 in human tumors with a lower incidence of metastasis [211, 212]. While other studies have found that miR-9 promotes metastasis and metastatic behavior [196, 197]. We found that in both the mouse skin SCC and human HNSCC cell lines, miR-9 overexpression increases migration and to a greater extent, increases invasion. Similarly knockdown of miR-9 in the mouse tumor lines inhibited migration and invasion. Since changes in miR-9 expression seemed to preferentially affect invasion, more than migration, future studies should look for putative miR-9 targets that may inhibit pro-invasive factors such as proteases. These results suggest that miR-9 promotes metastasis in SCC (Figure 36). While earlier studies of miR-9 overexpressing cells in the athymic nude mice did not show differences in metastasis, these results were hard to interpret due to the high levels of metastasis in the parent cell line. Studies are currently underway in the B6 mice to determine if miR-9 overexpression increases metastasis and miR-9 knockdown decreases metastasis. Additionally, further studies are needed to determine the effect of miR-9 overexpression on metastasis of human SCC cell lines.

In summary, we have generated a mouse model of skin SCC by generating mutations specifically in the hair follicle bulge stem cells. These tumors have regions of cells from multiple different hair follicle lineages, suggesting that the mutant stem cells maintain pluripotency and can give rise to tumor heterogeneity.

These SCCs are metastatic to the lung, and passing the tumors can increase the rate of metastasis. The tumor passing also increases the number of tumors with EMT phenotypes and increases the size of the SP TIC population. We identified a miRNA, miR-9 that is also increased in the EMT-like SPCC tumors. This miRNA is associated with increased SP size and in some cases overexpression of miR-9 increases the expression of the chemoresistance gene Abcb1a. Finally, we found that miR-9 increases migration, and to a greater extent, invasion of mouse SCC cells. Taken together, this study suggests that miR-9 is a major regulator of chemoresistance and metastasis of tumor-initiating cells in squamous cell carcinomas.

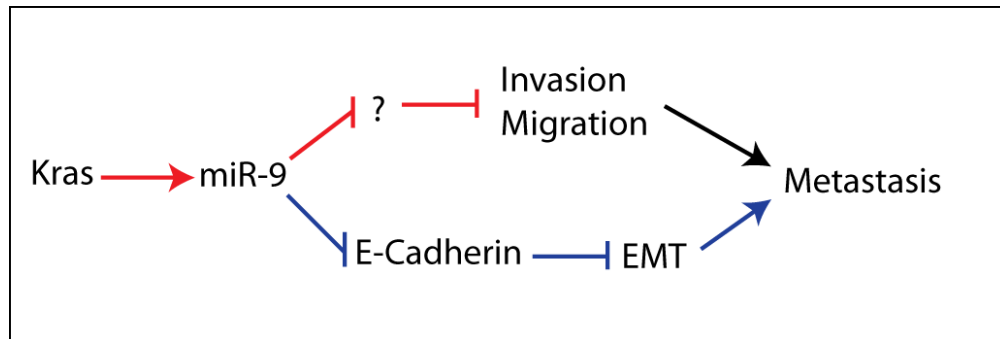


Figure 36. New mechanisms by which miR-9 may promote metastasis. In this thesis work we have shown that activation of *Kras* can induce miR-9 expression. Increased miR-9 promotes invasion and migration. Previous studies have shown miR-9 inhibition of *E-cadherin* and increased lung metastasis in breast cancer [196]. Blue arrows represent published findings. Red arrows represent findings of this study.

CHAPTER THREE

THE ROLE OF MICRORNA-9 IN HEAD AND NECK SQUAMOUS CELL CARCINOMA METASTASIS

METHODS

3.1 Generation of Stably Transduced Tumor Lines.

Lentivirus Production: Lentiviral particles were generated in the 293T packaging cell line. Prior to transfection the cells were changed in to Opti-MEM serum free media (Gibco, Carlsbad CA). Lentiviral vectors (see Appendix B for lentiviral vector information) containing precursor miRNA sequences or miRNA antagonists were transfected in to the 293T cells along with the appropriate lentiviral packaging mix (see Appendix B for packaging mixes used with lentivirus) using Lipofectamine 2000 (Invitrogen, Carlsbad CA). Four hours after transfection the media was changed to DMEM containing 30%FBS and antibiotics. The virus containing media was harvested at 24, 32 and 48 hours. Virus was not concentrated for these studies.

Transduction and Selection of Transduced Cells: After harvesting from 293T cells, the cell culture medium containing virus was centrifuged at 3000rpm for 15 minutes to pellet any cellular debris. The 8nM polybrene was added to the media to aid in transduction. For a 10cm plate, 6ml of virus containing medium was added to the target cells. The cells were then incubated with the viral media for 24-48 hours for transduction. Selection of transduced cells was done by puromycin selection or FACS for GFP or RFP positive cells.

3.2 Analysis of Gene and miRNA Expression

RNA Isolation:

Total RNA, consisting of both the small and large RNA species, was isolated using the Qiagen miRNeasy mini kit (Qiagen, Valencia CA) as per the manufacturer's instructions. Briefly, $800-10 \times 10^6$ pelleted cells were resuspended in 700 μ l of Qiazol lysis reagent. For sorted cells, where a small number of cells ($<3 \times 10^6$) were processed, homogenization was performed by vortexing the cells for 1 minute. For larger numbers of cells ($>3 \times 10^6$) and tissue samples, homogenization was performed using a bench top homogenizer. The total RNA was eluted from the column using 30 μ l of RNase free water.

Quantitative RT-PCR:

One-step qRT-PCR for gene expression: One-step qRT-PCR was used for gene expression when RNA samples were not limiting and amplification was not necessary. One-step qRT-PCR was performed using 100ng of RNA per reaction with the One-Step Brilliant II QRT-PCR system (Stratagene, Santa Clara CA). Expression of mRNA was measured using TaqMan® Assays-on-demand™ probes (Applied Biosystems, Carlsbad CA). All gene measurements were normalized to a GAPDH (human) or Gapdh (mouse) RNA probes. See appendix for TaqMan® probe details. Each sample was run in triplicate and the data was analyzed using a standard relative quantification ($\Delta\Delta$ Ct) method. Reactions were run on a Stratagene MX3000P qPCR machine (Stratagene, Santa Clara CA).

Two-step qRT-PCR for miRNA expression: All miRNA expression analysis by qRT-PCR was conducted using a two-step method. First miRNA specific cDNA was prepared using 10-300ng of starting RNA, and either individual miRNA specific RT primers, or a pooled RT primer mix containing all of the miRNAs on the Applied Biosystems Rodent A v2.0 TaqMan Low Density Array card. The RT reaction was carried out using the High Capacity RT Kit from Applied Biosystems according to the manufacturers instructions. Once the miRNA specific cDNA was prepared, the qRT-PCR reaction was run using TaqMan miRNA probes and TaqMan Universal Master Mix (Applied Biosystems, Carlsbad CA).

3.3 Invasion/Migration Assays

Invasion and migration assays were conducted using BD Bioscience Matrigel (Franklin Lakes, NJ) invasion chambers and transwell migration chambers. Prior to plating cells, the Matrigel layer was rehydrated in DMEM 10% FBS for 2 hours at 37°C. Once rehydrated 1×10^3 - 5×10^3 tumor cells transduced with miR-9 or miR-9 knockout vectors or controls were plated in the matrigel invasion chamber or transwell migration chamber in 500 μ l serum free medium. DMEM containing 10% FBS was used as a chemoattractant in the bottom well (750 μ l). The cells were then incubated at 37°C in a standard tissue culture incubator to allow for cell migration and invasion. After 24 hours the plates were removed from the incubator, and the cells that had not migrated or invaded were removed from the inside of the transwell by scrubbing the membrane with a cotton swab. The migrated/invaded cells were stained fixed in Diff-Quick fixing medium for 2 minutes, then stained with

0.05% crystal violet for an additional 2 minutes. The membranes were washed well in water then left overnight to dry. Once dry the membranes were removed from the transwells and placed on slides with Fluormount G (Southern Biotech, Birmingham AL). To quantify the invading and migrating cells, 3 microscopic fields (10x) were imaged per membrane and the average number of cells per field was counted. Each assay was done in triplicate such that a total of 9 fields were counted for each condition.

3.4 Cell Cycle Analysis

Control and miR-9 overexpressing of knockdown cells were harvested and washed with PBS. The cells were then pelleted by centrifugation and resuspended in 1ml Krishan Stain (produced as previously described [224]) at a concentration between $0.1-1 \times 10^6$ Cells/ml. The cells were vortexed to mix and incubated at 4°C overnight. Cell cycle analysis was performed with a FC500 flow cytometer and the data was analyzed using ModFit LT Software (Verity Software House, Topsham, ME).

3.5 Statistical Analysis

For all qRT-PCR data, error bars are represented as the standard deviation between samples (triplicate), unless otherwise noted. In these cases, the standard error was used instead. In general standard error was used when there was wider variation between samples and larger numbers of samples were used, as in the case of tumor samples. Standard deviation was generally used with *in vitro* studies and studies

with fewer replicates. In each case significance was assessed using a standard student's t-test.

3.6 Clinical Sample Collection

Human HNSCC samples were surgically resected between the years 2000 to 2005 from consenting patients at the Department of Otolaryngology, Oregon Health and Science University, and from the years 2008-2010 from consenting patients at the Department of Otolaryngology, University of Colorado Health Science Center. Samples were collected under Institutional Review Board-approved protocols at each institution. See Appendix F for tables of human samples included in this study.

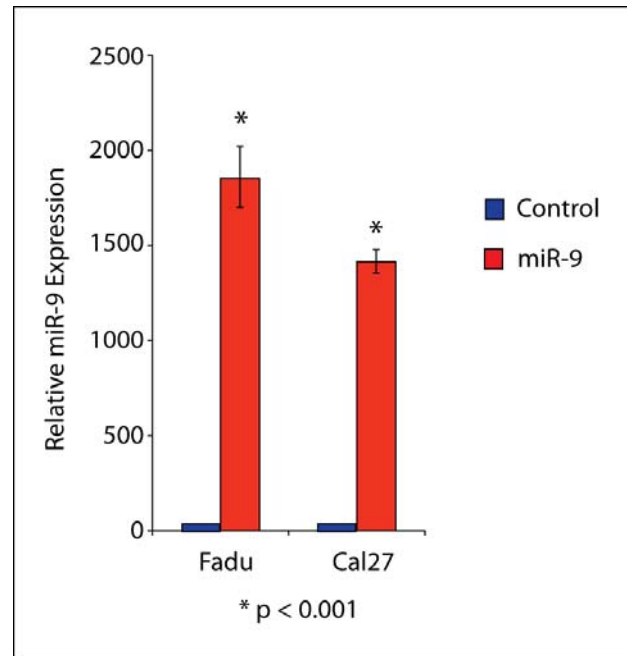
RESULTS

3.7 miR-9 Overexpression Inhibits Human HNSCC Cell Cycling.

The role of miR-9 in metastasis of human cancers is controversial. Methylation of miR-9 and subsequent downregulation of mature miR-9 has been associated with increased lymph node metastasis in clear cell renal cell carcinoma [211]. Conversely, in breast cancer [196] and colorectal carcinoma [197], increased miR-9 expression has been associated with distant metastasis. Further studies are needed to determine the role of miR-9 on SCC metastasis and to date no studies have examined the role of miR-9 in metastatic HNSCC. Since the K15.Kras^{G12D}.Smad4^{-/-} mouse cell lines used to study the function of miR-9 in Chapter 2 had relatively high levels of miR-9, even in the line with the lowest miR-9 expression (B911), we wanted to generate miR-9 overexpressing lines in cells that expressed little to no miR-9. The human HNSCC cell lines, Cal27 and Fadu, both have very low miR-9 levels, so we chose these cells to generate stable miR-9 overexpressing lines. Again, lentiviral pre-miR-9 vectors were transduced in to the cells and mature miR-9 levels were measured by qRT-PCR. Each of these human lines showed robust miR-9 expression compared to the parent lines (Figure 37).

Figure 37. Generation of miR-9

overexpressing human HNSCC cell lines. Cal27 and Fadu human HNSCC cell lines were transduced with a lentiviral vector containing the pre-miR-9 construct. Expression of mature miR-9 was measured using qRT-PCR compared to control transduced lines. Error bars represent



standard deviation and significance was determined using a Student's t-test.

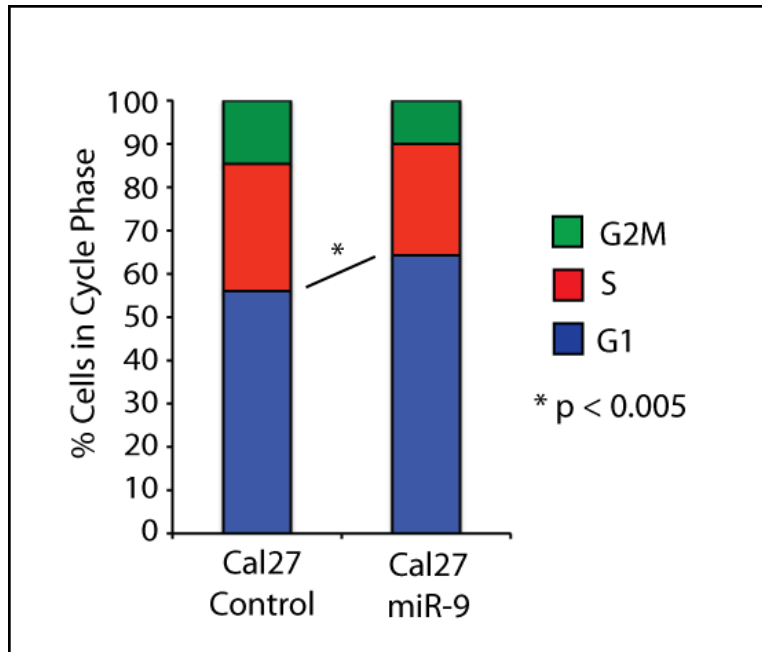
The effect of miR-9 on HNSCC cell cycle

To determine how miR-9 overexpression affects the behavior of HNSCC cells we looked at the effect of miR-9 overexpression on cell cycling. Cell cycle analysis of the high miR-9 expressing cells, Cal27-miR-9 cells (Figure 38), showed a significant increase in the percent of cells in G1 phase of the cell cycle compared to controls (p < 0.005). These result are consistent with the effect of miR-9 overexpression and knockdown in mouse skin SCC seen in Chapter 2. While the differences in the percent of cells in G1 between lines with high miR-9 and low miR-9 are not overly striking, again the consistency of the mouse skin and human HNSCC data indicates that miR-9 inhibits cell proliferation *in vitro*. Further *in vivo* studies are warranted

with the miR-9 overexpressing HNSCC cells to determine the effect of miR-9 on the growth of orthotopically xenografted tumors.

Figure 38. miR-9 slows

cell cycling. miR-9 overexpression increases the percent of cells in G1 in the Cal27 human HNSCC cell line. The cell cycle assay was done in triplicate and significance was assessed using a Student's t-test, $p < 0.005$ in each case.



3.8 miR-9 does not Affect the Expression of ABCB1 in Human HNSCC.

In Chapter 2 we found that increased expression of miR-9 in the mouse SCC lines was frequently correlated with increases in the expression of the ABC transporter Abcb1a and chemoresistance. Since the mouse Abcb1a gene has approximately 87% homology with the human ABCB1 gene [244], we wanted to determine whether the increased expression of miR-9 in the human HNSCC lines, Cal27 and Fadu, also resulted in increases in ABCB1. We assessed Abcb1a levels in Cal27 and Fadu cell lines transduced with lentiviral pre-miR-9. Each of the parental lines has very low levels of miR-9, and addition of the pre-miR-9, greatly increases

the mature miR-9 expression in these lines (Figure 39A). Nevertheless, there was no significant change in Abcb1a levels after miR-9 overexpression (Figure 39B), again suggesting that the association between miR-9 and Abcb1a may be cell type and/or context specific.

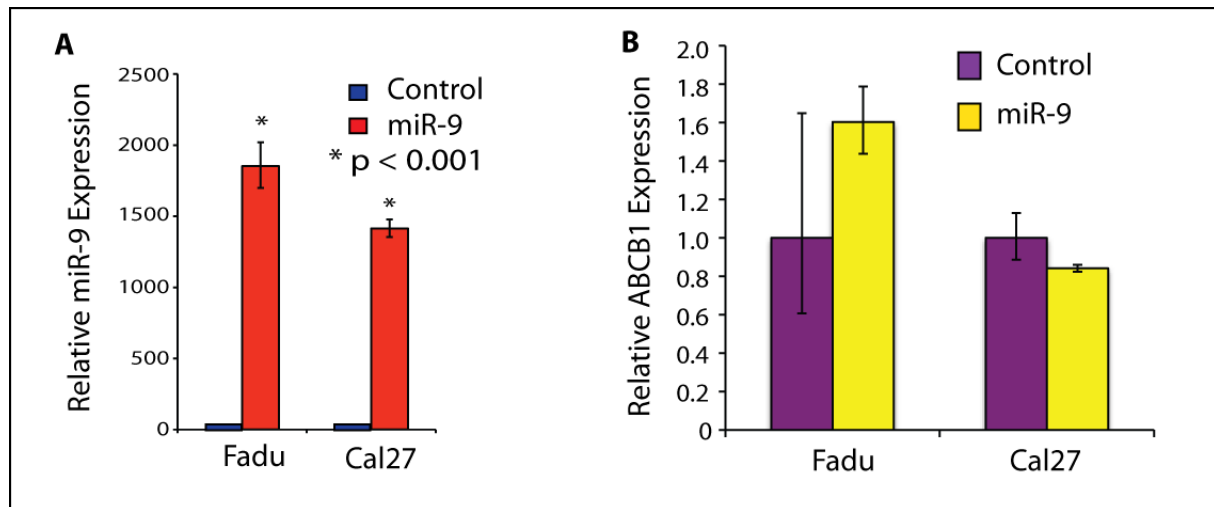


Figure 39. No increase in Abcb1a after miR-9 overexpression in Human HNSCC lines.. (A) Lentiviral pre-miR-9 transduced human HNSCC cell lines show robust mature miR-9 expression compared to controls. (B) No change in ABCB1 expression in the human cell lines after miR-9 overexpression. In each Figure, error bars represent standard deviation and significance was determined using a Student's t-test.

3.9. miR-9 Regulation of HNSCC Cell Invasion and Migration

Following our studies of the effect of miR-9 on invasion and migration of mouse SCC lines, we wanted to determine whether miR-9 also increased the invasion and migration of human HNSCC cells. Using a trans-well migration assay, we plated either miR-9 overexpressing cells or control cells in the trans-well in

serum free medium, the bottom well was filled with medium containing serum as a chemoattractant. Since the human HNSCC lines have more epithelial phenotypes than the mouse lines, we increased the time for migration and invasion to 48hrs from 24hrs to allow time for the cells to migrate. Similar to the mouse SCC studies in Chapter 2, we found that there was an increase in the migration of the Cal27 cell line after miR-9 overexpression (Figure 40A). While the Fadu human HNSCC line did show a slight increase in migration after miR-9 overexpression, this result was not significant (Figure 40B). To determine the invasive abilities of these cells, we used trans-wells coated with a matrigel basement membrane. Both the Cal27 and Fadu lines showed significantly increased invasion after miR-9 overexpression (Figures 40C, D). Again, the increase in invasion after miR-9 overexpression was far more pronounced than the increase in migration, suggesting that miR-9 may be more important for the invasive properties of metastatic tumor cells.

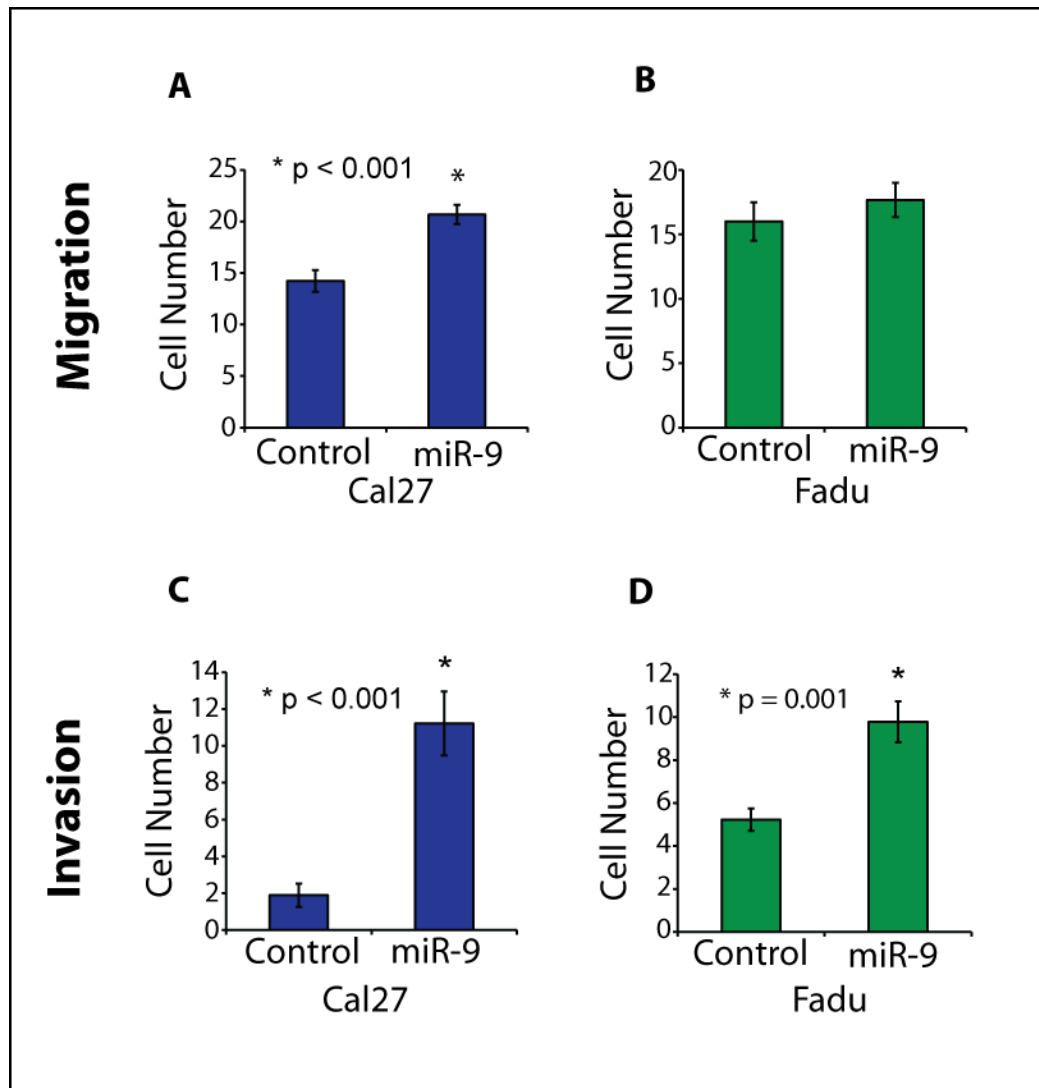


Figure 40. miR-9 regulates tumor cell invasion and migration. (A, B) Migration of control and miR-9 overexpressing tumor cells through 8 μ m pores. (A) miR-9 overexpression increases the migration of Cal27 human HNSCC cells. (B) miR-9 overexpression has little effect on the migration of Fadu human HNSCC cells. (C, D) Invasion of control and miR-9 overexpressing tumor cells through a matrigel basement membrane layer. miR-9 overexpression significantly increases the invasion of Cal27 (C), and Fadu (D) tumor cells (* p \leq 0.001). Each migration and invasion assay was

performed in triplicate. For each replicate three microscopic fields were taken in different regions of the membrane, and the number of cells per field were counted. Significance was determined using a Student's t-test.

3.10 miR-Expression in Human Tumors

There are a number of conflicting studies on the role of miR-9 in human tumors. On the one hand, a number of studies have found frequent methylation and decreased expression of miR-9 in tumors [211], while other studies have shown increased expression of miR-9 [196, 197]. The majority of *in vitro* studies of the mechanism of miR-9 have pointed towards a pro-tumorigenic function [196]. Therefore, to determine the role of miR-9 in human HNSCC, we analyzed tumor samples for methylation of miR-9 at the miR-9-3 locus on chromosome 15q26.1. Further, expression of miR-9 in the HNSCC tumors and normal mucosal controls obtained from sleep apnea patients was measured using qRT-PCR. miR-9 expression in the methylated and unmethylated tumors was then analyzed relative to the average expression of the normal controls (Figure 41) (Dr. Shi-Long Lu, unpublished data). Each of the tumors that was methylated at the miR-9-3 locus, showed reduced miR-9 expression, indicating that this methylation indeed inhibits expression of the miRNA. Interestingly, the miR-9 expression levels divided the unmethylated tumor samples in to two distinct groups, those with very high expression and those with very low expression.

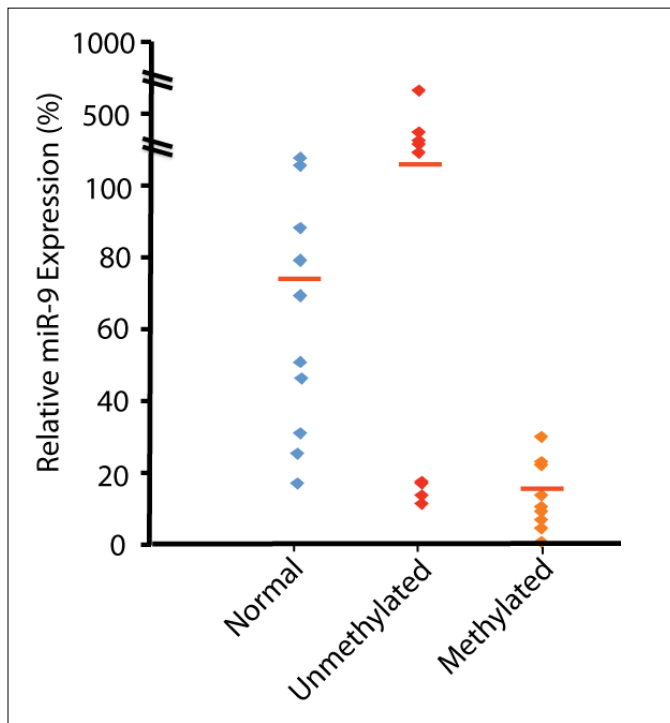


Figure 41. A small subset of human HNSCC has increased miR-9 expression. qRT-PCR expression analysis of miR-9 comparing normal uvula mucosa from sleep apnea patients with HNSCC with methylated and unmethylated miR-9-3. *Unpublished data contributed by Dr. Shi-Long Lu, department of

Otolaryngology, University of Colorado Health Sciences Center.

Since the miR-9 expression data showed such a large variation in expression, the data were further analyzed based on the location of each of the tumor samples (Table 3). While only 5/20 tumor samples showed increased miR-9 expression relative to normal mucosa, 4 out of these 5 samples were shown to be lymph node metastases. Further, of the 4 lymph node metastasis samples included in the study, 3 showed increased miR-9 expression, while only one was methylated and showed decreased expression.

Unmethylated		Methylated	
Tissue	miR-9 Expression	Tissue	miR-9 Expression
LN SCC	663	Floor of Mouth CIS	32
Base of Tongue SCC	376	Tonsil SCC	21
LN SCC	259	Tongue SCC	21
Tongue SCC	259	LN SCC	13
LN SCC	201	Alveolar Ridge SCC	13
Tongue SCC	18	Base of Tongue SCC	11
Buccal SCC	17	Base of Tongue SCC	7
Oral SCC	14	Larynx SCC	4
Tongue SCC	14	Glottic SCC	1
Retromolar Trigone	13	Tongue SCC	0

Table 3. Increased miR-9 expression in HNSCC lymph node metastasis. *miR-9 expression in human HNSCC from different sites. Decreased miR-9 expression compared to normal uvula tissue is represented in blue, and increased miR-9 expression is represented in yellow. Samples that are methylated on miR-9 transcripts all show decreased miR-9 and are displayed in the right hand columns. Samples that were not methylated on miR-9 are divided in to high and low miR-9 expression shown in the left hand columns. miR-9 expression is represented as a % of the average for normal control mucosa. *Unpublished data contributed by Dr. Shi-Long Lu, department of Otolaryngology, University of Colorado Health Sciences Center.*

Since passaging the mouse tumors resulted in increased miR-9 expression and enhanced size of SP cell fractions, we chose to look at miR-9 expression in human tumors that had also been passaged in nude mice. Human HNSCC collected

from the University of Colorado Health Sciences Center were subcutaneously transplanted in to the flanks of athymic nude mice. After harvesting the passaged tumors, RNA was isolated and qRT-PCR was used to measure miR-9 expression. The tumor samples were divided into node positive and node negative samples based on TNM tumor staging. The miR-9 expression in the node positive tumors was then compared to the expression in the node negative tumors (Figure 42). While there was a wide variation in miR-9 expression in the node positive tumors, the increase in miR-9 expression in this group was significant ($p = 0.04$). These data further support a pro-metastatic role for miR-9 in HNSCC.

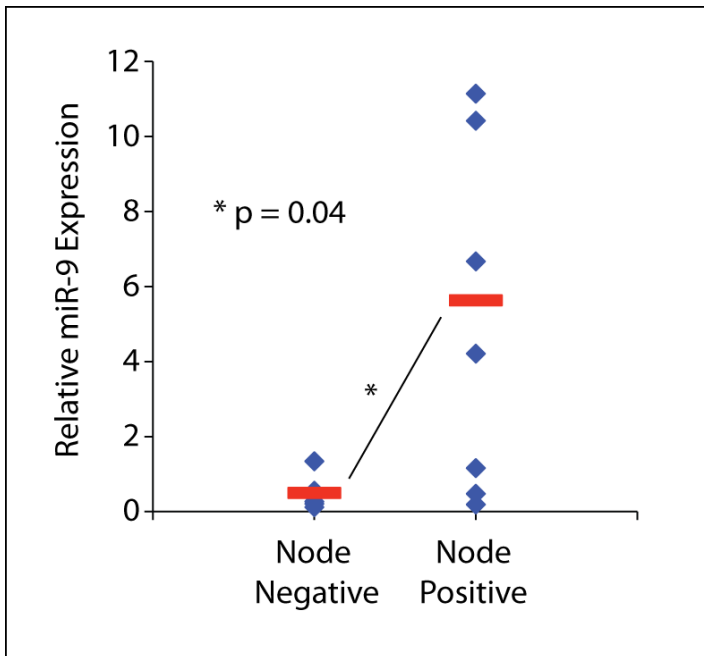


Figure 42. Increased miR-9 expression in node positive tumors after passaging. Human primary HNSCC was passaged in to athymic nude mice. Tumors were isolated and miR-9 expression was measured by qRT-PCR. miR-9 expression was compared between tumors that were

lymph node positive and lymph node negative based on TNM tumor staging. Blue diamonds represents individual tumor miR-9 expression and red bars represent the average expression for each group. Significance was determined using a Student's t-

*test. *Passaged human tumor samples were a gift from Dr. Antonio Jimeno at the University of Colorado Health Sciences Center.*

While each of the previous studies is promising, the sample size in each case is too small to accurately support any conclusions about the role of miR-9 in HNSCC. In order to address this problem, we looked at miR-9 expression in a larger number of primary human HNSCC (Figure 43). Of these tumors, 13 were node negative and 25 were node positive based on TNM staging. The expression of miR-9 in the tumor samples was compared to expression in normal control tissue obtained from pediatric tonsillectomy patients. Both the node positive and node negative samples showed a wide variation in miR-9 expression compared to control; however, there was no significant change in the median miR-9 expression between these groups. The wide variation of miR-9 expression in the tumor samples indicates that there may be significant deregulation of this miRNA in tumors, and that expression analysis needs to be further stratified based on other factors.

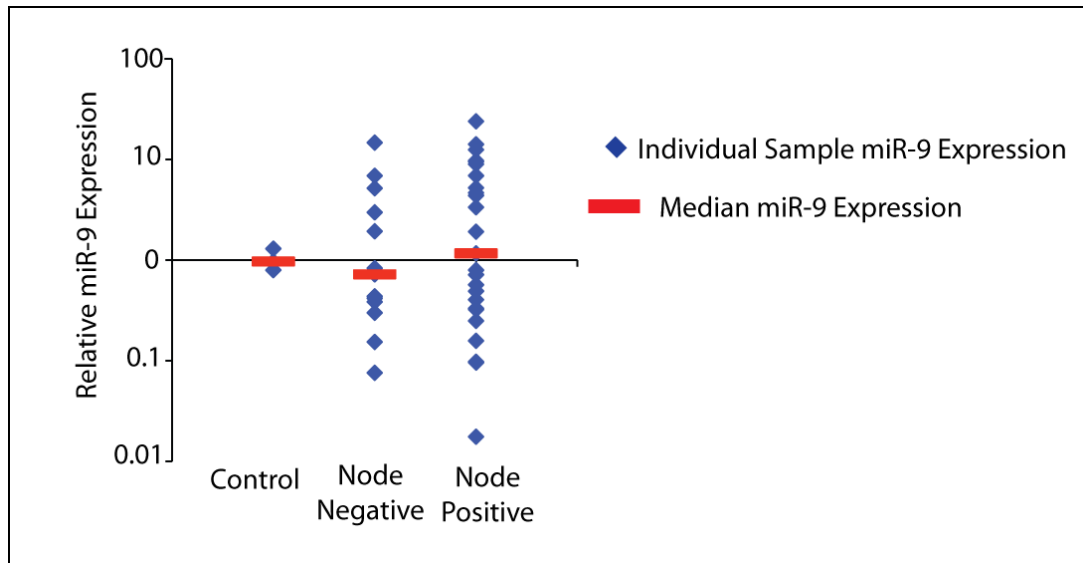


Figure 43. Wide variation in miR-9 expression in primary human HNSCC. miR-9 expression was measured by qRT-PCR in primary human HNSCC and control mucosa from pediatric tonsillectomies. Human HNSCCs were divided in to node positive and node negative tumors based on TNM staging, and expression was analyzed relative to miR-9 expression in control tissue. Blue diamonds represent individual samples and the red bars represent the median miR-9 expression for that group.

DISCUSSION

3.11 miR-9 Does Not Increase ABCB1 Expression in Human HNSCC Cells

Consistent with the studies in mouse skin SCC reported in chapter 2, we found that miR-9 can decrease the cycling of the human HNSCC line, Cal27, suggesting that this miRNA has similar functions in the mouse and human SCC lines. Unlike the mouse lines, however, overexpression of miR-9 in both Cal27 and Fadu did not alter the expression of ABCB1. The mouse *Abcb1a* and human ABCB1 genes share 37% homology [244], and as such would be predicted to share similar regulatory elements. One issue with comparing the human lines is the potential heterogeneity in the tumor lines. The Cal27 and Fadu lines have been well established, and as such, they are very genetically unstable. It is possible that genetic aberrations in the ABCB1 gene or regulatory regions may alter the effect miR-9 may have on expression of this gene. Another issue regarding miR-9 regulation of ABCB1 is the background expression of this gene in the tumor cells. The mouse lines all have some expression of the *Abcb1a* gene prior to overexpression of miR-9. In this case miR-9 may support the existing elements regulating *Abcb1a* expression and thus result in amplified expression. In the human HNSCC cell lines, however, there is very little background expression of ABCB1, and because of this, overexpression of miR-9 would may not support a further increase in ABCB1 expression. It is possible that other ABC transporters are highly expressed in these cells and future studies are needed to determine if miR-9 alters

the expression of any of these. Studies are also warranted to determine if miR-9 may affect chemoresistance by another mechanism, such as inhibition of apoptosis.

3.12 miR-9 Increases Invasion of Human HNSCC Cells

Studies of the effect of miR-9 overexpression on invasion and migration were consistent with those seen in the mouse SCC cells reported in chapter 2. Again, miR-9 increased both invasion and migration of the Cal27 and Fadu HNSCC cells, with a greater effect seen in the invasive properties of the cells. This consistency between cell types suggests that this regulation may be a major function of miR-9 in metastasis. Further studies are now needed to determine whether miR-9 affects metastasis of the human HNSCC cells *in vivo*.

3.13 miR-9 Expression may be Associated with Metastasis in Human HNSCC

The studies of miR-9 expression in human HNSCC were somewhat inconclusive. In the initial studies, miR-9 appeared to be increased preferentially in lymph node metastases. Unfortunately the sample size of metastasis samples was too small to generate any conclusions about miR-9 expression in metastasis. Similarly in the passaged human HNSCC samples, miR-9 expression in the tumors correlated with the presence of lymph node metastases in the patients, as determined by TNM staging. However this trend was not seen in the primary tumors. One reason for this could result from the selection of miR-9 expressing cells upon passaging, similar to the mouse tumors. If miR-9 is expressed at higher levels in the TIC populations it follows that miR-9 expression would be increased in the

passed and grafted tumors. In the primary tumors any differences in miR-9 expression may be masked because of the small size of the TIC populations compared to the bulk of the tumor.

A number of other factors may account for the wide variation in miR-9 expression in the primary human HNSCC samples. The precursor miR-9 is transcribed from three different chromosomes, but when processed the mature miR-9 has the same sequence regardless of its origin. In humans pre-miR-9-1 lies on chromosome 1, pre-miR-9-2 lies on chromosome 5 and pre-miR-9-3 lies on chromosome 15. In mice, pre-miRs 1-3 lie on chromosomes 3, 13 and 7 respectively. Of these different precursors, pre-miR-9-1 and pre-miR-9-2 have been shown to be highly methylated [211, 245] and increased methylation at these sites has been associated with increased metastasis in clear cell renal cell carcinoma [211] and colorectal cancer [212].

The wide variability in miR-9 expression in the primary human HNSCC may also be due to chromosomal aberrations. In humans, chromosome 5q14.3, the site of miR-9-2, is lost in approximately 20% of human oral SCC [97]. This loss may partially account for the tumors that exhibit very low levels of miR-9. On the other hand, chromosomal regions 1q22 (containing miR-9-1) and 15q26.1 (containing miR-9-3) are both gained in approximately 10% of oral SCCs [97] and may account for some of the samples with high miR-9 expression.

In the mouse model miR-9 expression clearly correlated with SPCC tumors. Based on this finding it would be interesting to examine the miR-9 levels in these tumors compared to more differentiated tumors, however human SPCC is rare and therefore, it would be difficult to attain enough patient samples for this study. One problem with studying EMT in human tissue is the relatively small proportion of tumor cells that undergo EMT. Because of this problem, a better mechanism for visualizing miR-9 expression in the human HNSCC may be to use *in situ* hybridization for miR-9 to potentially localize its expression to regions of EMT within the tumors.

CHAPTER FOUR

INCREASED SOX2 EXPRESSION IN THE SP⁻/CD34⁺/CD49f⁺ TUMOR-INITIATING CELL POPULATION FROM XENOGRAFTED TUMORS

METHODS

4.1 Tumor cell isolation and Fluorescence Activated Cell Sorting

Tumors were harvested from the mice and digested in a collagenase solution (250U/ml) (Worthington Biochemical, Lakewood, NJ) at 37°C for 30 minutes. After this time, the cells were manually dissociated by pipetting up and down approximately 10 times with a 10ml serological pipette. The cells were then incubated at 37°C for an additional 15 minutes. After a second round of manual dissociation the cells were filtered through a 70µm filter. The cells were then pelleted and resuspended in a solution of PBS 3% FBS at 1×10^6 cells/ml for Hoechst staining. The cells were stained at 25ng/ml Hoechst 33342 dye (Sigma-Aldrich, St. Louis, MO) in the dark in a 37°C water bath for 90 minutes [164]. Control cells were stained in the presence of 100µM verapamil to inhibit Hoechst dye efflux. After Hoechst staining the cells were pelleted and resuspended in 1ml PBS 3%FBS. The cells were then stained with FITC-CD31, FITC-CD45, Biotin-CD34 and PE-Cy5 CD49f for 20 minutes (for all antibodies and concentrations see Appendix A). In the case of sorting GFP positive cells, APC-CD31 and APC-CD45 were substituted for the FITC-conjugated antibodies. Secondary streptavidin-PE was then added to the cells to mark the CD34 positive cells and incubated for 20 minutes. Prior to flow sorting the cells were washed, filtered (40µm filter) and propidium iodide (PI) (1µg/ml) was added to select for live cells at least 5 minutes prior to sorting.

FACS analysis was performed by the UC Denver Flow Cytometry Core on a Beckman Coulter MoFlo-XDP (Beckman Coulter, Brea CA) data analysis was conducted using Summit Software V5.3 (Beckman Coulter, Brea CA). Single flurochrome stained Rat IgG control beads (BD Bioscience) were used for staining controls and setting compensation. Gating included forward/side scatter and dead cell exclusion with PI. Tumor cells were sorted for the Hoechst^{low} CD31⁻ CD45⁻ that was designated as the SP. A second cell population was sorted for Hoechst^{high} CD31⁻ CD45⁻ CD34⁺ CD49f⁺ and designated as the CD34⁺ CD49f⁺ population. The third cell population was sorted for Hoechst^{high} CD31⁻ CD45⁻ CD34⁻ CD49f⁻.

4.2 Analysis of Gene Expression

RNA Isolation:

Total RNA, consisting of both the small and large RNA species, was isolated using the Qiagen miRNeasy mini kit (Qiagen, Valencia CA) as per the manufacturer's instructions. Briefly, 800-10x10⁶ pelleted cells were resuspended in 700µl of Qiazol lysis reagent. For sorted cells, where a small number of cells (<3x10⁶) were processed, homogenization was performed by vortexing the cells for 1 minute. For larger numbers of cells (>3x10⁶) and tissue samples, homogenization was performed using a bench top homogenizer. The total RNA was eluted from the column using 30µl of RNase free water.

Quantitative RT-PCR:

One-step qRT-PCR for gene expression: One-step qRT-PCR was used for gene expression when RNA samples were not limiting and amplification was not necessary. One-step qRT-PCR was performed using 100ng of RNA per reaction with the One-Step Brilliant II QRT-PCR system (Stratagene, Santa Clara CA). Expression of mRNA was measured using TaqMan® Assays-on-demand™ probes (Applied Biosystems, Carlsbad CA). All gene measurements were normalized to a GAPDH (human) or Gapdh (mouse) RNA probes. See appendix for TaqMan® probe details. Each sample was run in triplicate and the data was analyzed using a standard relative quantification ($\Delta\Delta Ct$) method. Reactions were run on a Stratagene MX3000P qPCR machine (Stratagene, Santa Clara CA).

Two step qRT-PCR with pre-amplification for gene expression: For gene expression analysis on very small quantities of RNA, such as those generated from the sorted tumor cells, a two-step qRT-PCR reaction was performed with an amplification step. The first step involved an RT reaction starting with 2-200ng RNA. cDNA was generated using the High-Capacity cDNA Reverse Transcription kit (Applied Biosystems, Carlsbad CA), as per the manufacturers instructions. For the preamplification step, a pooled mix of TaqMan probes was made. Each of the probes were combined and diluted to 0.2x. The pooled assay mix was combined with 1-250ng cDNA and PreAmp Master Mix (Applied Biosystems, Carlsbad CA) as per the manufacturers instructions. The selected genes were amplified using 14 cycles to maintain amplification in the linear range. The qPCR reaction was performed using

TaqMan Universal master mix (Applied Biosystems, Carlsbad CA) according to the manufacturers instructions. The results were analyzed using the $\Delta\Delta C_t$ method and normalized to Gapdh. Reactions were run on a Stratagene MX3000P qPCR machine (Stratagene, Santa Clara CA).

Statistical Analysis

For all qRT-PCR data, error bars are represented as the standard deviation between samples (triplicate), unless otherwise noted. In these cases, the standard error was used instead. In general standard error was used when there was wider variation between samples and larger numbers of samples were used, as in the case of tumor samples. Standard deviation was generally used with *in vitro* studies and studies with fewer replicates. Significance was assessed using a standard student's t-test.

4.3 Cell culture

Generation of Primary Tumor Cultures:

Primary tumor cultures were generated from both primary and passaged tumors. Tumor tissue was harvested and the cells dissociated in collagenase (250U/ml) (Worthington Biochemical, Lakewood, NJ) for 45 minutes at 37°C. The cells were further dissociated manually by pipetting up and down. The cells were then filtered through a 40 μ m filter and washed in a culture medium of DMEM with 10% FBS. The cells were then plated in 10cm culture dishes and cultured at 5% CO₂ in a standard cell culture incubator. Prior to subculturing, the cells were treated with TrypLE (Invitrogen, Carlsbad CA) for 2 min and the floating cells discarded to

select for epithelial cells. This selection was repeated prior to the subsequent 3-5 subcultures or as needed to remove fibroblast contamination. In total, 10 separate cell lines were generated from primary tumors and passaged tumors. However, three lines were used in this study all of which were generated from passaged tumors, B931, B911 and S4#8.

Retrovirus production

Retroviruses (Appendix B) were produced in a similar manner to the lentivirus with the exception that the Θ nX-E packaging cell line was used and the pCL-ECO packaging vector was cotransfected with the retroviral vector. For human retroviruses, 293T packaging cells were used, and PUMVC, and pCMV-VSV-G were used for packaging (Appendix B). Virus harvesting was the same as for lentiviral particles.

Transduction and Selection of Transduced Cells

After harvesting from 293T cells or Θ nX-E cells, the culture medium containing virus was centrifuged at 3000rpm for 15 minutes to pellet any cellular debris. The 8nM polybrene was added to the media to aid in transduction. For a 10cm plate, 6ml of virus containing medium was added to the target cells. The cells were then incubated with the viral media for 24-48 hours for transduction. Selection of transduced cells was done by puromycin selection.

4.4 Cell Growth Assays

In vitro cell proliferation was measured using a WST-8 [2-(2-methoxy-4-nitrophenyl)-3-(4-nitrophenyl)-5-(2, 4-disulfophenyl)-2H-tetrazolium, monosodium salt] Cell Count Reagent (Nacalai Tesque, Inc. Japan). Cell proliferation assays were performed on tumor cell lines transduced with miR-9 or GFP transduced control cell lines. For the cell growth assay, 50 cells were plated in a series of 96 well plates in triplicate. The proportion of viable cells was measured at 24, 48, and 72 hours by adding 10 μ l of WST-8 Cell Count Reagent to each well. The plates were incubated for at 37°C in a standard tissue culture incubator for 2 hours and then the absorbance of the reaction was measured at 450nm using a micro plate reader. At an absorbance 450nm the WST-8 reagent is proportional to the number of viable cells.

4.5 Invasion/Migration Assays

Invasion and migration assays were conducted using BD Bioscience Matrigel (Franklin Lakes, NJ) invasion chambers and transwell migration chambers. Prior to plating cells, the Matrigel layer was rehydrated in DMEM 10% FBS for 2 hours at 37°C. Once rehydrated 1x10³-5x10³ tumor cells transduced with miR-9 or miR-9 knockout vectors or controls were plated in the matrigel invasion chamber or transwell migration chamber in 500 μ l serum free medium. DMEM containing 10% FBS was used as a chemoattractant in the bottom well (750 μ l). The cells were then incubated at 37°C in a standard tissue culture incubator to allow for cell migration

and invasion. After 24 hours the plates were removed from the incubator, and the cells that had not migrated or invaded were removed from the inside of the transwell by scrubbing the membrane with a cotton swab. The migrated/invaded cells were stained fixed in Diff-Quick fixing medium for 2 minutes, then stained with 0.05% crystal violet for an additional 2 minutes. The membranes were washed well in water then left overnight to dry. Once dry the membranes were removed from the transwells and placed on slides with Fluormount G (Southern Biotech, Birmingham AL). To quantify the invading and migrating cells, 3 microscopic fields (10x) were imaged per membrane and the average number of cells per field was counted. Each assay was done in triplicate such that a total of 9 fields were counted for each condition.

RESULTS

4.6 Sox2 is increased in the SP⁻/CD34⁺/CD49f⁺ TIC from Passage 1 Tumors

Sox2 is increased in the SP⁻/CD34⁺/CD49f⁺ cell populations from Passage 1 tumors

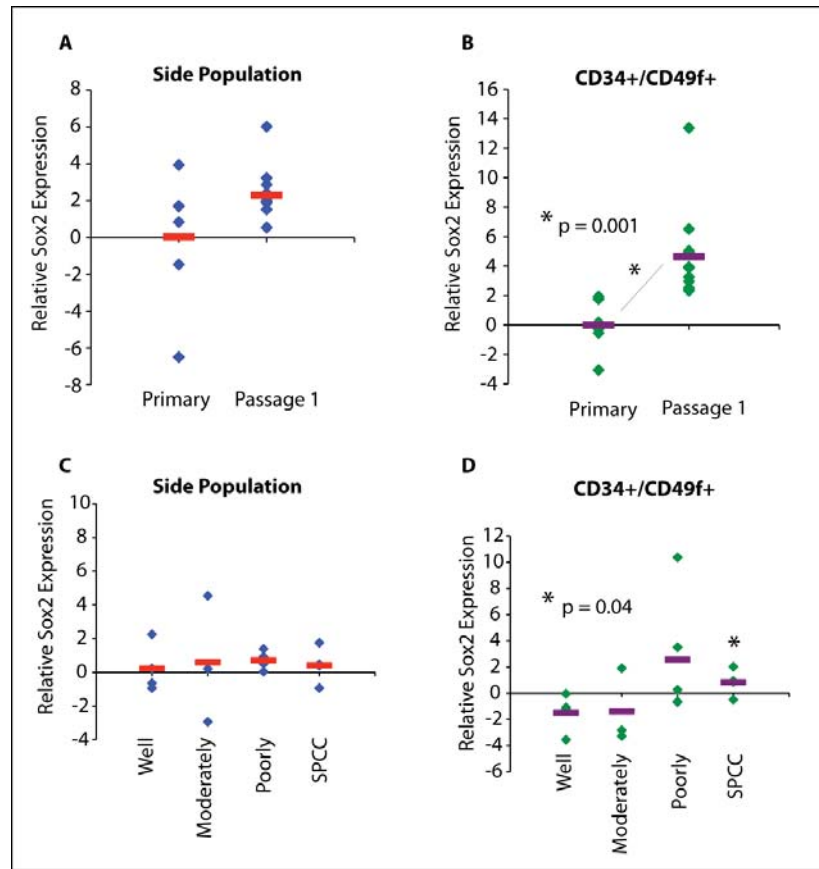
One of the major characteristics of TICs is the acquisition of stem-like traits, such as self-renewal and relative quiescence. Therefore, we wanted to determine if the TICs from the Passage 1 tumors characterized in Chapter 2 showed increased expression of stem cell genes contributing to the increased stem cell populations of these tumors. We used qRT-PCR to screen for a number of well-established stem cell genes including, Sox2, Oct4, Nanog and Bmi1, in the TIC populations from the Primary and Passage 1 tumors. We found that Oct4, Nanog and Bmi1 were not expressed in the TICs from either the Primary or the Passage 1 tumors. While Sox2 was expressed, there was no difference in expression between the TIC and non-TIC populations. However, when we compared the expression between the TICs from the Primary and Passage 1 TICs, we saw a slight, but insignificant, increase in Sox2 between the Primary and Passage 1 SP populations ($p = 0.1$) (Figure 44A). Interestingly, we found that there was a significant increase in Sox2 expression between the SP⁻/CD34⁺/CD49f⁺ populations from the Primary and Passage 1 tumors ($p = 0.001$) (Figure 44B). Similarly, when we compared the Sox2 expression in the SP and SP⁻/CD34⁺/CD49f⁺ populations with the tumor histology, we found that there was no significant difference in the SP Sox2 expression between tumor types (Figure 44C). There was, however, a significant increase in the SP⁻/CD34⁺/CD49f⁺ Sox2 expression in SPCC tumors compared to well-differentiated tumors (Figure

44D). There was also an increase in SP⁻/CD34⁺/CD49f⁺ Sox2 expression in the poorly-differentiated tumors; however, these data were not significant due to the large variation in expression between tumor samples.

Figure 44. Increased Sox2 expression in the SP⁻/CD34⁺/CD49f⁺ cell population of

Passage 1 tumors

and SPCC. (A) Relative Sox2 expression in the SP cells from Passage 1 tumors compared to SP cells from Primary tumors. Blue diamonds represent individual tumor samples, and red



lines represent average expression for each tumor type. (B) Relative Sox2 expression in the SP⁻/CD34⁺/CD49f⁺ cells from Passage 1 tumors compared to SP⁻/CD34⁺/CD49f⁺ cells from Primary tumors. Green diamonds represent individual tumor samples, and purple lines represent average expression for each tumor type. (C) Sox2 expression in SP cells compared to tumor histology. (D) Sox2 expression in SP⁻/CD34⁺/CD49f⁺ cells compared to tumor histology. Significant increase in Sox2 expression in SPCC

*compared to well differentiated tumors in SP⁻/CD34⁺/CD49f⁺ cells was determined using a Student's t-test: * p = 0.04. In each case Sox2 expression was measured by qRT-PCR and normalized to Gapdh expression. Relative expression was then determined by comparing Sox2 expression in Passage 1 tumors to Primary tumors (A, B) or by comparing Sox2 expression to the average Sox2 expression of all samples (C, D).*

To further study the role of Sox2 in the regulation of the K15.Kras^{G12D}.Smad4^{-/-} tumors, we used the cell cultures from these tumors to alter Sox2 expression. We conducted qRT-PCR to determine the relative levels of Sox2 in each of the tumor lines (Figure 45A). From this analysis, we chose the line with the lowest Sox2 levels (B911) for overexpression and the line with the highest expression for the knockdown (B931). Unfortunately, we were not successful in knocking down Sox2 using transient siRNAs or lentiviral shRNAs against Sox2. Sox2 overexpression in the B911 line was accomplished by retroviral integration of the Sox2 gene. We also overexpressed Sox2 in a normal WT keratinocyte cell line to determine the effect of Sox2 expression in non-tumorigenic cells. Sox2 overexpression was confirmed by qRT-PCR in both cell lines, and was significantly increased to levels greater than 100 fold higher than the control cells (Figure 45B). Cell proliferation assays showed that increased expression of Sox2 resulted in slower growth of the non-tumorigenic WT keratinocyte cell lines (Figure 45C), but had no effect on the growth of the tumor cells (Figure 45D). This discrepancy is potentially due to dysregulation of the cell cycle in the tumor cell line, which allows them to tolerate elevated Sox2 expression.

Since there was an increase in Sox2 expression in the SP⁻/CD34⁺/CD49f⁺ populations from the more metastatic Passage 1 tumors we wanted to see if the increase in Sox2 expression contributed to the metastatic behavior of these cells. We used trans-well assays to compare the differences in invasion and migration between control and Sox2 overexpressing cells. The WT keratinocytes were not invasive and migratory enough to accurately study the effect of Sox2 on these behaviors. However, the tumor cell lines showed a significant decrease in both migration (Figure 45E) through the transwell and invasion (Figure 45F) through a matrigel basement membrane layer in the Sox2 overexpressing cells compared to control. Since Sox2 overexpression was more closely correlated with the SP⁻/CD34⁺/CD49f⁺ cells than the SP cells, this Sox2-mediated decrease in metastatic behavior further provides evidence that the SP and SP⁻/CD34⁺/CD49f⁺ TIC populations may play different roles in tumor progression.

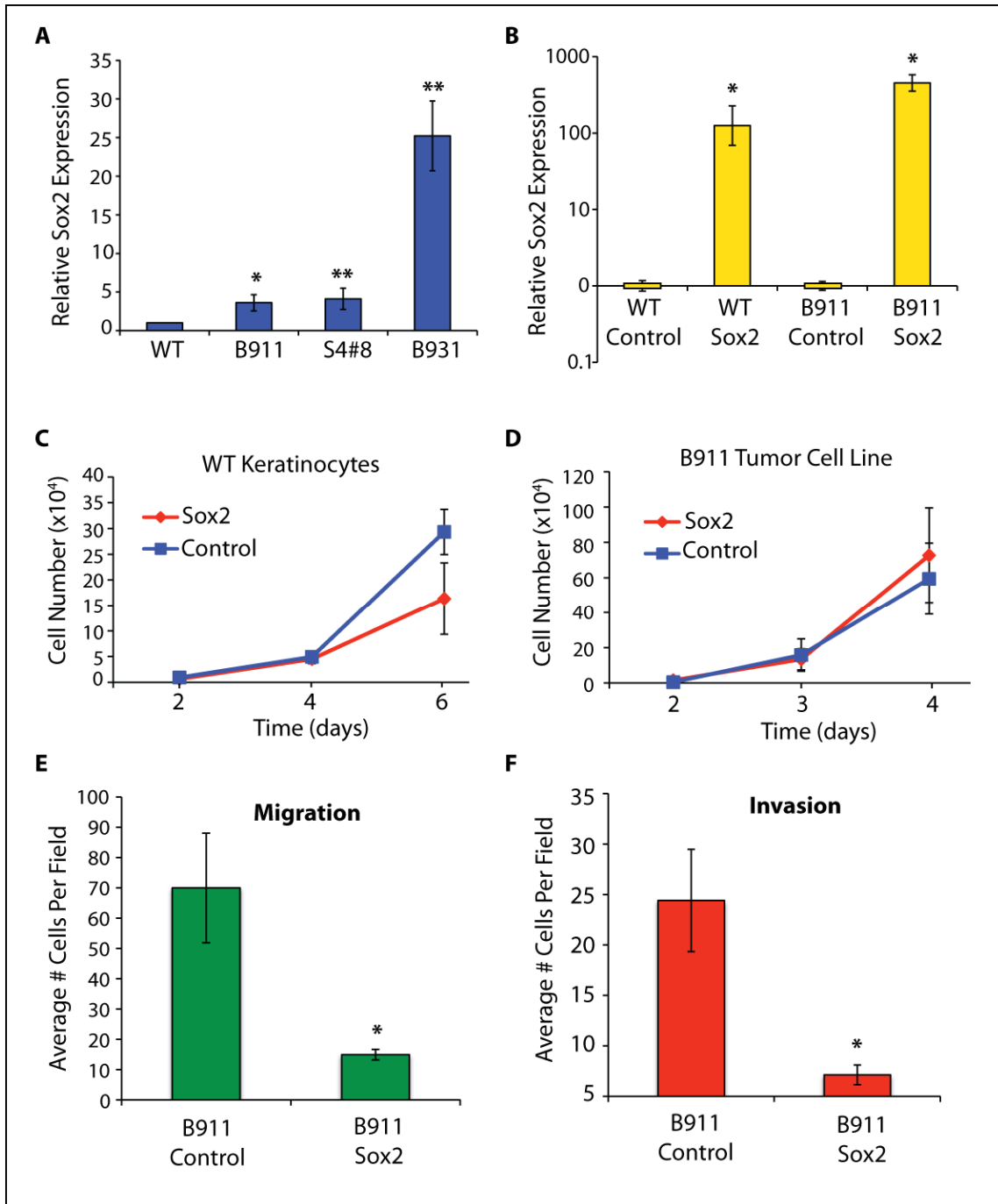


Figure 45. Sox2 overexpression slows cell growth in non-tumorigenic keratinocytes and decreases invasion and migration in tumor cells. (A) Sox2 expression in K15.Kras^{G12D}.Smad4^{-/-} tumor cell lines, relative to normal WT

keratinocyte cell lines. * $p < 0.05$ and ** $p < 0.005$. (B) Forced overexpression of Sox2 in WT keratinocytes and B911 tumor cell line. * $p < 0.001$. Sox2 expression was measured by qRT-PCR and normalized to Gapdh expression. Significance was determined using a Student's t-test. (C) Growth curves of control and Sox2 overexpressing WT keratinocytes. (D) Growth curve of control and Sox2 overexpressing B911 tumor cells. (E) Transwell migration assay of control and Sox2 overexpressing B911 tumor cells. * $p < 0.005$. (F) Matrigel invasion assay of control and Sox2 overexpressing B911 tumor cells. * $p < 0.005$. In each Figure, error bars represent standard deviation.

DISCUSSION

4.7 The CD34⁺/CD49f⁺ TIC Population has Increased Expression of the Stem Cell Gene, Sox2, after Passaging.

One of the known characteristics of TICs is the acquisition of stem-like traits. When we screened for the expression of a number of stem cell genes in the TIC populations, we only found Sox2 to be expressed in the tumors. Surprisingly, there was no increase in Sox2 expression when we compared the TICs with the non-TIC populations, however we did see an increase in Sox2 expression in the Passage 1 tumor TICs compared to the Primary tumor TICs. This increase further supported the idea that the Passage 1 tumors are enriched for TICs. Unlike the miRNA profiles of the TICs, Sox2 was not increased in the Passage 1 SP cells compared to the Primary tumor SP cells; instead the difference was seen in the SP⁻/CD34⁺/CD49f⁺ population. This difference was also seen when comparing Sox2 expression with tumor histology. While there was no correlation between Sox2 expression and histology in the SP cells, there was a significant increase in the Sox2 expression in SP⁻/CD34⁺/CD49f⁺ cells from the SPCC tumors.

Our functional studies of Sox2 overexpression *in vitro*, showed that Sox2 decreases the proliferation of non-tumorigenic epithelial cell lines, but not tumor lines. The decrease in proliferation after expression of a stem cell gene is expected due to the relative quiescence of stem cells to more mature progenitors; however

the tumor lines may have defects in cell cycling that overcome the Sox2 induced quiescence.

To determine if Sox2 might play a role in metastasis in the Passage 1 tumors, we conducted invasion and migration assays on the Sox2 overexpressing cell lines. Interestingly, Sox2 expression appeared to reduce both invasion and migration of the tumor cells. While these experiments need to be repeated in other cell lines, these data suggest that the Sox2 expressing cells may not be metastatic. Taken together these observations further support the idea that the SP⁻/CD34⁺/CD49f⁺ and SP are distinct TIC populations with different functions in tumor initiation. Additionally, each population appears to have different regulatory elements, for example, these studies suggest that the SP⁻/CD34⁺/CD49f⁺ population requires Sox2 for maintaining “stemness”, while the SP is not dependent on this gene. While the SP TIC appears to play a role in metastasis, the SP⁻/CD34⁺/CD49f⁺ population shows increased expression of stem cell genes and decreased motility. It is possible that this population may function in other tumor-initiating situations such as tumor recurrence.

CHAPTER FIVE

SUMMARY AND CONCLUSIONS

Squamous cell carcinoma of the head and neck and skin are common forms of cancer arising from squamous epithelial tissue. HNSCC is the sixth most common cancer worldwide, however, few advances have been made in the treatment of this cancer over the last 50 years [1]. Most patients with HNSCC present with locally advanced disease involving the loco-regional lymph nodes, and this late presentation contributes to treatment failure [3]. Skin SCC is one of the most frequently occurring forms of cancer [1]. In most cases, skin SCC can be well controlled if caught early, however, in immunocompromised patients, skin SCC can be quite aggressive and highly metastatic. Metastasis and tumor recurrence after treatment are the major causes of patient mortality with SCC. Tumor-initiating cells are believed to be the source of both metastases and tumor recurrence [128] and as such development of therapies targeted at this cell population is essential to improving prognosis these diseases.

In this dissertation work we developed a mouse model in which Smad4 and Kras^{G12D} mutations are targeted to the hair follicle bulge stem cells. These mice develop metastatic SCC as well as sebaceous adenomas and BCC-like SCC suggesting that the mutant stem cells maintain pluripotency. Using this model we identified two distinct TIC populations that appear to have different functions. Our results

suggest that the side population is associated with metastasis. We identified a number of miRNAs that are differentially expressed in the SPs from highly metastatic Passage 1 tumors. Of these miRNAs, increased levels of miR-9 and miR-132 are associated with larger SP size and SPCC tumor histology. The increase in miR-9 expression is regulated in part by Kras activation. miR-9 has been shown to target E-cadherin [196] and may promote EMT in these tumors resulting in SPCC histology. Our data further suggests that miR-9 may be associated with increases in the expression of *Abcb1a* in the mouse tumors resulting in amplification of the SP size and chemoresistance. Additionally, miR-9 promotes increased migration and invasion of tumor cells *in vitro* and may support tumor growth in immunocompetent mice. Finally, we showed that the SP⁻/CD34⁺/CD49f⁺ population has increased expression of the stem cell gene, *Sox2*, in the more aggressive Passage 1 tumors, but that *Sox2* overexpression decreases invasion and migration of tumor cells. These data suggest that the SP⁻/CD34⁺/CD49f⁺ population is not associated with metastasis, but may have other tumor initiating functions such as tumor recurrence.

Taken together our results from this study suggest that in the skin the slow cycling stem cell population is likely the target of oncogenic mutations leading to skin SCC. By generating mutations in the hair follicle bulge stem cells we were able to generate tumors containing regions of cells from multiple different hair follicle lineages, demonstrating that the mutant epithelial stem cells maintain pluripotency.

Identification and analysis of TICs in our K15.Kras^{G12D}.Smad4^{-/-} tumors showed that there are distinct populations of TICs within tumors and that these populations have different genetic identities. Our results suggest that the SP and SP⁻/CD34⁺/CD49f⁺ TICs in the K15.Kras^{G12D}.Smad4^{-/-} tumors may contribute to tumor progression in different ways as summarized in Figure 46. The increased size of the SP in the metastatic SPCC tumors suggests that this population is involved in metastasis. Increased expression of miR-9 in the SP promotes invasion and migration of the tumor cells and subsequently is likely to increase metastasis. This population also has increased levels of the Abcb1a, or other ABC transporters, which contribute to chemoresistance and survival of these metastatic cells. Our results also suggest that the SP⁻/CD34⁺/CD49f⁺ population is distinct from the SP and plays a different role in tumor progression. We found that the SP⁻/CD34⁺/CD49f⁺ population has increased Sox2 expression in the aggressive passage 1 tumors, however, reduction in invasion and migration of tumor cells after Sox2 overexpression suggests that this population is not involved in metastasis. Rather, these cells may play other roles in cancer progression where tumor-initiation is required, such as tumor recurrence.

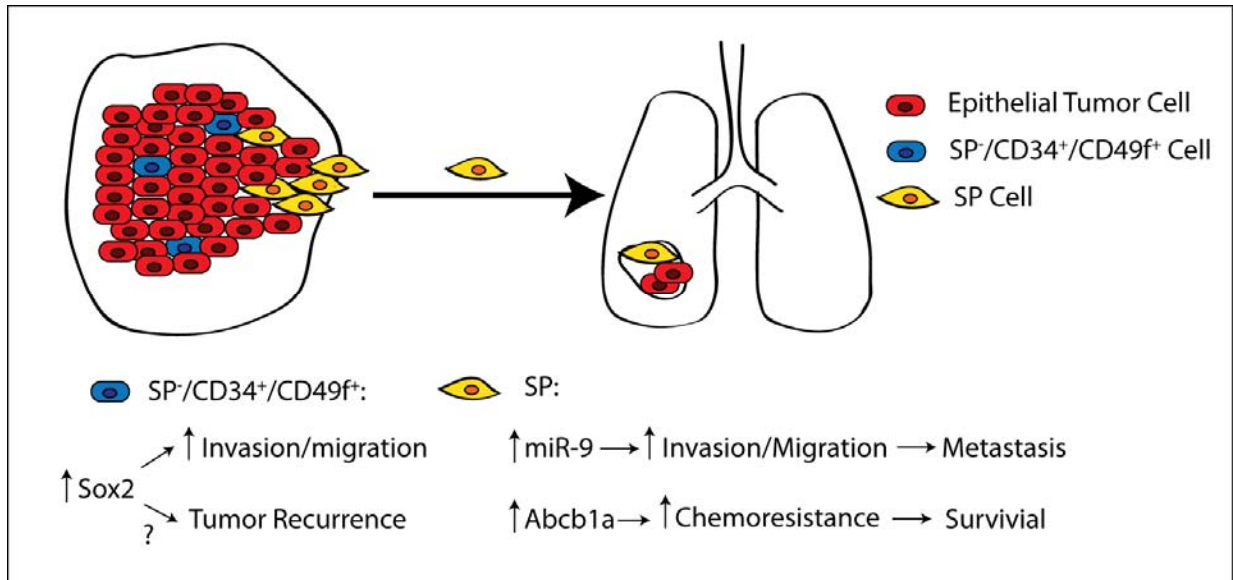


Figure 46. Potential Roles of Distinct Tumor-Initiating Cells in Cancer Progression. Increased miR-9 in the side population (SP) results in increased migration and invasion of the TIC, survival of this cell population is supported by increased expression of the ABC transporter, Abcb1a. These properties allow the TIC to escape from the parent tumor and surviving in the circulation before the TIC lands at the distant metastatic site. The tumor-initiating capabilities of this cell allows for development of the metastasis. Increased expression of Sox2 in the SP-/CD34+/CD49f+ TIC population inhibits invasion and migration and therefore these cells may play a different tumor-initiating role such as tumor recurrence.

CHAPTER SIX

FUTURE DIRECTIONS

6.1 Studying the Tumor-Initiating and Metastatic Potential of the SP and SP⁻/CD34⁺/CD49f⁺ Cell Populations

In chapter 2 we showed that 1×10^4 SP or SP⁻/CD34⁺/CD49f⁺ cells were sufficient to form grafted tumors from the K15.Kras^{G12D}.Smad4^{-/-} tumors. Further studies are needed in these tumors to determine the minimum number of sorted tumor cells required for tumor initiation. We predict that that this number is lower for the passage 1 tumors compared to the primary tumors due to the rate at which the passage 1 tumor can form subsequent tumor passages. A series of sorting and grafting experiments from primary and passage 1 tumors with decreasing numbers of TICs are needed to answer this question. *In vitro* soft agar assays may support these results by comparing the relative numbers of colonies formed after equal numbers of primary and passage 1 tumor cells are plated.

Another question that remaining, is whether the SP is the metastatic population. To help answer this question it would be interesting to sort SP and SP⁻/CD34⁺/CD49f⁺ cell populations as well as the corresponding non-TIC population and conduct invasion and migration assays on these cells. If the SP is a metastatic population, it should be more invasive and migratory than either the SP⁻

/CD34⁺/CD49f⁺ or the non-TIC population. Analysis of metastasis after grafting the SP and SP⁻/CD34⁺/CD49f⁺ populations may also indicate whether the SP is more of a metastatic population. This *in vivo* study, however, may be confounded by the ability of the TIC populations to form heterogeneous tumor populations, i.e. the SP TIC can generate tumors containing CD34⁺/CD49f⁺ cells. Another interesting study that could help determine if the SP is a metastatic population, would be to FACS sort the metastases to determine the relative percent of SP (and SP⁻/CD34⁺/CD49f⁺) cells in the metastases compared to the parent tumor. Unfortunately, the very small size and paucity of metastatic cells may also prohibit this study.

6.2 Transcriptional Regulation of miR-9 in SCC

This study only briefly touched on the transcriptional regulation of miR-9 in SCC. Kras activation only modestly increased the expression of miR-9 in the HaCaT cells, however, since these cells are not tumorigenic further study of the effect of Kras in tumor cell lines is warranted. For example, it would be interesting to activate Kras in the human HNSCC cell lines, Cal27 and Fadu, both of which are deficient in Smad4, and look at the effect of Kras on miR-9 expression in this context. Conversely, it would be interesting to block Kras activity in the K15.Kras^{G12D}.Smad4^{-/-} cell lines and determine whether this reduces the expression of miR-9. Similarly, to look at the effect of Smad4 on miR-9 expression in the oncogenic context, we could replace Smad4 in the K15.Kras^{G12D}.Smad4^{-/-} cell lines and examine the effect on miR-9 expression.

Other possible mechanisms of miR-9 transcriptional, and post-transcriptional regulation should be examined. For example, CREB has been shown to control the expression of miR-9 in neurons [210]. Expression levels of Creb should be studied in the TIC populations from primary and passage 1 tumors to determine if this gene is increased in the passage 1 SP cells. Finally, since methylation of miR-9 primary transcripts is commonly seen in human cancers [211], the methylation status in the TIC populations compared to the non-TIC cells should be examined.

6.3. The Role of miR-9 in SCC Chemoresistance

The data concerning the role of miR-9 in chmoresistance is somewhat inconclusive. On one hand miR-9 overexpression in the K15.Kras^{G12D}.Smad4^{-/-} tumor cells appears to promote an increase in Abcb1a expression, while on the other hand knockdown of miR-9 in the same cells has no effect on Abcb1a expression and miR-9 overexpression in human HNSCC cells also has no effect on ABCB1 expression. However, miR-9 expression is closely associated with the SP size in the K15.Kras^{G12D}.Smad4^{-/-} tumors, while Abcb1a is not. Therefore it is likely that other ABC transporters may be dysregulated in the Passage 1 tumors. Further studies are needed in the miR-9 overexpressing and knockdown cells to determine whether other ABC transporters are under the control of miR-9. The best method of studying this would be to perform gene expression microarrays on the miR-9 overexpressing and knockdown cells. Not only would this tell us about the relative expression of the ABC tansporters, it could also identify other potential mechanisms

of chemoresistance regulated by miR-9 such as anti-apoptotic mechanisms. Finally, since a number of miRNAs were found to be dysregulated in the SP cells between primary and passage 1 tumors, it would be interesting to examine the combined effects of these miRNAs in the regulation of chemoresistance.

6.4 The role of miR-9 in SCC Metastasis

The results from this study show a clear correlation between the EMT-like SPCC tumors and high miR-9 expression. This raises the question whether miR-9 promotes EMT, or whether increased expression of miR-9 is a result of EMT. To answer this, cell lines overexpressing miR-9 and/or with miR-9 knockdown could be stained for markers of EMT such as E-cadherin, vimentin, and N-cadherin and compared to control cells. If miR-9 promotes EMT in these cells, we would expect to see the staining shift to an EMT pattern after miR-9 overexpression. To determine if EMT promotes an increase in miR-9 expression, tumor cells, and/or other epithelial cell lines could be forced to undergo EMT through treatment with TGF β , or ectopic expression of Snail or Twist, and the effect on miR-9 determined. To further examine whether miR-9 expression is associated with metastases, a study comparing the expression of miR-9 in the metastases with the expression in the parent tumor should be conducted. If miR-9 is associated with increased metastasis, we would predict that there would be increased miR-9 expression in the metastasis.

Perhaps the most important studies needed to determine the effect of miR-9 in metastasis are *in vivo* studies. The current studies reported in this dissertation

work were confounded by the rapid growth of the K15.Kras^{G12D}.Smad4^{-/-} tumor cell growth and baseline metastatic rate after grafting the cell lines. These studies need to be repeated with much smaller number of cells to both slow growth and provide time to measure a difference in metastasis. Additionally, these experiments should be repeated with the miR-9 knockdown K15.Kras^{G12D}.Smad4^{-/-} cells since we predict that miR-9 should increase the metastatic potential of the tumor cells. Similarly, *in vivo* orthotopic injection of the human HNSCC lines, Cal27 and Fadu, with forced expression of miR-9 should be conducted to determine the effect of miR-9 on human SCC. Unpublished studies from our lab have shown that both the Fadu and Cal27 cell lines metastasize to the loco regional lymph nodes after orthotopic injection in to the floor of the mouth. Since our mouse model and previous studies with miR-9 have consistently shown differences in lung metastasis, it will be interesting to see if miR-9 overexpression re-directs the Cal27 and Fadu metastasis to the lung.

6.5 Does Sox2 Contribute to Tumor-Initiation and Chemoresistance in the SP⁻/CD34⁺/CD49f⁺ Population?

Since the SP⁻/CD34⁺/CD49f⁺ population expresses increased Sox2 in the passaged tumors, but increases in Sox2 appear to inhibit invasion and migration, we predict that this cell population may have other roles in tumor progression such as tumor recurrence. To further study whether help promote tumor-initiation in the SP⁻/CD34⁺/CD49f⁺ cells it would be interesting to conduct limiting dilution studies in mouse grafts of tumor cells overexpressing Sox2 compared to controls. To strengthen these studies, it would be important to generate Sox2 knockdown lines

and include them in these grafting studies, as well as in the invasion and migration studies. *In vitro* soft agar studies may also help support the *in vivo* studies on the regulation of tumor-initiation by Sox2. Finally, since tumor recurrence occurs as the result of treatment failure, it will be important to determine whether Sox2 plays a role in chemo- and/or radiation resistance in the tumor cells.

CHAPTER SEVEN

REFERENCES

1. Parkin, D.M., et al., *Global cancer statistics, 2002*. CA Cancer J Clin, 2005. **55**(2): p. 74-108.
2. Edwards, B.K., et al., *Annual report to the nation on the status of cancer, 1975-2006, featuring colorectal cancer trends and impact of interventions (risk factors, screening, and treatment) to reduce future rates*. Cancer, 2009.
3. Argiris, A., et al., *Head and neck cancer*. Lancet, 2008. **371**(9625): p. 1695-709.
4. Curado, M.P. and M. Hashibe, *Recent changes in the epidemiology of head and neck cancer*. Curr Opin Oncol, 2009. **21**(3): p. 194-200.
5. Hecht, S.S., *Tobacco carcinogens, their biomarkers and tobacco-induced cancer*. Nat Rev Cancer, 2003. **3**(10): p. 733-44.
6. Licitra, L., et al., *High-risk human papillomavirus affects prognosis in patients with surgically treated oropharyngeal squamous cell carcinoma*. J Clin Oncol, 2006. **24**(36): p. 5630-6.
7. Prime, S.S., et al., *A review of inherited cancer syndromes and their relevance to oral squamous cell carcinoma*. Oral Oncol, 2001. **37**(1): p. 1-16.
8. Forastiere, A., et al., *Head and neck cancer*. N Engl J Med, 2001. **345**(26): p. 1890-900.

9. Mao, L., W.K. Hong, and V.A. Papadimitrakopoulou, *Focus on head and neck cancer*. Cancer Cell, 2004. **5**(4): p. 311-6.
10. Hunter, K.D., E.K. Parkinson, and P.R. Harrison, *Profiling early head and neck cancer*. Nat Rev Cancer, 2005. **5**(2): p. 127-35.
11. McCaul, J.A., et al., *Telomerase inhibition and the future management of head-and-neck cancer*. Lancet Oncol, 2002. **3**(5): p. 280-8.
12. Leemans, C.R., B.J. Braakhuis, and R.H. Brakenhoff, *The molecular biology of head and neck cancer*. Nat Rev Cancer. **11**(1): p. 9-22.
13. Grandis, J.R. and D.J. Tweardy, *Elevated levels of transforming growth factor alpha and epidermal growth factor receptor messenger RNA are early markers of carcinogenesis in head and neck cancer*. Cancer Res, 1993. **53**(15): p. 3579-84.
14. Song, J.I. and J.R. Grandis, *STAT signaling in head and neck cancer*. Oncogene, 2000. **19**(21): p. 2489-95.
15. Grandis, J.R., et al., *Constitutive activation of Stat3 signaling abrogates apoptosis in squamous cell carcinogenesis in vivo*. Proc Natl Acad Sci U S A, 2000. **97**(8): p. 4227-32.
16. Shin, D.M., et al., *Dysregulation of epidermal growth factor receptor expression in premalignant lesions during head and neck tumorigenesis*. Cancer Res, 1994. **54**(12): p. 3153-9.
17. van Oijen, M.G., et al., *Increased expression of epidermal growth factor receptor in normal epithelium adjacent to head and neck carcinomas independent of tobacco and alcohol abuse*. Oral Dis, 1998. **4**(1): p. 4-8.

18. Karamouzis, M.V., J.R. Grandis, and A. Argiris, *Therapies directed against epidermal growth factor receptor in aerodigestive carcinomas*. JAMA, 2007. **298**(1): p. 70-82.
19. Chang, S.E., et al., *Ras mutations in United Kingdom examples of oral malignancies are infrequent*. Int J Cancer, 1991. **48**(3): p. 409-12.
20. Lu, S.L., et al., *Loss of transforming growth factor-beta type II receptor promotes metastatic head-and-neck squamous cell carcinoma*. Genes Dev, 2006. **20**(10): p. 1331-42.
21. Saranath, D., et al., *High frequency mutation in codons 12 and 61 of H-ras oncogene in chewing tobacco-related human oral carcinoma in India*. Br J Cancer, 1991. **63**(4): p. 573-8.
22. Johnson, T.M., et al., *Squamous cell carcinoma of the skin (excluding lip and oral mucosa)*. J Am Acad Dermatol, 1992. **26**(3 Pt 2): p. 467-84.
23. Adamson, R., et al., *High incidence and clinical course of aggressive skin cancer in heart transplant patients: a single-center study*. Transplant Proc, 1998. **30**(4): p. 1124-6.
24. Euvrard, S., J. Kanitakis, and A. Claudy, *Skin cancers after organ transplantation*. N Engl J Med, 2003. **348**(17): p. 1681-91.
25. Tsai, K.Y. and H. Tsao, *The genetics of skin cancer*. Am J Med Genet C Semin Med Genet, 2004. **131C**(1): p. 82-92.
26. Weinberg, A.S., C.A. Ogle, and E.K. Shim, *Metastatic cutaneous squamous cell carcinoma: an update*. Dermatol Surg, 2007. **33**(8): p. 885-99.

27. Friedman, H.I., P.H. Cooper, and H.J. Wanebo, *Prognostic and therapeutic use of microstaging of cutaneous squamous cell carcinoma of the trunk and extremities*. *Cancer*, 1985. **56**(5): p. 1099-105.
28. Dinehart, S.M. and S.V. Pollack, *Metastases from squamous cell carcinoma of the skin and lip. An analysis of twenty-seven cases*. *J Am Acad Dermatol*, 1989. **21**(2 Pt 1): p. 241-8.
29. Rowe, D.E., R.J. Carroll, and C.L. Day, Jr., *Prognostic factors for local recurrence, metastasis, and survival rates in squamous cell carcinoma of the skin, ear, and lip. Implications for treatment modality selection*. *J Am Acad Dermatol*, 1992. **26**(6): p. 976-90.
30. Petter, G. and U.F. Haustein, *Histologic subtyping and malignancy assessment of cutaneous squamous cell carcinoma*. *Dermatol Surg*, 2000. **26**(6): p. 521-30.
31. Nakazawa, H., et al., *UV and skin cancer: specific p53 gene mutation in normal skin as a biologically relevant exposure measurement*. *Proc Natl Acad Sci U S A*, 1994. **91**(1): p. 360-4.
32. Jonason, A.S., et al., *Frequent clones of p53-mutated keratinocytes in normal human skin*. *Proc Natl Acad Sci U S A*, 1996. **93**(24): p. 14025-9.
33. Ling, G., et al., *Persistent p53 mutations in single cells from normal human skin*. *Am J Pathol*, 2001. **159**(4): p. 1247-53.
34. Ren, Z.P., et al., *Two distinct p53 immunohistochemical patterns in human squamous-cell skin cancer, precursors and normal epidermis*. *Int J Cancer*, 1996. **69**(3): p. 174-9.

35. Kubo, Y., et al., *Mutations of the INK4a locus in squamous cell carcinomas of human skin*. Biochem Biophys Res Commun, 1997. **232**(1): p. 38-41.
36. Popp, S., et al., *UV-B-type mutations and chromosomal imbalances indicate common pathways for the development of Merkel and skin squamous cell carcinomas*. Int J Cancer, 2002. **99**(3): p. 352-60.
37. Quinn, A.G., S. Sikkink, and J.L. Rees, *Delineation of two distinct deleted regions on chromosome 9 in human non-melanoma skin cancers*. Genes Chromosomes Cancer, 1994. **11**(4): p. 222-5.
38. Boukamp, P., *Non-melanoma skin cancer: what drives tumor development and progression?* Carcinogenesis, 2005. **26**(10): p. 1657-67.
39. van der Schroeff, J.G., et al., *Ras oncogene mutations in basal cell carcinomas and squamous cell carcinomas of human skin*. J Invest Dermatol, 1990. **94**(4): p. 423-5.
40. Pierceall, W.E., et al., *Ras gene mutation and amplification in human nonmelanoma skin cancers*. Mol Carcinog, 1991. **4**(3): p. 196-202.
41. Campbell, C., A.G. Quinn, and J.L. Rees, *Codon 12 Harvey-ras mutations are rare events in non-melanoma human skin cancer*. Br J Dermatol, 1993. **128**(2): p. 111-4.
42. Spencer, J.M., et al., *Activated ras genes occur in human actinic keratoses, premalignant precursors to squamous cell carcinomas*. Arch Dermatol, 1995. **131**(7): p. 796-800.
43. Perez-Losada, J. and A. Balmain, *Stem-cell hierarchy in skin cancer*. Nat Rev Cancer, 2003. **3**(6): p. 434-43.

44. Shi, Y. and J. Massague, *Mechanisms of TGF-beta signaling from cell membrane to the nucleus*. Cell, 2003. **113**(6): p. 685-700.
45. Massague, J., *TGFbeta in Cancer*. Cell, 2008. **134**(2): p. 215-30.
46. Massague, J., *How cells read TGF-beta signals*. Nat Rev Mol Cell Biol, 2000. **1**(3): p. 169-78.
47. Massague, J., J. Seoane, and D. Wotton, *Smad transcription factors*. Genes Dev, 2005. **19**(23): p. 2783-810.
48. Ebisawa, T., et al., *Smurf1 interacts with transforming growth factor-beta type I receptor through Smad7 and induces receptor degradation*. J Biol Chem, 2001. **276**(16): p. 12477-80.
49. Zhang, Y.E., *Non-Smad pathways in TGF-beta signaling*. Cell Res, 2009. **19**(1): p. 128-39.
50. Pardali, K., et al., *Smad pathway-specific transcriptional regulation of the cell cycle inhibitor p21(WAF1/Cip1)*. J Cell Physiol, 2005. **204**(1): p. 260-72.
51. Ten Dijke, P., et al., *Regulation of cell proliferation by Smad proteins*. J Cell Physiol, 2002. **191**(1): p. 1-16.
52. Bertolino, P., et al., *Transforming growth factor-beta signal transduction in angiogenesis and vascular disorders*. Chest, 2005. **128**(6 Suppl): p. 585S-590S.
53. Gomis, R.R., et al., *C/EBPbeta at the core of the TGFbeta cytostatic response and its evasion in metastatic breast cancer cells*. Cancer Cell, 2006. **10**(3): p. 203-14.

54. Seoane, J., et al., *Integration of Smad and forkhead pathways in the control of neuroepithelial and glioblastoma cell proliferation*. Cell, 2004. **117**(2): p. 211-23.
55. Chen, C.R., et al., *E2F4/5 and p107 as Smad cofactors linking the TGFbeta receptor to c-myc repression*. Cell, 2002. **110**(1): p. 19-32.
56. Kang, Y., C.R. Chen, and J. Massague, *A self-enabling TGFbeta response coupled to stress signaling: Smad engages stress response factor ATF3 for Id1 repression in epithelial cells*. Mol Cell, 2003. **11**(4): p. 915-26.
57. Pardali, K. and A. Moustakas, *Actions of TGF-beta as tumor suppressor and pro-metastatic factor in human cancer*. Biochim Biophys Acta, 2007. **1775**(1): p. 21-62.
58. Yanagisawa, K., et al., *Induction of apoptosis by Smad3 and down-regulation of Smad3 expression in response to TGF-beta in human normal lung epithelial cells*. Oncogene, 1998. **17**(13): p. 1743-7.
59. Sorrentino, A., et al., *The type I TGF-beta receptor engages TRAF6 to activate TAK1 in a receptor kinase-independent manner*. Nat Cell Biol, 2008. **10**(10): p. 1199-207.
60. Yamashita, M., et al., *TRAF6 mediates Smad-independent activation of JNK and p38 by TGF-beta*. Mol Cell, 2008. **31**(6): p. 918-24.
61. Zhang, S., et al., *TGFbeta1-induced activation of ATM and p53 mediates apoptosis in a Smad7-dependent manner*. Cell Cycle, 2006. **5**(23): p. 2787-95.

62. Wang, J., et al., *Transforming growth factor beta induces apoptosis through repressing the phosphoinositide 3-kinase/AKT/survivin pathway in colon cancer cells*. *Cancer Res*, 2008. **68**(9): p. 3152-60.
63. Levy, L. and C.S. Hill, *Alterations in components of the TGF-beta superfamily signaling pathways in human cancer*. *Cytokine Growth Factor Rev*, 2006. **17**(1-2): p. 41-58.
64. Bornstein, S., et al., *Smad4 loss in mice causes spontaneous head and neck cancer with increased genomic instability and inflammation*. *J Clin Invest*, 2009. **119**(11): p. 3408-19.
65. Li, A.G., et al., *Smad3 knockout mice exhibit a resistance to skin chemical carcinogenesis*. *Cancer Res*, 2004. **64**(21): p. 7836-45.
66. Cui, W., et al., *TGFbeta1 inhibits the formation of benign skin tumors, but enhances progression to invasive spindle carcinomas in transgenic mice*. *Cell*, 1996. **86**(4): p. 531-42.
67. Yang, L., et al., *Targeted disruption of Smad4 in mouse epidermis results in failure of hair follicle cycling and formation of skin tumors*. *Cancer Res*, 2005. **65**(19): p. 8671-8.
68. Qiao, W., et al., *Hair follicle defects and squamous cell carcinoma formation in Smad4 conditional knockout mouse skin*. *Oncogene*, 2006. **25**(2): p. 207-17.
69. Lewandoski, M., *Conditional control of gene expression in the mouse*. *Nat Rev Genet*, 2001. **2**(10): p. 743-55.
70. Jonkers, J. and A. Berns, *Conditional mouse models of sporadic cancer*. *Nat Rev Cancer*, 2002. **2**(4): p. 251-65.

71. Byrne, C., M. Tainsky, and E. Fuchs, *Programming gene expression in developing epidermis*. *Development*, 1994. **120**(9): p. 2369-83.
72. Wang, X., et al., *Transgenic studies with a keratin promoter-driven growth hormone transgene: prospects for gene therapy*. *Proc Natl Acad Sci U S A*, 1997. **94**(1): p. 219-26.
73. Ornitz, D.M., R.W. Moreadith, and P. Leder, *Binary system for regulating transgene expression in mice: targeting int-2 gene expression with yeast GAL4/UAS control elements*. *Proc Natl Acad Sci U S A*, 1991. **88**(3): p. 698-702.
74. Kellendonk, C., et al., *Regulation of Cre recombinase activity by the synthetic steroid RU 486*. *Nucleic Acids Res*, 1996. **24**(8): p. 1404-11.
75. Jackson, E.L., et al., *Analysis of lung tumor initiation and progression using conditional expression of oncogenic K-ras*. *Genes Dev*, 2001. **15**(24): p. 3243-8.
76. Balmain, A. and I.B. Pragnell, *Mouse skin carcinomas induced in vivo by chemical carcinogens have a transforming Harvey-ras oncogene*. *Nature*, 1983. **303**(5912): p. 72-4.
77. Yuan, B., et al., *Harvey ras (H-ras) point mutations are induced by 4-nitroquinoline-1-oxide in murine oral squamous epithelia, while squamous cell carcinomas and loss of heterozygosity occur without additional exposure*. *Cancer Res*, 1994. **54**(20): p. 5310-7.
78. Hawkins, B.L., et al., *4NQO carcinogenesis: a mouse model of oral cavity squamous cell carcinoma*. *Head Neck*, 1994. **16**(5): p. 424-32.

79. Muro-Cacho, C.A., et al., *Defective transforming growth factor beta signaling pathway in head and neck squamous cell carcinoma as evidenced by the lack of expression of activated Smad2*. Clin Cancer Res, 2001. **7**(6): p. 1618-26.
80. Chen, T., et al., *Novel inactivating mutations of transforming growth factor-beta type I receptor gene in head-and-neck cancer metastases*. Int J Cancer, 2001. **93**(5): p. 653-61.
81. Li, A.G., et al., *Current view of the role of transforming growth factor beta 1 in skin carcinogenesis*. J Investig Dermatol Symp Proc, 2005. **10**(2): p. 110-7.
82. Lu, S.L., et al., *Overexpression of transforming growth factor beta1 in head and neck epithelia results in inflammation, angiogenesis, and epithelial hyperproliferation*. Cancer Res, 2004. **64**(13): p. 4405-10.
83. Bian, Y., et al., *Progressive tumor formation in mice with conditional deletion of TGF-beta signaling in head and neck epithelia is associated with activation of the PI3K/Akt pathway*. Cancer Res, 2009. **69**(14): p. 5918-26.
84. Weeks, B.H., et al., *Inducible expression of transforming growth factor beta1 in papillomas causes rapid metastasis*. Cancer Res, 2001. **61**(20): p. 7435-43.
85. Teicher, B.A., *Transforming growth factor-beta and the immune response to malignant disease*. Clin Cancer Res, 2007. **13**(21): p. 6247-51.
86. Wrzesinski, S.H., Y.Y. Wan, and R.A. Flavell, *Transforming growth factor-beta and the immune response: implications for anticancer therapy*. Clin Cancer Res, 2007. **13**(18 Pt 1): p. 5262-70.
87. Moutsopoulos, N.M., J. Wen, and S.M. Wahl, *TGF-beta and tumors--an ill-fated alliance*. Curr Opin Immunol, 2008. **20**(2): p. 234-40.

88. Boucek, J., et al., *Regulatory T cells and their prognostic value for patients with Squamous Cell Carcinoma of the Head and Neck*. J Cell Mol Med, 2009.
89. van Vlasselaer, P., J. Punnonen, and J.E. de Vries, *Transforming growth factor-beta directs IgA switching in human B cells*. J Immunol, 1992. **148**(7): p. 2062-7.
90. Veldhoen, M., et al., *TGFbeta in the context of an inflammatory cytokine milieu supports de novo differentiation of IL-17-producing T cells*. Immunity, 2006. **24**(2): p. 179-89.
91. Mangan, P.R., et al., *Transforming growth factor-beta induces development of the T(H)17 lineage*. Nature, 2006. **441**(7090): p. 231-4.
92. Bierie, B. and H.L. Moses, *Tumour microenvironment: TGFbeta: the molecular Jekyll and Hyde of cancer*. Nat Rev Cancer, 2006. **6**(7): p. 506-20.
93. Hahn, S.A., et al., *DPC4, a candidate tumor suppressor gene at human chromosome 18q21.1*. Science, 1996. **271**(5247): p. 350-3.
94. Zhang, Y., et al., *Receptor-associated Mad homologues synergize as effectors of the TGF-beta response*. Nature, 1996. **383**(6596): p. 168-72.
95. Hoot, K.E., et al., *Keratinocyte-specific Smad2 ablation results in increased epithelial-mesenchymal transition during skin cancer formation and progression*. J Clin Invest, 2008. **118**(8): p. 2722-32.
96. Bierie, B. and H.L. Moses, *TGF-beta and cancer*. Cytokine Growth Factor Rev, 2006. **17**(1-2): p. 29-40.

97. Snijders, A.M., et al., *Rare amplicons implicate frequent deregulation of cell fate specification pathways in oral squamous cell carcinoma*. *Oncogene*, 2005. **24**(26): p. 4232-42.
98. Kim, S.K., et al., *DPC4, a candidate tumor suppressor gene, is altered infrequently in head and neck squamous cell carcinoma*. *Cancer Res*, 1996. **56**(11): p. 2519-21.
99. Papadimitrakopoulou, V.A., et al., *Presence of multiple incontiguous deleted regions at the long arm of chromosome 18 in head and neck cancer*. *Clin Cancer Res*, 1998. **4**(3): p. 539-44.
100. Takebayashi, S., et al., *Identification of new minimally lost regions on 18q in head and neck squamous cell carcinoma*. *Cancer Res*, 2000. **60**(13): p. 3397-403.
101. Pearlstein, R.P., et al., *Loss of 18q predicts poor survival of patients with squamous cell carcinoma of the head and neck*. *Genes Chromosomes Cancer*, 1998. **21**(4): p. 333-9.
102. Iamaroon, A., K. Pattamapun, and S.O. Piboonniyom, *Aberrant expression of Smad4, a TGF-beta signaling molecule, in oral squamous cell carcinoma*. *J Oral Sci*, 2006. **48**(3): p. 105-9.
103. Xie, W., et al., *Frequent alterations of Smad signaling in human head and neck squamous cell carcinomas: a tissue microarray analysis*. *Oncol Res*, 2003. **14**(2): p. 61-73.

104. Sirard, C., et al., *The tumor suppressor gene Smad4/Dpc4 is required for gastrulation and later for anterior development of the mouse embryo*. *Genes Dev*, 1998. **12**(1): p. 107-19.
105. Yang, X., et al., *The tumor suppressor SMAD4/DPC4 is essential for epiblast proliferation and mesoderm induction in mice*. *Proc Natl Acad Sci U S A*, 1998. **95**(7): p. 3667-72.
106. Kitamura, T., et al., *SMAD4-deficient intestinal tumors recruit CCR1+ myeloid cells that promote invasion*. *Nat Genet*, 2007. **39**(4): p. 467-75.
107. Takaku, K., et al., *Intestinal tumorigenesis in compound mutant mice of both Dpc4 (Smad4) and Apc genes*. *Cell*, 1998. **92**(5): p. 645-56.
108. Izeradjene, K., et al., *Kras(G12D) and Smad4/Dpc4 haploinsufficiency cooperate to induce mucinous cystic neoplasms and invasive adenocarcinoma of the pancreas*. *Cancer Cell*, 2007. **11**(3): p. 229-43.
109. Bardeesy, N., et al., *Smad4 is dispensable for normal pancreas development yet critical in progression and tumor biology of pancreas cancer*. *Genes Dev*, 2006. **20**(22): p. 3130-46.
110. Teng, Y., et al., *Synergistic function of Smad4 and PTEN in suppressing forestomach squamous cell carcinoma in the mouse*. *Cancer Res*, 2006. **66**(14): p. 6972-81.
111. Xu, X., et al., *Induction of intrahepatic cholangiocellular carcinoma by liver-specific disruption of Smad4 and Pten in mice*. *J Clin Invest*, 2006. **116**(7): p. 1843-52.

112. Xu, X., et al., *Haploid loss of the tumor suppressor Smad4/Dpc4 initiates gastric polyposis and cancer in mice*. *Oncogene*, 2000. **19**(15): p. 1868-74.
113. Li, W., et al., *Squamous cell carcinoma and mammary abscess formation through squamous metaplasia in Smad4/Dpc4 conditional knockout mice*. *Development*, 2003. **130**(24): p. 6143-53.
114. Malumbres, M. and M. Barbacid, *RAS oncogenes: the first 30 years*. *Nat Rev Cancer*, 2003. **3**(6): p. 459-65.
115. Perona, R. and I. Sanchez-Perez, *Control of oncogenesis and cancer therapy resistance*. *Br J Cancer*, 2004. **90**(3): p. 573-7.
116. Bernhard, E.J., et al., *Direct evidence for the contribution of activated N-ras and K-ras oncogenes to increased intrinsic radiation resistance in human tumor cell lines*. *Cancer Res*, 2000. **60**(23): p. 6597-600.
117. Caulin, C., et al., *Inducible activation of oncogenic K-ras results in tumor formation in the oral cavity*. *Cancer Res*, 2004. **64**(15): p. 5054-8.
118. Kojima, K., et al., *Inactivation of Smad4 accelerates Kras(G12D)-mediated pancreatic neoplasia*. *Cancer Res*, 2007. **67**(17): p. 8121-30.
119. Kutler, D.I., et al., *High incidence of head and neck squamous cell carcinoma in patients with Fanconi anemia*. *Arch Otolaryngol Head Neck Surg*, 2003. **129**(1): p. 106-12.
120. Marsit, C.J., et al., *Inactivation of the Fanconi anemia/BRCA pathway in lung and oral cancers: implications for treatment and survival*. *Oncogene*, 2004. **23**(4): p. 1000-4.

121. Sparano, A., et al., *Genome-wide profiling of oral squamous cell carcinoma by array-based comparative genomic hybridization*. *Laryngoscope*, 2006. **116**(5): p. 735-41.
122. Weber, F., et al., *Microenvironmental genomic alterations and clinicopathological behavior in head and neck squamous cell carcinoma*. *JAMA*, 2007. **297**(2): p. 187-95.
123. Wreesmann, V.B., et al., *Downregulation of Fanconi anemia genes in sporadic head and neck squamous cell carcinoma*. *ORL J Otorhinolaryngol Relat Spec*, 2007. **69**(4): p. 218-25.
124. Berton, T.R., et al., *Tumor formation in mice with conditional inactivation of Brca1 in epithelial tissues*. *Oncogene*, 2003. **22**(35): p. 5415-26.
125. Kim, B.G., et al., *Smad4 signalling in T cells is required for suppression of gastrointestinal cancer*. *Nature*, 2006. **441**(7096): p. 1015-9.
126. Bharathy, S., et al., *Cancer-associated transforming growth factor beta type II receptor gene mutant causes activation of bone morphogenic protein-Smads and invasive phenotype*. *Cancer Res*, 2008. **68**(6): p. 1656-66.
127. Liu, I.M., et al., *TGFbeta-stimulated Smad1/5 phosphorylation requires the ALK5 L45 loop and mediates the pro-migratory TGFbeta switch*. *EMBO J*, 2009. **28**(2): p. 88-98.
128. Campbell, L.L. and K. Polyak, *Breast tumor heterogeneity: cancer stem cells or clonal evolution?* *Cell Cycle*, 2007. **6**(19): p. 2332-8.
129. Park, C.Y., D. Tseng, and I.L. Weissman, *Cancer stem cell-directed therapies: recent data from the laboratory and clinic*. *Mol Ther*, 2009. **17**(2): p. 219-30.

130. Visvader, J.E. and G.J. Lindeman, *Cancer stem cells in solid tumours: accumulating evidence and unresolved questions*. Nat Rev Cancer, 2008. **8**(10): p. 755-68.
131. Zhao, R. and G.Q. Daley, *From fibroblasts to iPS cells: induced pluripotency by defined factors*. J Cell Biochem, 2008. **105**(4): p. 949-55.
132. Takahashi, K. and S. Yamanaka, *Induction of pluripotent stem cells from mouse embryonic and adult fibroblast cultures by defined factors*. Cell, 2006. **126**(4): p. 663-76.
133. Lapidot, T., et al., *A cell initiating human acute myeloid leukaemia after transplantation into SCID mice*. Nature, 1994. **367**(6464): p. 645-8.
134. Clarke, M.F., et al., *Cancer stem cells--perspectives on current status and future directions: AACR Workshop on cancer stem cells*. Cancer Res, 2006. **66**(19): p. 9339-44.
135. Al-Hajj, M., et al., *Prospective identification of tumorigenic breast cancer cells*. Proc Natl Acad Sci U S A, 2003. **100**(7): p. 3983-8.
136. Harper, L.J., et al., *Stem cell patterns in cell lines derived from head and neck squamous cell carcinoma*. J Oral Pathol Med, 2007. **36**(10): p. 594-603.
137. Wu, M.J., et al., *Elimination of head and neck cancer initiating cells through targeting glucose regulated protein78 signaling*. Mol Cancer. **9**: p. 283.
138. Prince, M.E., et al., *Identification of a subpopulation of cells with cancer stem cell properties in head and neck squamous cell carcinoma*. Proc Natl Acad Sci U S A, 2007. **104**(3): p. 973-8.

139. Clay, M.R., et al., *Single-marker identification of head and neck squamous cell carcinoma cancer stem cells with aldehyde dehydrogenase*. *Head Neck*. **32**(9): p. 1195-201.
140. Chen, Y.C., et al., *Aldehyde dehydrogenase 1 is a putative marker for cancer stem cells in head and neck squamous cancer*. *Biochem Biophys Res Commun*, 2009. **385**(3): p. 307-13.
141. Blanpain, C. and E. Fuchs, *Epidermal stem cells of the skin*. *Annu Rev Cell Dev Biol*, 2006. **22**: p. 339-73.
142. Cotsarelis, G., T.T. Sun, and R.M. Lavker, *Label-retaining cells reside in the bulge area of pilosebaceous unit: implications for follicular stem cells, hair cycle, and skin carcinogenesis*. *Cell*, 1990. **61**(7): p. 1329-37.
143. Lyle, S., et al., *The C8/144B monoclonal antibody recognizes cytokeratin 15 and defines the location of human hair follicle stem cells*. *J Cell Sci*, 1998. **111** (Pt 21): p. 3179-88.
144. Trempus, C.S., et al., *Enrichment for living murine keratinocytes from the hair follicle bulge with the cell surface marker CD34*. *J Invest Dermatol*, 2003. **120**(4): p. 501-11.
145. Li, A., P.J. Simmons, and P. Kaur, *Identification and isolation of candidate human keratinocyte stem cells based on cell surface phenotype*. *Proc Natl Acad Sci U S A*, 1998. **95**(7): p. 3902-7.
146. Blanpain, C., et al., *Self-renewal, multipotency, and the existence of two cell populations within an epithelial stem cell niche*. *Cell*, 2004. **118**(5): p. 635-48.

147. Liang, L. and J.R. Bickenbach, *Somatic epidermal stem cells can produce multiple cell lineages during development*. *Stem Cells*, 2002. **20**(1): p. 21-31.
148. Hanahan, D. and R.A. Weinberg, *The hallmarks of cancer*. *Cell*, 2000. **100**(1): p. 57-70.
149. Gupta, G.P. and J. Massague, *Cancer metastasis: building a framework*. *Cell*, 2006. **127**(4): p. 679-95.
150. Xu, J., S. Lamouille, and R. Derynck, *TGF-beta-induced epithelial to mesenchymal transition*. *Cell Res*, 2009. **19**(2): p. 156-72.
151. Polyak, K. and R.A. Weinberg, *Transitions between epithelial and mesenchymal states: acquisition of malignant and stem cell traits*. *Nat Rev Cancer*, 2009. **9**(4): p. 265-73.
152. Cano, A., et al., *The transcription factor snail controls epithelial-mesenchymal transitions by repressing E-cadherin expression*. *Nat Cell Biol*, 2000. **2**(2): p. 76-83.
153. Bindels, S., et al., *Regulation of vimentin by SIP1 in human epithelial breast tumor cells*. *Oncogene*, 2006. **25**(36): p. 4975-85.
154. Yang, J., et al., *Twist, a master regulator of morphogenesis, plays an essential role in tumor metastasis*. *Cell*, 2004. **117**(7): p. 927-39.
155. Ansieau, S., et al., *Induction of EMT by twist proteins as a collateral effect of tumor-promoting inactivation of premature senescence*. *Cancer Cell*, 2008. **14**(1): p. 79-89.

156. Deckers, M., et al., *The tumor suppressor Smad4 is required for transforming growth factor beta-induced epithelial to mesenchymal transition and bone metastasis of breast cancer cells*. *Cancer Res*, 2006. **66**(4): p. 2202-9.
157. Takano, S., et al., *Smad4 is essential for down-regulation of E-cadherin induced by TGF-beta in pancreatic cancer cell line PANC-1*. *J Biochem*, 2007. **141**(3): p. 345-51.
158. Mani, S.A., et al., *The epithelial-mesenchymal transition generates cells with properties of stem cells*. *Cell*, 2008. **133**(4): p. 704-15.
159. Yang, M.H., et al., *Bmi1 is essential in Twist1-induced epithelial-mesenchymal transition*. *Nat Cell Biol*. **12**(10): p. 982-92.
160. Fletcher, J.I., et al., *ABC transporters in cancer: more than just drug efflux pumps*. *Nat Rev Cancer*. **10**(2): p. 147-56.
161. Dean, M., *The genetics of ATP-binding cassette transporters*. *Methods Enzymol*, 2005. **400**: p. 409-29.
162. Yamada, T., et al., *Suppression of intestinal polyposis in Mdr1-deficient Apc^{Min/+} mice*. *Cancer Res*, 2003. **63**(5): p. 895-901.
163. Mochida, Y., et al., *The role of P-glycoprotein in intestinal tumorigenesis: disruption of mdr1a suppresses polyp formation in Apc(Min/+) mice*. *Carcinogenesis*, 2003. **24**(7): p. 1219-24.
164. Goodell, M.A., et al., *Isolation and functional properties of murine hematopoietic stem cells that are replicating in vivo*. *J Exp Med*, 1996. **183**(4): p. 1797-806.

165. Goodell, M.A., et al., *Dye efflux studies suggest that hematopoietic stem cells expressing low or undetectable levels of CD34 antigen exist in multiple species.* Nat Med, 1997. **3**(12): p. 1337-45.
166. Zhou, S., et al., *The ABC transporter Bcrp1/ABCG2 is expressed in a wide variety of stem cells and is a molecular determinant of the side-population phenotype.* Nat Med, 2001. **7**(9): p. 1028-34.
167. Gussoni, E., et al., *Dystrophin expression in the mdx mouse restored by stem cell transplantation.* Nature, 1999. **401**(6751): p. 390-4.
168. Hirschmann-Jax, C., et al., *A distinct "side population" of cells with high drug efflux capacity in human tumor cells.* Proc Natl Acad Sci U S A, 2004. **101**(39): p. 14228-33.
169. Schinkel, A.H., et al., *Disruption of the mouse mdr1a P-glycoprotein gene leads to a deficiency in the blood-brain barrier and to increased sensitivity to drugs.* Cell, 1994. **77**(4): p. 491-502.
170. Zhou, S., et al., *Bcrp1 gene expression is required for normal numbers of side population stem cells in mice, and confers relative protection to mitoxantrone in hematopoietic cells in vivo.* Proc Natl Acad Sci U S A, 2002. **99**(19): p. 12339-44.
171. Robinson, L.J., et al., *Human MDR 1 protein overexpression delays the apoptotic cascade in Chinese hamster ovary fibroblasts.* Biochemistry, 1997. **36**(37): p. 11169-78.

172. Smyth, M.J., et al., *The drug efflux protein, P-glycoprotein, additionally protects drug-resistant tumor cells from multiple forms of caspase-dependent apoptosis.* Proc Natl Acad Sci U S A, 1998. **95**(12): p. 7024-9.
173. Johnstone, R.W., E. Cretney, and M.J. Smyth, *P-glycoprotein protects leukemia cells against caspase-dependent, but not caspase-independent, cell death.* Blood, 1999. **93**(3): p. 1075-85.
174. Weinstein, R.S., et al., *Relationship of the expression of the multidrug resistance gene product (P-glycoprotein) in human colon carcinoma to local tumor aggressiveness and lymph node metastasis.* Cancer Res, 1991. **51**(10): p. 2720-6.
175. Miletti-Gonzalez, K.E., et al., *The CD44 receptor interacts with P-glycoprotein to promote cell migration and invasion in cancer.* Cancer Res, 2005. **65**(15): p. 6660-7.
176. Colone, M., et al., *The multidrug transporter P-glycoprotein: a mediator of melanoma invasion?* J Invest Dermatol, 2008. **128**(4): p. 957-71.
177. Naor, D., R.V. Sionov, and D. Ish-Shalom, *CD44: structure, function, and association with the malignant process.* Adv Cancer Res, 1997. **71**: p. 241-319.
178. Yamada, T., et al., *Transactivation of the multidrug resistance 1 gene by T-cell factor 4/beta-catenin complex in early colorectal carcinogenesis.* Cancer Res, 2000. **60**(17): p. 4761-6.
179. Bentires-Alj, M., et al., *NF-kappaB transcription factor induces drug resistance through MDR1 expression in cancer cells.* Oncogene, 2003. **22**(1): p. 90-7.

180. Bourguignon, L.Y., et al., *Hyaluronan-CD44 interaction with protein kinase C(epsilon) promotes oncogenic signaling by the stem cell marker Nanog and the Production of microRNA-21, leading to down-regulation of the tumor suppressor protein PDCD4, anti-apoptosis, and chemotherapy resistance in breast tumor cells.* J Biol Chem, 2009. **284**(39): p. 26533-46.
181. Brodersen, P. and O. Voinnet, *Revisiting the principles of microRNA target recognition and mode of action.* Nat Rev Mol Cell Biol, 2009. **10**(2): p. 141-8.
182. Calin, G.A., et al., *Frequent deletions and down-regulation of micro- RNA genes miR15 and miR16 at 13q14 in chronic lymphocytic leukemia.* Proc Natl Acad Sci U S A, 2002. **99**(24): p. 15524-9.
183. Cimmino, A., et al., *miR-15 and miR-16 induce apoptosis by targeting BCL2.* Proc Natl Acad Sci U S A, 2005. **102**(39): p. 13944-9.
184. Takamizawa, J., et al., *Reduced expression of the let-7 microRNAs in human lung cancers in association with shortened postoperative survival.* Cancer Res, 2004. **64**(11): p. 3753-6.
185. Johnson, S.M., et al., *RAS is regulated by the let-7 microRNA family.* Cell, 2005. **120**(5): p. 635-47.
186. Kong, W., et al., *MicroRNA-155 is regulated by the transforming growth factor beta/Smad pathway and contributes to epithelial cell plasticity by targeting RhoA.* Mol Cell Biol, 2008. **28**(22): p. 6773-84.
187. Davis, B.N., et al., *SMAD proteins control DROSHA-mediated microRNA maturation.* Nature, 2008. **454**(7200): p. 56-61.

188. Meng, F., et al., *MicroRNA-21 regulates expression of the PTEN tumor suppressor gene in human hepatocellular cancer*. *Gastroenterology*, 2007. **133**(2): p. 647-58.
189. Asangani, I.A., et al., *MicroRNA-21 (miR-21) post-transcriptionally downregulates tumor suppressor Pcd4 and stimulates invasion, intravasation and metastasis in colorectal cancer*. *Oncogene*, 2008. **27**(15): p. 2128-36.
190. Kim, Y.J., et al., *MiR-21 regulates adipogenic differentiation through the modulation of TGF-beta signaling in mesenchymal stem cells derived from human adipose tissue*. *Stem Cells*, 2009. **27**(12): p. 3093-102.
191. Chen, R., et al., *Regulation of IKKbeta by miR-199a affects NF-kappaB activity in ovarian cancer cells*. *Oncogene*, 2008. **27**(34): p. 4712-23.
192. Gregory, P.A., et al., *The miR-200 family and miR-205 regulate epithelial to mesenchymal transition by targeting ZEB1 and SIP1*. *Nat Cell Biol*, 2008. **10**(5): p. 593-601.
193. Korpala, M., et al., *The miR-200 family inhibits epithelial-mesenchymal transition and cancer cell migration by direct targeting of E-cadherin transcriptional repressors ZEB1 and ZEB2*. *J Biol Chem*, 2008. **283**(22): p. 14910-4.
194. Burk, U., et al., *A reciprocal repression between ZEB1 and members of the miR-200 family promotes EMT and invasion in cancer cells*. *EMBO Rep*, 2008. **9**(6): p. 582-9.

195. Ma, L., J. Teruya-Feldstein, and R.A. Weinberg, *Tumour invasion and metastasis initiated by microRNA-10b in breast cancer*. *Nature*, 2007. **449**(7163): p. 682-8.
196. Ma, L., et al., *miR-9, a MYC/MYCN-activated microRNA, regulates E-cadherin and cancer metastasis*. *Nat Cell Biol.* **12**(3): p. 247-56.
197. Zhu, L., et al., *MicroRNA-9 up-regulation is involved in colorectal cancer metastasis via promoting cell motility*. *Med Oncol.*
198. Kanellopoulou, C., et al., *Dicer-deficient mouse embryonic stem cells are defective in differentiation and centromeric silencing*. *Genes Dev*, 2005. **19**(4): p. 489-501.
199. Murchison, E.P., et al., *Characterization of Dicer-deficient murine embryonic stem cells*. *Proc Natl Acad Sci U S A*, 2005. **102**(34): p. 12135-40.
200. Andl, T., et al., *The miRNA-processing enzyme dicer is essential for the morphogenesis and maintenance of hair follicles*. *Curr Biol*, 2006. **16**(10): p. 1041-9.
201. Yi, R., et al., *A skin microRNA promotes differentiation by repressing 'stemness'*. *Nature*, 2008. **452**(7184): p. 225-9.
202. Lena, A.M., et al., *miR-203 represses 'stemness' by repressing DeltaNp63*. *Cell Death Differ*, 2008. **15**(7): p. 1187-95.
203. Yi, R., et al., *Morphogenesis in skin is governed by discrete sets of differentially expressed microRNAs*. *Nat Genet*, 2006. **38**(3): p. 356-62.
204. Shimono, Y., et al., *Downregulation of miRNA-200c links breast cancer stem cells with normal stem cells*. *Cell*, 2009. **138**(3): p. 592-603.

205. Wellner, U., et al., *The EMT-activator ZEB1 promotes tumorigenicity by repressing stemness-inhibiting microRNAs*. Nat Cell Biol, 2009. **11**(12): p. 1487-95.
206. Saunders, L.R., et al., *miRNAs regulate SIRT1 expression during mouse embryonic stem cell differentiation and in adult mouse tissues*. Aging (Albany NY). **2**(7): p. 415-31.
207. Wan, H.Y., et al., *Regulation of the transcription factor NF-kappaB1 by microRNA-9 in human gastric adenocarcinoma*. Mol Cancer. **9**: p. 16.
208. Rotkrua, P., et al., *MiR-9 down-regulates CDX2 expression in gastric cancer cells*. Int J Cancer.
209. Myatt, S.S., et al., *Definition of microRNAs that repress expression of the tumor suppressor gene FOXO1 in endometrial cancer*. Cancer Res. **70**(1): p. 367-77.
210. Laneve, P., et al., *A minicircuitry involving REST and CREB controls miR-9-2 expression during human neuronal differentiation*. Nucleic Acids Res. **38**(20): p. 6895-905.
211. Hildebrandt, M.A., et al., *Hsa-miR-9 methylation status is associated with cancer development and metastatic recurrence in patients with clear cell renal cell carcinoma*. Oncogene. **29**(42): p. 5724-8.
212. Bandres, E., et al., *Epigenetic regulation of microRNA expression in colorectal cancer*. Int J Cancer, 2009. **125**(11): p. 2737-43.
213. Lu, J., et al., *MicroRNA expression profiles classify human cancers*. Nature, 2005. **435**(7043): p. 834-8.

214. Esquela-Kerscher, A. and F.J. Slack, *Oncomirs - microRNAs with a role in cancer*. Nat Rev Cancer, 2006. **6**(4): p. 259-69.
215. Childs, G., et al., *Low-level expression of microRNAs let-7d and miR-205 are prognostic markers of head and neck squamous cell carcinoma*. Am J Pathol, 2009. **174**(3): p. 736-45.
216. Krutzfeldt, J., et al., *Silencing of microRNAs in vivo with 'antagomirs'*. Nature, 2005. **438**(7068): p. 685-9.
217. Owens, P., et al., *Smad4-dependent desmoglein-4 expression contributes to hair follicle integrity*. Dev Biol, 2008. **322**(1): p. 156-66.
218. Liu, Y., et al., *Keratin 15 promoter targets putative epithelial stem cells in the hair follicle bulge*. J Invest Dermatol, 2003. **121**(5): p. 963-8.
219. Yang, X., et al., *Generation of Smad4/Dpc4 conditional knockout mice*. Genesis, 2002. **32**(2): p. 80-1.
220. Braun, B.S., et al., *Somatic activation of a conditional KrasG12D allele causes ineffective erythropoiesis in vivo*. Blood, 2006. **108**(6): p. 2041-4.
221. Han, G., et al., *Distinct mechanisms of TGF-beta1-mediated epithelial-to-mesenchymal transition and metastasis during skin carcinogenesis*. J Clin Invest, 2005. **115**(7): p. 1714-23.
222. Aldaz, C.M., et al., *Progressive dysplasia and aneuploidy are hallmarks of mouse skin papillomas: relevance to malignancy*. Proc Natl Acad Sci U S A, 1987. **84**(7): p. 2029-32.
223. Lichti, U., J. Anders, and S.H. Yuspa, *Isolation and short-term culture of primary keratinocytes, hair follicle populations and dermal cells from newborn*

- mice and keratinocytes from adult mice for in vitro analysis and for grafting to immunodeficient mice.* Nat Protoc, 2008. **3**(5): p. 799-810.
224. Krishan, A., *Rapid flow cytofluorometric analysis of mammalian cell cycle by propidium iodide staining.* J Cell Biol, 1975. **66**(1): p. 188-93.
225. Owens, P., et al., *Epidermal Smad4 deletion results in aberrant wound healing.* Am J Pathol. **176**(1): p. 122-33.
226. Gerdes, M.J. and S.H. Yuspa, *The contribution of epidermal stem cells to skin cancer.* Stem Cell Rev, 2005. **1**(3): p. 225-31.
227. Boukamp, P., et al., *Normal keratinization in a spontaneously immortalized aneuploid human keratinocyte cell line.* J Cell Biol, 1988. **106**(3): p. 761-71.
228. Pietenpol, J.A., et al., *Transforming growth factor beta 1 suppression of c-myc gene transcription: role in inhibition of keratinocyte proliferation.* Proc Natl Acad Sci U S A, 1990. **87**(10): p. 3758-62.
229. Guo, L.M., et al., *MicroRNA-9 inhibits ovarian cancer cell growth through regulation of NF-kappaB1.* FEBS J, 2009. **276**(19): p. 5537-46.
230. Song, J., et al., *Characterization of side populations in HNSCC: highly invasive, chemoresistant and abnormal Wnt signaling.* PLoS One. **5**(7): p. e11456.
231. Yanaihara, N., et al., *Unique microRNA molecular profiles in lung cancer diagnosis and prognosis.* Cancer Cell, 2006. **9**(3): p. 189-98.
232. Iorio, M.V., et al., *MicroRNA gene expression deregulation in human breast cancer.* Cancer Res, 2005. **65**(16): p. 7065-70.

233. Jiang, S., et al., *MicroRNA-155 functions as an OncomiR in breast cancer by targeting the suppressor of cytokine signaling 1 gene*. *Cancer Res.* **70**(8): p. 3119-27.
234. Xiang, X., et al., *miR-155 promotes macroscopic tumor formation yet inhibits tumor dissemination from mammary fat pads to the lung by preventing EMT*. *Oncogene*.
235. Lee, Y.B., et al., *Twist-1 regulates the miR-199a/214 cluster during development*. *Nucleic Acids Res*, 2009. **37**(1): p. 123-8.
236. Yin, G., et al., *TWISTing stemness, inflammation and proliferation of epithelial ovarian cancer cells through MIR199A2/214*. *Oncogene.* **29**(24): p. 3545-53.
237. Lin, E.A., et al., *miR-199a, a bone morphogenic protein 2-responsive MicroRNA, regulates chondrogenesis via direct targeting to Smad1*. *J Biol Chem*, 2009. **284**(17): p. 11326-35.
238. Yang, H., et al., *MicroRNA expression profiling in human ovarian cancer: miR-214 induces cell survival and cisplatin resistance by targeting PTEN*. *Cancer Res*, 2008. **68**(2): p. 425-33.
239. Magill, S.T., et al., *microRNA-132 regulates dendritic growth and arborization of newborn neurons in the adult hippocampus*. *Proc Natl Acad Sci U S A.* **107**(47): p. 20382-7.
240. Wayman, G.A., et al., *An activity-regulated microRNA controls dendritic plasticity by down-regulating p250GAP*. *Proc Natl Acad Sci U S A*, 2008. **105**(26): p. 9093-8.

241. Park, J.K., et al., *miR-132 and miR-212 are increased in pancreatic cancer and target the retinoblastoma tumor suppressor*. *Biochem Biophys Res Commun.* **406**(4): p. 518-23.
242. Anand, S., et al., *MicroRNA-132-mediated loss of p120RasGAP activates the endothelium to facilitate pathological angiogenesis*. *Nat Med.* **16**(8): p. 909-14.
243. Lewis, D.A., et al., *Aberrant NF-kappaB activity in HaCaT cells alters their response to UVB signaling*. *J Invest Dermatol*, 2006. **126**(8): p. 1885-92.
244. Wolf, S.J., et al., *An update on ABCB1 pharmacogenetics: insights from a 3D model into the location and evolutionary conservation of residues corresponding to SNPs associated with drug pharmacokinetics*. *Pharmacogenomics J.*
245. Lehmann, U., et al., *Epigenetic inactivation of microRNA gene hsa-mir-9-1 in human breast cancer*. *J Pathol*, 2008. **214**(1): p. 17-24.

APPENDIX A

ANTIBODIES

Antibody	Protocol	Host	Vendor	Catalog #	Tissue Species	Primary Conc.	Secondary Conc.
FITC-CD31	Flow Cytometry	Rat	eBioscience	11-0311	Mouse	1:50	N/A
FITC-CD45	Flow Cytometry	Rat	eBioscience	11-0451	Mouse	1:200	N/A
CD34-biotin	Flow Cytometry	Rat	eBioscience	13-0341	Mouse	1:20	N/A
Streptavidin-PE	Flow cytometry	N/A	eBioscience	12-4317	Mouse	N/A	1:20
PE-Cy5-CD49f	Flow Cytometry	Rat	BD Bioscience	551129	Mouse	1:20	N/A
APC-CD45	Flow Cytometry	Rat	BD Bioscience	559864	Mouse	1:200	N/A
APC-CD31	Flow Cytometry	Rat	BD Bioscience	551262	Mouse	1:50	N/A
Keratin 15	Frozen IF	Chicken	Covance	PCK-153P	Human, Mouse	1:500	1:200
CD34	Frozen IF	Rat	BD Bioscience	553507	Human, Mouse	1:200	1:200
Smad4 (B-8)	IHC	Mouse	Santa Cruz	Sc-7966	Human, Mouse	1:100	1:200
Sox2	IHC	Rabbit	Millipore	Ab5603	Human, Mouse	1:400	1:200
E-cadherin	IF	Mouse	BD Bioscience	610182	Human, Mouse	1:100	1:200
Vimentin	IF	Mouse	Sigma	V2258	Human, Mouse	1:400	1:200
Keratin 5	IF	Rabbit	Abcam	Ab24647	Mouse	1:200	1:200
β -Cateinin	IF/IHC	Rabbit	Abcam	Ab16051	Human, Mouse	1:400	1:200
Mdr1/p-glycoprotein	Frozen IF	Mouse	Abcam	Ab3364	Human, Mouse	1:200	1:200

APPENDIX B

LENTI/RETROVIRAL STUDY VECTORS

Construct Name	Company	Cat #	Retro/Lenti	Purpose	Packaging line	Packaging Mix	Selection
pGIPZ Non-Silencing Control Vector	Thermo Scientific Open biosystems	RHS4346	Lentivirus	GFP labeled control	293T	TransLenti Viral Packaging Mix	GFP Puromycin
pCDH-CMV-MCS-EF1-RFP	System Bioscience	CD512A-1	Lentivirus	RFP labeled control	293T	pPACKH1 Lentivector packaging kit	RFP
pCDH-EF1-CymR-T2A-Puro	System Bioscience	QM200PA-1	Lentivirus	Generation of repressor lines for cumate inducible switch	293T	pPACKH1 Lentivector packaging kit	Puromycin
CuO-CMV-miR-9-1-IRES-GFP	System Bioscience	Custom	Lentivirus	Cumate inducible expression of miR-9	293T	pPACKH1 Lentivector packaging kit	GFP Puromycin
pMIRNA1-pre-miR9-1	System Bioscience	PMIRH9-1PA-1	Lentivirus	Stable overexpression of miR-9	293T	pPACKH1 Lentivector packaging kit	GFP
pmiR-ZIP-anti-miR-9	System Bioscience	MZIP9-PA-1	Lentivirus	Stable knockdown of miR-9	293T	pPACKH1 Lentivector packaging kit	GFP Puromycin
pMXs-Sox2	From Roop Lab (Shinya Yakamanaka Lab original)	N/A	Retrovirus	Stable overexpression of mouse Sox2	Ønx-E	pCL-Eco	None
pMiR-9-Luc Reporter	Signosis	LR-0054	Luciferase	Analysis of miR-9 activity	N/A	N/A	N/A
pBABE-puro-Kras12V	Addgene William Hahn (REF)	Addgene Plasmid #9052 William Hahn Lab	Retrovirus	Constitutive activation of Kras	293T	pUMVC, pCMV-VSV-G	Puromycin
pBABE-puro	Addgene	Addgene Plasmid #1764 Bob Weinberg Lab	Retrovirus	Empty expression vector	293T	pUMVC, pCMV-VSV-G	Puromycin
SMAD4 shRNA	UC Denver Functional Genomics Core/ Sigma	TRCN0000010321	Lentivirus	Human SMAD4 Knockdown	293T	MISSION lentiviral packaging mix (Sigma)	Puromycin
pSIH1-H1-siLuc-copGFP	System Bioscience	LV601B-1	Lentivirus	Positive control GFP	293T	pPACKH1 Lentivector packaging kit	GFP

APPENDIX C

GENOTYPING PRIMERS

Transgene	Primer Sequence
K15.CrePR1	CGGTCGATGCAACGAGTGAT
	CCACCGTCAGTACGTGAGAT
Smad4 Floxed	GGGCAGCGTAGCATATAAGA (P9)
	GACCCAAACGTCACCTTCA (P10)
LSL-Kras ^{G12D}	CCTTTACAAGCGCACGCAGACTGTAGA
	AGCTAGCCACCATGGCTTGAGTAAGTCTGC
Smad4 deletion	AAGAGCCACAGGTCAAGCAG (P8)
	GACCCAAACGTCACCTTCA (P10)
LSL-Kras ^{G12D} recombination	GGGTAGGTGTTGGGATAGCTG
	TCCGAATTCAGTGACTACAGATGTACAGAG

APPENDIX D

TAQMAN® GENE EXPRESSION PROBES

Probe Target	Species	Filter	Vendor	Catalog #
GAPDH	Human	VIC	Applied Biosystems	4326317E
GAPDH	Mouse	VIC	Applied Biosystems	4352339E
Smad4	Human	FAM	Applied Biosystems	Hs00232068
Smad4	Mouse	FAM	Applied Biosystems	Mm00484724_m1
Smad3	Mouse	FAM	Applied Biosystems	Mm00489637_m1
Smad2	Mouse	FAM	Applied Biosystems	Mm00487530_m1
Sox2	Mouse	FAM	Applied Biosystems	Mm00488369_s1
Keratin 1	Mouse	FAM	Applied Biosystems	Mm00492992_g1
Abcg2	Mouse	FAM	Applied Biosystems	Mm00496364_m1
Vimentin	Mouse	FAM	Applied Biosystems	Mm00449201_m1
Abcb1a	Mouse	FAM	Applied Biosystems	Mm00440761_m1*
Abcb1b	Mouse	FAM	Applied Biosystems	Mm00440736_m1
Abcc1	Mouse	FAM	Applied Biosystems	Mm00456156_m1
Nfkb1	Mouse	FAM	Applied Biosystems	Mm00476361_m1*
ABCB1	Human	FAM	Applied Biosystems	Hs01067802_m1*

APPENDIX E

TAQMAN® MICRORNA EXPRESSION PROBES

Assay	Assay type	Assay ID	Vendor	Mature miRNA sequence	miRBase names	miRBase Accession
miR-9	Mature miRNA	000583	Applied Biosystems	UCUUUGGUUAUCUAGCUGUAUGA	hsa-miR-9	MIMAT0000441
					mmu-miR-9	MIMAT0000142
miR-132	Mature miRNA	000457	Applied biosystems	UAACAGUCUACAGCCAUGGUCG	hsa-miR-132	MIMAT0000426
					mmu-miR-132	MIMAT0000144
U6 snRNA	Control	001973	Applied biosystems	GTGCTCGCTTCGGCAGCACATATACTAAAA TTGGAACGATACAGAGAAGATTAGCATGGC CCCTGCGCAAGGATGACACGCAAATTCGTG AAGCGTCCATATTTT	715680	N/A

APPENDIX F
HUMAN SAMPLES

UC Denver IRB# 08-0552			Number	Percent
TNM	T	1	2	10
		2	6	29
		3	7	33
		4	6	29
	N	0	6	29
		1	4	19
		2	11	52
	M	0	19	90
		1	1	5
		X	1	5
Differentiation		Well	3	14
		Moderately	15	71
		Poorly	3	14

OHSU IRB# e809			Number	Percent
TNM	T	1	4	21
		2	10	53
		3	2	11
		4	3	16
	N	0	7	37
		1	4	21
		2	5	26
		3	1	5
	M	X	19	100
Differentiation		Well	0	0
		Moderately	14	74
		Poorly	5	26

APPENDIX G
CURRICULUM VITAE

Ruth Aroon White

MD/PhD Student
Oregon Health and Science University

E-Mail: whiter@OHSU.edu

Education

2005-present	MD/PhD Cell and Developmental Biology Oregon Health and Science University, Portland OR
1998-2002	BA Honors in Biology-Chemistry Scripps College, Claremont CA

Professional Experience

2003-2005	Senior Research Technician Laboratory of Dr. David Livingston Dana Farber Cancer Institute, Boston MA
2002-2003	Research Technician Laboratory of Dr. Bruce Spiegelman Dana Farber Cancer Institute, Boston MA
June-Aug 2001	Student Intern Laboratory of Dr. Wolfgang Berger Max Plank Institute for Molecular Genetics, Berlin Germany
June-Aug 2000	Student Intern Laboratory of Dr. Peter Lichter German Cancer Research Institute, Heidelberg Germany

Honors and Awards

AACR Bristol Meyer Squibb scholar in training award: American Association for Cancer Research annual meeting, Denver CO, April 2009.

Distinguished Poster Award: 7th International conference on Head and Neck Cancer, San Francisco CA, July 19-23 2008

Barbara McClintock Award for Best Scientific Thesis: Scripps College, Claremont CA, 2002.

Memberships

American Medical Student Association, 2005-present

Oregon Medical Association, 2005-present

Sigma Xi Scientific Honors Society, elected to membership 2002.

American Association for the Advancement of Science, 2007-present

American Association for Cancer Research, April 2009-present

Teaching

Mentor, Minds Matters, Portland OR, September 2007 to 2009.

Service

Medical Student volunteer, Wallace Medical Concern, Portland OR, May 2007-present.

Medical student volunteer, SW Medical Clinic, Portland OR, November 2005-present.

Publications

1. Zimmer SN, Zhou Q, Zhou T, Cheng Z, Abboud-Werner SL, Horn D, Lecoche M, **White R**, Krivtsov AV, Armstrong SA, Kung AL, Livingston DM, Rebel VI. *Crebbp haploinsufficiency in mice alters the bone marrow microenvironment leading to loss of stem cells and excessive myelopoiesis*. Blood, 2011.
2. **White RA**, Malkoski SP, Wang XJ. *TGF β signaling in head and neck squamous cell carcinoma*. Oncogene, 2010. 7;29(40): p5437-46.
3. Bornstein S, **White R**, Malkoski S, Oka M, Han G, Cleaver T, Reh D, Andersen P, Gross N, Olson S, Deng C, Lu S, and Wang XJ. *Smad4 loss in mice causes spontaneous head and neck cancer with increased genomic instability and inflammation*. J Clin Invest, 2009. **119**(11): p3408-19.

Abstracts

1. **White R**, Bornstein S, Malkoski S, Lu S.L., Wang X.J. MicroRNAs in Metastatic Stem Cells. **Keystone Symposium on Stem Cells, Cancer and Metastasis**. Keystone, CO. May 6-11th 2011.
2. **White R**, Lu SL, Bornstein S, Salter K, Olson S, Anderson P, Reh D, Malkoski S, Deng C, Wang X. Smad4 Deletion Leads to Spontaneous Head and Neck Cancer Formation Associated with Genomic Instability. **American Association for Cancer Research 100th Annual Meeting**, Denver, Colorado, April 18-22, 2009. *AACR Bristol Meyer Squibb Scholar in Training Award.
3. **White R**, Lu SL, Bornstein S, Salter K, Olson S, Anderson P, Reh D, Malkoski S, Deng C, Wang X. Smad4 Deletion Leads to Spontaneous Head and Neck Cancer Formation Associated with Reduced Expression of FancA and Brca1. **Twentieth Annual Fanconi Anemia Research Fund Scientific Symposium**, Eugene, Oregon, October 4-7, 2008.
4. **White R**, Lu SL, Bornstein S, Salter K, Olson S, Anderson P, Reh D, Malkoski S, Deng C, Wang X. Smad4 Deletion Leads to Spontaneous Head and Neck Cancer Formation Associated with Genomic Instability. **7th International Conference on Head and Neck Cancer**. San Francisco, California, July 19-23, 2008. *Poster of Distinction.
5. Bornstein S, Lu, SL, Hoot K, **White R**, Anderson P, Corless C, Deng C, Wang X. Role of TGF β Signaling-Mediated Inflammation in HNSCC Carcinogenesis. **7th International Conference on Head and Neck Cancer**. San Francisco, California, July 19-23, 2008.

APPENDIX H

SMAD4 LOSS IN MICE CAUSES SPONTANEOUS HEAD AND NECK CANCER WITH INCREASED GENOMIC INSTABILITY AND INFLAMMATION

Journal of Clinical Investigation

2009;119(11):3408-3419

Sophia Bornstein¹, Ruth White^{1,2}, Stephen Malkoski³, Masako Oka², Gangwen Han²,
Timothy Cleaver³, Douglas Reh¹, Peter Andersen¹, Neil Gross¹, Susan Olson⁴, Chuxia
Deng⁵, Shi-Long Lu⁶ and Xiao-Jing Wang^{1,2}

¹Department of Otolaryngology, Oregon Health & Science University (OHSU), Portland, Oregon,
USA.

²Department of Pathology and

³Department of Medicine, Division of Pulmonary Sciences and Critical Care Medicine,
University of Colorado Denver, Aurora, Colorado, USA.

⁴Department of Molecular and Medical Genetics, OHSU, Portland, Oregon, USA.

⁵Genetics of Development and Disease Branch, NIDDK, NIH, Bethesda, Maryland, USA.

⁶Department of Otolaryngology, University of Colorado Denver, Aurora, Colorado, USA